Collective dynamics of excitons and exciton-polaritons in nanoscale heterostructures

Dmitri Visnevski

N° d'Ordre: D. U. 2366

UNIVERSITE BLAISE PASCAL - CLERMONT-FERRAND

U. F. R. Science et Technologies

ECOLE DOCTORALE DES SCIENCES FONDAMANTALES

N° 753

THESE DE DOCTORAT

Pour accéder au grade de

Docteur d'université en sciences

de l'université Blaise Pascal - Clermont-Ferrand

Specialité : Science des matériaux

Défendue par

Dmitri VISNEVSKI

Collective dynamics of excitons and exciton-polaritons in nanoscale heterostructures

Soutenue publiquement le 09 Juillet 2013

Commission d'examen:

Rapporteurs :	Pr. Mikhail Glazov
	Pr. Fabrice Laussy
Examinateurs :	Pr. Dmitry Yakovlev
	Pr. Ivan Shelykh
	Dr. Dmitry Solnyshkov
Directeur de thèse :	Dr. Guillaume Malpuech
	Pr. Nikolay Gippius

Acknowledgments

Like the quasi-particles in semiconductor structures, living their short but undoubtedly useful life, cannot be treated outside the media, so are the scientists and their works, which could not be considered stand-alone, out of the context of the scientific society. The time I have been writing this manuscript, I was wondering at the elegant consistency and regularity which underlay the evolution of the physics. When I tried to investigate the cause of any discovery or invention, I always went deeper and deeper into the history of physics, and if I did not stop myself at will, I certainly would have had to parse the manuscripts of the ancient Greeks.

Thus, the work that I have done is nothing but a natural continuation to all what has been done before, and a lot of other people have contributed to it not less than I did. I want to mention here some of them, who have made an invaluable contribution to the development of me as a person and as a scientist. First of all, of course, I want to thank my family and particularly my father, who, sometimes against my will and laziness, has been introducing me into the world of physics and mathematics in the times of my adolescence. Then, I would like to thank my first true scientific advisor Prof. Ivan Vladimirovich Ignatiev. The first tentative steps in the semiconductor physics I did under his experienced and wise leadership.

Of course, one could hardly overestimate the influence of my three doctorate supervisors, who, contrary to the Russian proverb about seven nannies, each being a bright personality, harmoniously complement each other and provided me with a full-fledged supervision. Thus, for example, infinite optimism, vitality and incredible scientific intuition of Dr. Guillaume Malpuech have been continuously inspiring me and driving me forward, when sensible criticism and I would say even skepticism of Prof. Nikolay Gippius stopped me and cooled me down just in time, preventing of the making serious mistakes. Dr. Dmitry Solnyshkov helped me a lot with my pressing problems, I was admired by his ability to understand my needs at a glance (and not only because we speak the same language), accurately get the point of the problem and to provide the solution very quickly.

Also I wish to thank other PhD-students and one post-doctoral researcher I have worked with: Hugo Flayac, Goran Pavlovic, Anton Nalitov and Hugo Terças. It was very pleasant to collaborate with them, since we often have been sharing the same "joys and sorrows". I would like to mention a great team of the European International Training Network "Spin-optronics". We have been passing a very good time on numerous conferences and meetings which were held in different, sometimes quite exotic places.

Contents

Chapter 1

Introduction

Contents

Undoubtedly, the successes in the investigation of the microworld in the beginning of XX century have provoked a rapid development of the quantum theory. Together with the works of Einstein on theory of relativity it has made a revolution in the conception of theoretical physics. New theories, whose progress was bounded just by the imagination of scientists, developed rapidly, often leaving the experiment behind. This way, for example, Bose-Einstein condensation was predicted by Einstein in 1925 [1]. Conditions for the formation of an atomic condensate were so extreme, that technologies allowed its observation only 70 years after its theoretical description[2].

One could say that the pioneer works on X-ray diffraction in different crystal structures performed by von Laue, Bragg and others in early 1910s [3, 4, 5, 6] have initiated the modern solid-state physics (SSP). Since that time it has been continuously evolving during the XXth century. Progress in growth technologies has been allowing to create more and more complicated and perfect structures - starting with simple transistors in 1940s up to high-quality nanostructures nowadays. Most of them, based on the specifics of heterojunctions between different materials, are efficiently driving forward micro- and nanoelectronics, optoelectronics, spintronics etc.

In addition, it's important to say about one more aspect - information technologies (IT). A lot of theoretical problems have no analytical solution. Previously,

scientists had to make numerous approximations to solve them and this limited the applicability of solutions. The strong boom in the IT of the last 30 year has allowed to solve very wide range of problems with high accuracy for a reasonable time. In the solid-state physics numerical calculations are extremely important, so the progress in computer technologies strongly assists the development of the solid-state theory. Summarizing, it seems, that we live in the age where the development of science becomes less and less limited by objective constraints.

Huge number of particles, which compose solids, gives rise to numerous collective excitation effects. They can be described in terms of quasiparticles (excitons, phonons, etc), which behave like real particles having its own effective mass, charge, spin etc, but which appear in media only. The solid medium strongly defines the behavior of quasiparticles, so tuning the medium properties one could strongly vary the properties of the quasiparticles under study. This is why nowadays there are so many different nanostructures. Solid-state physics provides a handy platform to study and develop different effects which could be hardly studied in other systems. So, for example, considering very light quasiparticles (whose mass is 10^8 times smaller than atomic mass) one could raise the critical temperature of Bose-Einstein condensation from microKelvins up to room temperature. Amazing properties of semiconductor nanostructures have inspired me to dedicate this work to them. Of course, modern solid-state physics is a huge scientific field, but I want to believe that my studies will find their small but useful place inside.

This manuscript is divided into 5 chapters. The first chapter is an introduction, where I will describe the basics aspects of nanostructure physics which are relevant to my work, such as basic facts about structures of different types, idea of Bose-Einstein condensation and basic mathematical tools for its description. Each of the four others chapters will be dedicated to a separate topic. In the second chapter I will discuss the interaction between exciton condensates and strong coherent acoustic fields. I will show that at some conditions strong-coupling regime could be obtained what gives rise to a new-type quasiparticles. Chapter 3 will be dedicated to the lasing of quantum dots ensemble embedded into a cavity. The effect of the lasing amplification by ultrafast acoustic pulse will be described. In chapter 4, the multistability effect in the system of cavity polaritons will be discussed. It will be shown that under strong resonant pumping of the ground state, the high-populated excitonic reservoir could appear, which strongly modifies the effective polariton-polariton interactions. And finally, in chapter 5 I will speak about polarization patterns in the condensates of indirect excitons. Also, I have added a small Appendix, where I discuss some features of numerical methods I used in my calculations.

1.1 Excitons and Exciton-polaritons

1.1.1 The basics. Band structure.

The propagation of the free carriers (electrons and holes) in the periodic potential of semiconductor lattice can be described by the Bloch-type wave-functions $u_{n\mathbf{k}}(\mathbf{r})$ multiplied by plane wave [7]:

$$\psi_{n\mathbf{k}} = e^{i\mathbf{kr}} u_{n\mathbf{k}}(\mathbf{r}), \tag{1.1}$$

where the function $u_{n\mathbf{k}}(\mathbf{r}+\mathbf{R}) = u_{n\mathbf{k}}(\mathbf{r})$ has the same periodicity as crystal structure. $\mathbf{r}$ is a radius-vector, $\mathbf{k}$ is called electron (hole) wave-vector and n is a band number. Thus, the carriers in semiconductor could be considered as quasiparticles with their own dispersion defined by the medium.

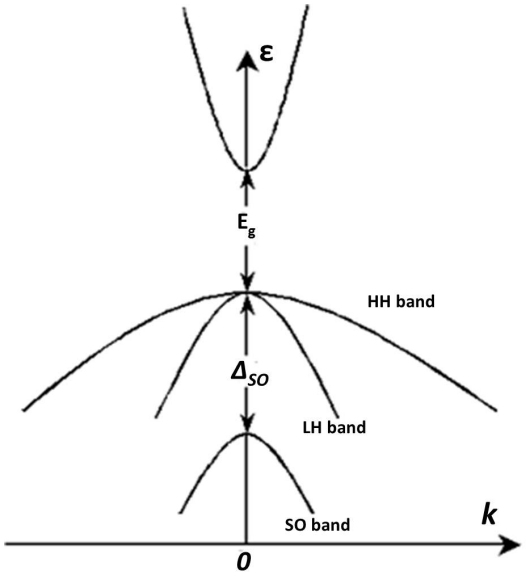

Figure 1.1: Band structure of GaAs for electrons with small wave-vector. Valence band consists of three subbands (SO, LH and HH). E_g is the width of the energy gap, Δ_{SO} is a split-off value

Hereinafter we will speak generally about semiconductors of zinc-blende type and particularly about GaAs. In such crystals the highest valence band is formed by p-shell electrons while the conduction band is formed by s-shell electrons. Electrons in p-states have angular momentum $\mathbf{L}$ equal to 1 so its projection L_z on the chosen axis (let's call it $\mathbf{Z}$ axis) could be either 0 or ± 1. Electrons with $L_z = 0$ are split in energy from the bottom of the valence band and they form the so-called split-off band (SO). Total angular momentum $\mathbf{J}$ of a carrier is defined by the sum of its angular momentum $\mathbf{L}$ and its spin $\mathbf{S}$. So, the split-off band is double degenerate when the spin is taken into account. The projection of $\mathbf{J}$ on chosen axis for the states with $L_z = \pm 1$ could take for values $(J_z = \pm\frac{1}{2}, \pm\frac{3}{2})$. This gives rise to two

double degenerate bands called light-hole band (LH) for $J_z = \pm\frac{1}{2}$ and heavy-hole (HH) band for $J_z = \pm\frac{3}{2}$ which show the same energy when carrier has zero wave-vector $\mathbf{k} = 0$ [8]. In our work we will not consider the SO band and will discuss LH and HH bands only.

The total angular momentum of s-type electrons which form the conduction band is defined by the electron spin only. Thus, there is only one double degenerate conduction band. Band structure of GaAs for the carriers with small $\mathbf{k}$ is schematically illustrated on figure 1.1.

If a photon is propagating in a semiconductor and its energy is larger than the gap energy E_g, it could be absorbed by the medium and a free electron and a hole would appear. Physical laws require the conservation of the wave-vector ($\mathbf{k_{ph}} = \mathbf{k_e} + \mathbf{k_h}$) and of the angular momentum. Taking into account the fact that photons have angular momentum equal to 1, the latter requirement provides certain selection rules:

$$J_z^e + J_z^h = \pm 1, 0. \tag{1.2}$$

Selection rules for photon absorption are schematically shown in figure 1.2[8]. Circularly polarized photons with $J_z^{ph} = \pm 1$ are shown by circle arrows, while linearly polarized photons with $J_z^{ph} = 0$ are plotted by straight double arrows.

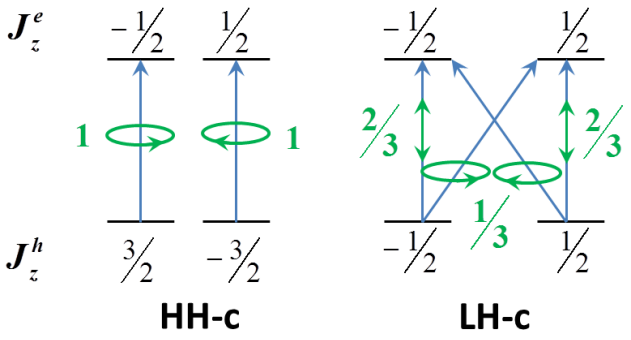

Figure 1.2: Selection rules for light absorption. Black numbers show the z-projections of total angular momentum of carriers. Green arrows show the polarization of the absorbed light when green numbers state relative intensity of transitions.

Also, an electron and a hole could recombine emitting a photon. The selection rules for emission are similar to ones for absorption. Thus by illuminating samples by polarized light one can create certain spin states in the system and by analyzing the polarization of emitted light, one can collect the information about spin states. This is what lies in the principles of the light-based control of spin.

1.1.2 Excitons

An electron interacts with a hole by the Coulomb force. If their relative distance $r_{e-h} = |\mathbf{r_e} - \mathbf{r_h}|$ is much larger than the size of a unit cell of the crystal, then the

Schrodinger equation for the system could be written in a form:

$$\left(\frac{\hat{p}_e^2}{2m_e} + \frac{\hat{p}_h^2}{2m_h} - \frac{e^2}{\varepsilon r_{e-h}}\right)\Psi = E\Psi. \tag{1.3}$$

Here $\hat{p}_{e,h}$ are momentum operators for electron and hole, $m_{e,h}$ are their effective masses, Ψ is a wave-function of the system and E is the energy. The semiconductor medium is introduced in this equation by the dielectric constant ε. In such description, the electron-hole pair forms a hydrogen atom-like system and one can speak about new quasi-particle - *exciton* [9]. The exciton energy spectrum is described by:

$$E_n^X(k_X) = -\frac{R_X}{n^2} + \frac{\hbar^2 k_X^2}{2M}, \tag{1.4}$$

$R_X = \frac{\mu e^4}{2\hbar^2\varepsilon^2}$ is called exciton Rydberg, k_X is an exciton wave-vector, $M = m_e + m_h$ - its effective mass and $\mu = \left(\frac{1}{m_e} + \frac{1}{m_h}\right)^{-1}$ is the reduced mass. Here, the lowest energy of free electron and hole is taken as zero reference. Equation 1.4 describes the parabolic dispersion of excitons. Bohr radius of an exciton could be written as:

$$a_X = \frac{\hbar^2\varepsilon}{\mu e^2}. \tag{1.5}$$

Dielectric constant ε of GaAs is 13 which makes Bohr radius of an GaAs exciton much larger than the size of its unit cell ($a_X = 112$ Å). Thus our assumption about relative position of the electron and the hole is correct, and effective mass approximation (1.3) is legal. Such excitons with large Bohr radius are commonly found in crystal semiconductors and are called Wannier-Mott excitons as opposed to Frenkel excitons of small Bohr radius which could be found in molecular crystals. In this work we shall be dealing only with Wannier-Mott excitons.

The main property of excitons is their ability to interact with light (theory was developed first in [10, 11, 12]) An exciton could be created by light as well as it could decay, emitting photon. Exciton-photon interaction is strongest at resonance. If we introduce into the Hamiltonian the exciton-photon interaction term, the eigenstates of the system at the wavevector where the dispersions cross each other would not be pure exciton and photon states, but a mixing between them. In fact we could speak about a new quasi-particle - *exciton-polariton* [7]. Thanks to light-matter interaction, an anticrossing between the two dispersion curves appears. However, in most bulk materials, exciton-photon interaction is weak, so the magnitude of the anticrossing is smaller than broadening of exciton and photon lines. In these cases, the eigenstates of system are almost completely excitonic or photonic and we can still speak about two independent quasi-particles in medium.

Sum of the total angular momentum of hole and electron forming the exciton is called for simplicity the exciton spin ($\mathbf{S^X}$). Its projection on the chosen axis can take five values: $\mathbf{S_z^X} = \pm 2, \pm 1, 0$. Selection rules and conservation laws here are the same as for free electrons and holes, this is why excitons with $\mathbf{S_z^X} = \pm 2$ do not interact with light and are called dark excitons.

1.2 Nanostructures

Growth technologies have been advancing very much during the last decades. This gave opportunity to fabricate different semiconductor heterostructures with very high quality interfaces. As a result, numerous nanoscale heterostructures appeared. The main idea is to strongly modify motion of carriers by heterotransitions. For example, placing a thin layer of one semiconductor with small band gap (for example GaAs) between two layers of another crystal with large band gap (AlAs) one can create a potential well for carriers in the growth direction (**Z**-axis). If the size of potential well is small enough, the motion of carriers along **Z** becomes quantized. Such structures are called *Quantum wells* or QWs. Particularly, if electrons and holes are trapped in the same layer, such QWs (or, rather, the heterojunctions) are said to be of the 1st type.

Electrons and holes in QWs form a quasi 2D system. Their motion in the plane is free, while they are quantized in the growth direction. Nowadays, there are plenty of different types of heterostructures possessing different effective dimensionality. However, in this work we will discuss only few of them.

1.2.1 Quantum Wells

As it was said, quantum wells are thin layers of one semiconductor sandwiched between thicker layers of another. The motion of the carriers becomes quantized in the **Z** direction and a number of energy subbands appears. Because each state trapped in QW has a fixed nonzero $\mathbf{k_z}$, the degeneracy between LH and HH bands in Γ point is lifted and even with zero in-plane wave vector $\mathbf{k}_{||}$ there is a gap in energy between the two bands. For an infinite potential well one should expect the following expression for the width of this gap [13]:

$$\Delta E^{\Gamma}_{lh-hh} = \frac{(\pi n\hbar)^2}{2L^2_{QW}}\left(\frac{1}{m_{lh}} - \frac{1}{m_{hh}}\right), \tag{1.6}$$

where L_{QW} is the width of the well and n is a number of state quantized in **Z**.

However, far from the Γ point, the eigenstates in the valence band are no longer pure heavy-hole or pure light-hole states, but a mixture of them. This gives rise to additional non-parabolicity of the valence band.

In quantum wells, electrons and holes could couple to excitons as well, but quantum confinement of their motion imposes certain changes on their energy structure. Thus, in excitons formed by an electron and by a heavy hole, optically active states ($\mathbf{S^X_z} = \pm 1$) are split from dark states ($\mathbf{S^X_z} = \pm 2$) by short-range electron-hole exchange interaction.

For spin dynamics of carriers in QWs one should consider two different cases: when carriers are free and when they are bound into excitons. The general mechanism of spin relaxation for free carriers is a Dyakonov-Perel mechanism of spin-orbit interaction. This gives rise to non-zero splitting between spin-states proportional to **k**. In bulk there is only one type of spin-orbit interaction - the Dresselhaus or bulk

inversion asymmetry (BIA)[14]. For electrons in a basis $\begin{pmatrix} \frac{1}{2} & -\frac{1}{2} \end{pmatrix}^T$ one can read a Hamiltonian term:

$$H_e^D = \beta(\sigma_x k_x(k_y^2 - k_z^2) + \sigma_y k_y(k_z^2 - k_x^2) + \sigma_z k_z(k_x^2 - k_y^2)), \tag{1.7}$$

where β is a Dresselhaus coefficient.

To obtain the corresponding term in Hamiltonian for electrons in QWs one should take an averaging over k_z. For [001] direction of growth axis one could get:

$$H_{2De}^D = \beta_e(\sigma_+ k_-^e + \sigma_- k_+^e). \tag{1.8}$$

Here $(\sigma_\pm, k_\pm) = (\sigma_x, k_x) \pm i(\sigma_y, k_y)$.

Also in confined structures there is an additional energy splitting due to the structural inversion asymmetry (SIA) in the presence of electric fields also known as Rashba spin-orbit interaction[15]:

$$H_e^R = \gamma(\sigma_+(k_y^e + ik_x^e) + \sigma_-(k_y^e - ik_x^e)). \tag{1.9}$$

Here γ is Rasba coefficient.

For holes the situation is a bit more complicated. In bulk, the hole spin relaxes very fast due to the mixing between heavy-hole and light-hole subbands [8, 16]. In 2D systems, because of the degeneracy lifting near the Γ-point this mechanism is suppressed and holes are also affected by SOI. Several recent papers claim the cubic by $\mathbf{k}$ dependence of splitting[17, 18]. However, to my knowledge it is the result of the group delusion and the Dresselhaus term in the Hamiltonian for 2D holes is linear by wave-vector $\mathbf{k}$ as it was stated in the paper of Rashba and Sherman [19]. The energy splitting between two subbands in the heavy-hole band reads as:

$$\Delta E_{hh}(\mathbf{k}) = \beta_h^{'}\left(\frac{\pi}{L_{QW}}\right)^2 \mathbf{k}. \tag{1.10}$$

Because of the HH-LH subband splittings in 2D-systems, the lowest in energy exciton is formed from heavy-holes. The short-range exchange interaction between holes and electrons bound into an exciton causes a splitting in energy between bright and dark exciton states in quantum well for a value [13] (here and after we will consider the infinite barrier model):

$$\Delta_0 \approx \frac{9}{16}\Delta_0^{3D}\left(\frac{E_B}{E_B^{3D}}\right)^2 \frac{a_B^{3D}}{L_{QW}}. \tag{1.11}$$

Here Δ_0^{3D} is the corresponding splitting in bulk, E_B^{3D},E_B are the exciton binding energies in bulk and in QW, a_B^{3D} is a Bohr radius.

Also, thanks to the long-range electron-hole exchange interaction there is an additional splitting in energy between the longitudinal and transverse exciton states, which in 2D systems is linear with respect to the wave-vector of the exciton center of mass $\mathbf{k}^{\mathbf{X}}$ [20]:

$$\Delta_{LT} = \frac{3}{16}\Delta_{LT}^{3D}\left(\frac{E_B}{E_B^{3D}}\right)^2 |\langle\chi_{e,l}|\chi_{h,l}\rangle|^2 a_B^{3D} k^X, \tag{1.12}$$

where $\chi_{e,h,l}$ are the single particle envelope functions describing the electron and heavy-hole motion along the growth axis, and Δ_{LT}^{3D} is a longitudinal-transverse splitting for the bulk, which does not depend on k^X.

1.2.2 Quantum Dots

Another very important type of semiconductor nanostructures, in which motion of carriers is confined in all directions, are called *quantum dots* (QD). The history of QDs starts in 1981 with the work of Ekimov and Onushchenko [21], who observed discrete lines in the absorption spectra of CuCl nanocrystals in a silicate glass matrix. However, the energy structure of such objects was very sensitive to the interfaces. Since that time, numerous methods of quantum dots growth appeared, but most popular nowadays is *Stranski-Krastanov* method of self-assembled quantum dots formation under molecular-beam epitaxy (MBE). This method is based on the formation of semiconductor droplets under the forces of surface tension. Then these droplets are covered by another wide-gap semiconductor. However, between the QDs there still remains a thin layer of the same material which is called wetting layer. Such growth method leads to the formation of a large ensemble of quantum dots. However, studies of single quantum dots selected from such ensemble, are also popular.

A scheme and a HRTEM image of quantum dots are presented on fig. 1.3.

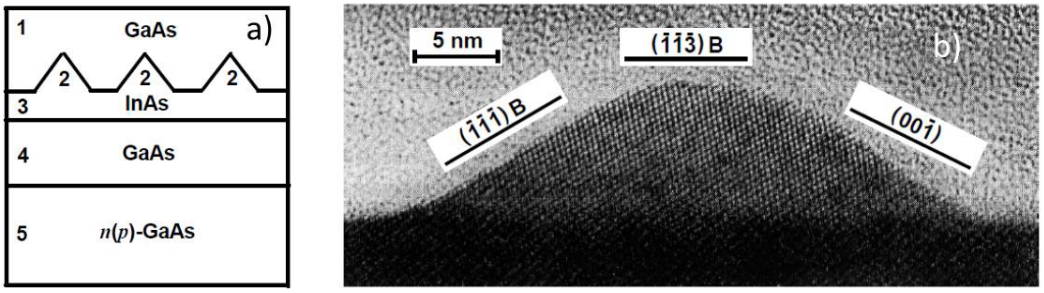

Figure 1.3: a) Schematic representation of self-assembled quantum dots. 1, 4 - buffer layers of GaAs, 2 - InAs quantum dots, 3 - wetting layer, 5 - n-doped GaAs substrate. b) HRTEM image of single InAs quantum dot. Pictures are taken from [22, 23]

As it was said, in QDs the motion of carriers is confined in all directions which results in the formation of a set of discrete states. Considering an approximation of the infinite potential well for carriers and considering a parallelepiped QD with dimensions $L_{x,y,z}$, one can easily find the values for the energy of the quantized states:

$$E_n^{QD} = \frac{\hbar^2\pi^2}{2m_{e,h}}\left(\frac{n_x^2}{L_x^2} + \frac{n_y^2}{L_y^2} + \frac{n_z^2}{L_z^2}\right), \tag{1.13}$$

where $n_{x,y,z}$ are the quantum numbers of the eigenstates. Thus, the ground exciton state has the energy:

$$E_{X1}^{QD} = \frac{\hbar^2\pi^2}{2\mu}\left(\frac{1}{L_x^2} + \frac{1}{L_y^2} + \frac{1}{L_z^2}\right). \tag{1.14}$$

Obviously it depends strongly on the size of the dot. The Stranski-Krastanov method assumes self-assembling of the quantum dots which leads to a statistical distribution of their sizes. As a result, there is a broadening of the QD spectra up to tens meV which is called *inhomogeneous broadening* (fig. 1.4). Annealing of the structure at high temperature provokes the diffusion of atoms and blurs the interfaces of the quantum dots. This procedure leads to a smoothing of the dots sizes and to a narrowing of their spectra. At the same time, the average ground state energy is increased.

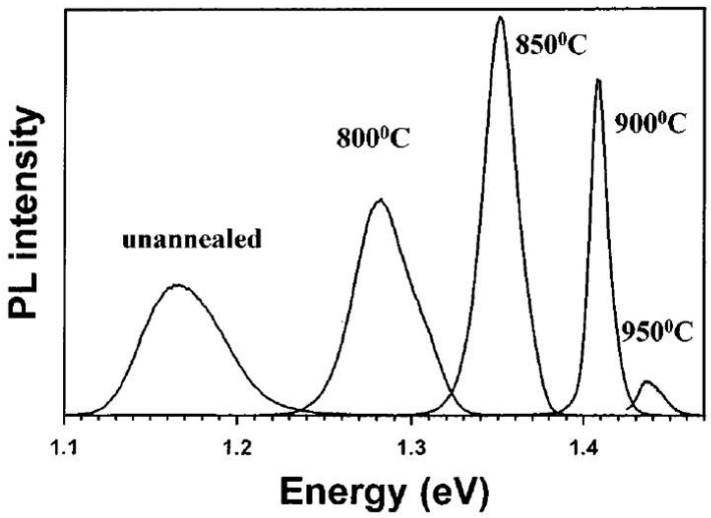

Figure 1.4: Spectra of InAs/GaAs QDs photoluminescence for different values of the annealing temperature.

The main method of study of QDs is based on the analysis of their photoluminescence (PL). Investigation of the effects based on polarization properties of PL takes a large part in the QD field, however, it is not the principal subject of this thesis, so we will not discuss the features determined by the spin dynamics of the carriers.

Nowadays, the quantum dots are considered as very promising objects. They are already widely exploited in light-emitting devices: light-emitting diodes and lasers. Recently, displays on quantum dots appeared. Also, they have been used as

active media for solar cells, single electron transistors and even qubits for quantum computation.

1.2.3 Microcavities. Cavity polaritons

Confinement of light in resonators has been studied since a very long time, and maybe the most well-known resonator is the Fabry-Perot resonator. The most used method is the confinement in *optical microcavities* (MC). Nowadays, the microcavities are usually composed of two Bragg mirrors situated parallel each to other with some spacing between. Each Bragg mirror presents a periodical structure of two semiconductors with different dielectric constants (fig. 1.5)

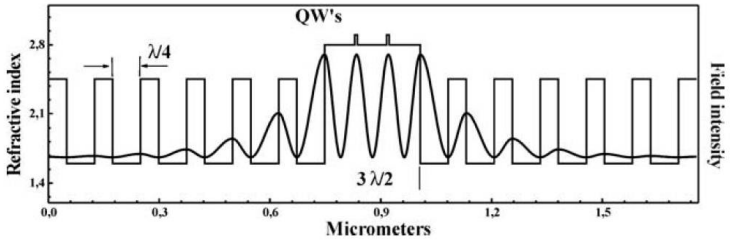

Figure 1.5: Scheme of a microcavity. A number of quantum wells or quantum dots are embedded at the antinodes of the light mode. Image is taken from [24]

Tuning the thickness of layers, one can obtain the situation when the incident light is almost totally reflected due to the interference inside the mirror. The spectral width of the total reflection band is called *stop-band*. However, for two parallel mirrors, a dip may appear in the reflection spectrum. This dip corresponds to the resonant frequency of the light mode confined inside the resonator. Due to the fact that cavity photons have fixed wave-vector along the growth axis, their dispersion is parabolic for small in-plane wave-vectors. The main feature of microcavities is that photons could live inside very long time (up to tens picoseconds) thanks to numerous reflections from the two Bragg mirrors. This requires the reflection coefficient to be very high, and this is why the Bragg mirrors are preferred over metallic ones, for example.

In general, the photonic dispersion law is linear versus its wave-vector and could be written in a form:

$$E_\phi = \hbar k c_\phi, \tag{1.15}$$

where c_ϕ is a speed of light in the medium. However, in the microcavities, where the motion of photons is confined in the Z direction, the value of k_z is fixed and one should express the total photon wave-vector as $k = \sqrt{k_z^2 + k_{||}^2}$, where $k_{||}$ is an in-plane wave-vector. Thanks to this, the dispersion in a case of small $k_{||}$ gets the standard parabolic form:

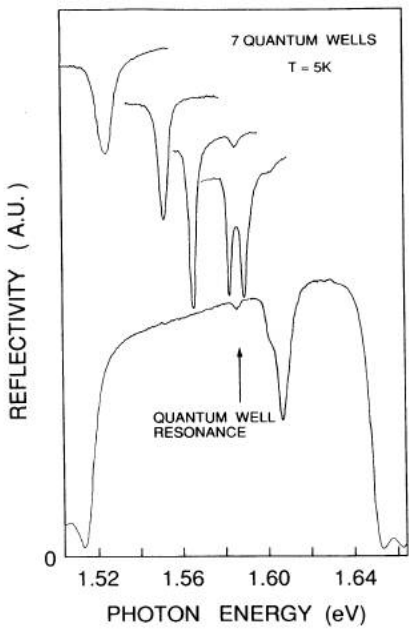

Figure 1.6: Reflection spectra of the quantum wells in a microcavity measured for different values of detunings. The presence of a double dip is a signature of the transition to strong coupling regime. The image is taken from [25]

$$E_\phi \sim \frac{\hbar^2 k_{||}^2}{2m_\phi}. \tag{1.16}$$

The effective mass of cavity photon is given by $m_\phi = k_z/2c_\phi$ and it usually takes values of the order of $10^{-5}m_e$.

Usually, the microcavities are used to study the light-matter interaction and the number of quantum wells or quantum dots are embedded inside (fig. 1.5). They are placed at the antinodes of the confined light mode to increase the strength of the interaction. If the light-exciton interaction is strong enough, one can obtain the *strong coupling* regime which is exhibited by anticrossing between the light and the exciton mode. In microcavities the strong-coupling regime for the first time was observed by Claude Weisbuch et al.[25]. They studied the dip in the reflectivity spectrum of the QWs embedded in MC and they found that at some conditions the dip was split (fig. 1.6), which is a signature of the anticrossing of quantum levels because of their interaction.

To describe light-matter interaction in microcavities mathematically we could write the following Hamiltonian:

$$H = \sum_{\mathbf{k}} E_\phi(\mathbf{k})\, \phi_{\mathbf{k}}^\dagger \phi_{\mathbf{k}} + \sum_{\mathbf{k}} E_\chi(\mathbf{k})\, \chi_{\mathbf{k}}^\dagger \chi_{\mathbf{k}} + \hbar\Omega_R \sum_{\mathbf{k}} \left(\phi_{\mathbf{k}}^\dagger \chi_{\mathbf{k}} + \chi_{\mathbf{k}}^\dagger \phi_{\mathbf{k}}\right). \tag{1.17}$$

It is a simple Hamiltonian for two interacting oscillators (exciton and photon).

Here $\phi_{\mathbf{k}}^{\dagger}$ and $\phi_{\mathbf{k}}$ ($\chi_{\mathbf{k}}^{\dagger}$ and $\chi_{\mathbf{k}}$) are the creation and destruction operators for a photon (exciton). $E_{\phi}(\mathbf{k}) = \hbar^2 k^2/2m_{\phi} + \delta$ and $E_{\chi}(\mathbf{k}) = \hbar^2 k^2/2m_{\chi}$ describe the parabolic dispersions of photons and excitons. The ground state energy of the photon could be shifted with respect to the ground state energy of the exciton by a value of δ which is called *detuning*. The strength of the exciton-photon interaction is described by the so-called *Rabi frequency* Ω_R.

In the two-component basis (pure exciton and pure photon states) the 1.17 Hamiltonian could be presented in a matrix form:

$$M = \begin{pmatrix} E_{\phi}(\mathbf{k}) & \hbar\Omega_R \\ \hbar\Omega_R & E_{\chi}(\mathbf{k}) \end{pmatrix}. \tag{1.18}$$

It can be easily diagonalized. As a result, one can write the in-plane dispersion expressions for the two new eigenstates:

$$E_L(\mathbf{k}) = \frac{1}{2}\left(E_{\phi}(\mathbf{k}) + E_{\chi}(\mathbf{k}) - \sqrt{\left[E_{\phi}(\mathbf{k}) - E_{\chi}(\mathbf{k})\right]^2 + 4\hbar^2\Omega_R^2}\right), \tag{1.19}$$

$$E_U(\mathbf{k}) = \frac{1}{2}\left(E_{\phi}(\mathbf{k}) + E_{\chi}(\mathbf{k}) + \sqrt{\left[E_{\phi}(\mathbf{k}) - E_{\chi}(\mathbf{k})\right]^2 + 4\hbar^2\Omega_R^2}\right). \tag{1.20}$$

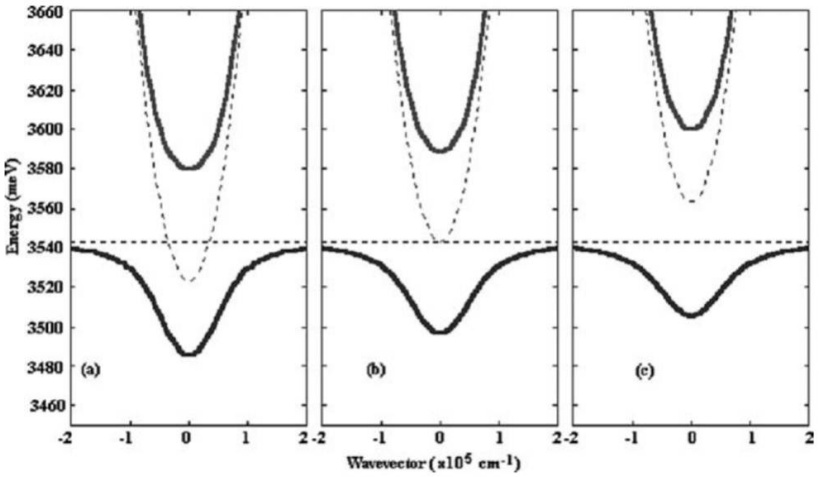

Figure 1.7: Polariton dispersion calculated for a) negative, b)zero and c) positive detuning. Image is taken from [24]

As stated in 1.1.2, the new eigenstates can be treated as new quasiparticles which are called in general exciton-polaritons or particularly cavity polaritons (because they appear in a microcavity). Polariton dispersion for different values of detuning is presented on fig. 1.7.

The expression for the energy splitting between the lower and the upper polariton branches for zero in-plane wave vector reads:

$$\Delta E_{UL}(0) = \sqrt{\delta^2 + \hbar^2\Omega_R^2}. \tag{1.21}$$

If the broadening of polariton lines is smaller than this splitting, then the double dip in the reflectivity spectrum could be observed. This is a practical criterion for the strong-coupling regime.

The polariton dispersion at small in-plane wave-vectors is almost parabolic and could be described by an effective mass whose value lies between m_ϕ and m_χ. The value of the mass strongly depends on the detuning. Thus, δ is a very important parameter in polaritonics. In practice, microcavities are grown that way that Bragg mirrors are not absolutely parallel, but slightly mutually inclined (because there is a wedge in the cavity thickness due to a special growth procedure). This allows to tune the energy of photonic ground state and the δ by studying different points on the cavity surface.

As it was said before, the long-range exchange interaction between electron and hole coupled to an exciton gives rise to a so-called longitudinal-transverse (or TE-TM) energy splitting between differently polarized exciton states. However, for cavity polaritons there is an additional TE-TM splitting originating from the one of cavity photons. Since now we should no longer consider the model of two coupled oscillators (photons and excitons) but a model of four oscillators (TE- and TM-polarized excitons and photons), each of them has its own effective mass and a bare dispersion:

$$E_\phi^{TE}(\mathbf{k}) = \frac{\hbar^2 k^2}{2m_\phi^{TE}} + \delta,\ E_\chi^{TE}(k) = \frac{\hbar^2 k^2}{2m_\chi^{TE}}, \tag{1.22}$$

$$E_\phi^{TM}(\mathbf{k}) = \frac{\hbar^2 k^2}{2m_\phi^{TM}} + \delta,\ E_\chi^{TM}(k) = \frac{\hbar^2 k^2}{2m_\chi^{TM}}. \tag{1.23}$$

This leads to 4 polariton branches:

$$E_L^{TE} = \frac{E_\phi^{TE} + E_\chi^{TE}}{2} - \frac{1}{2}\sqrt{\left(E_\phi^{TE} - E_\chi^{TE}\right)^2 + 4\hbar^2\Omega_R^2}, \tag{1.24}$$

$$E_L^{TM} = \frac{E_\phi^{TM} + E_\chi^{TM}}{2} - \frac{1}{2}\sqrt{\left(E_\phi^{TM} - E_\chi^{TM}\right)^2 + 4\hbar^2\Omega_R^2}, \tag{1.25}$$

$$E_U^{TE} = \frac{E_\phi^{TE} + E_\chi^{TE}}{2} + \frac{1}{2}\sqrt{\left(E_\phi^{TE} - E_\chi^{TE}\right)^2 + 4\hbar^2\Omega_R^2}, \tag{1.26}$$

$$E_U^{TM} = \frac{E_\phi^{TM} + E_\chi^{TM}}{2} + \frac{1}{2}\sqrt{\left(E_\phi^{TM} - E_\chi^{TM}\right)^2 + 4\hbar^2\Omega_R^2}. \tag{1.27}$$

For the lower polariton branch in a case of small wave-vectors, the additional energy coming from the TE-TM splitting could be written in a basis of $(1, -1)^T$:

$$\Delta E_{LT} = \begin{pmatrix} 0 & \beta_{LT}(k_y - ik_x)^2 \\ \beta_{LT}(k_y + ik_x)^2 & 0 \end{pmatrix}, \tag{1.28}$$

where β_{LT} is an effective constant of the TE-TM splitting.

Physically, it means that at some certain k one can consider an effective in-plane magnetic field which causes "Zeeman" splitting between differently polarized polaritons (we describe the splitting between polarizations as being caused by an effective field). The direction of this field changes as we change the direction of the wave-vector.

1.3 Bose-Einstein condensates

1.3.1 Basics

The story has started in 1925 by the work of Einstein [1]. Basing on the theoretical work of Bose [26], he predicted a new phase transition in a system of noniteracting bosons. Let us consider a ν-dimensional bosonic gas. Its distribution function is:

$$f_B(\mathbf{k}, T, \mu) = \frac{1}{\exp\left(\frac{E(\mathbf{k})-\mu}{k_B T}\right) - 1}. \tag{1.29}$$

Here $E(\mathbf{k})$ is a dispersion of a boson, μ is a chemical potential, T is a temperature and k_B - the Boltzmann constant. It's necessary to notice that 1.29 requires μ to be negative if $E(0) = 0$.

To obtain the total density of particles one should integrate 1.29 over all states in the reciprocal space:

$$n(T, \mu) = \frac{1}{(2\pi)^\nu} \int_0^{+\infty} f_B(\mathbf{k}, T, \mu)\, d^\nu \mathbf{k}. \tag{1.30}$$

Also we can extract the density of particles in the ground state from the integral:

$$n_0(T, \mu) = \lim_{R \to +\infty} \frac{1}{R^\nu} \frac{1}{\exp\left(\frac{-\mu}{k_B T}\right) - 1}. \tag{1.31}$$

Where the size of the system R tends to infinity.

So we have:

$$n(T, \mu) = n_0 + \frac{1}{(2\pi)^\nu} \int f_B(\mathbf{k}, T, \mu)\, d^\nu \mathbf{k}. \tag{1.32}$$

So far as μ is negative and it grows with the number of particles in system, there could be a finite $n_c(T, 0)$ for which the chemical potential turns to zero and it seems to be the maximum particle density in the system:

$$n_c(T, 0) = \lim_{\mu \to 0} \frac{1}{(2\pi)^\nu} \int f_B(\mathbf{k}, T)\, d^\nu \mathbf{k}. \tag{1.33}$$

For the 3D-case this integral converges and could be calculated analytically, while for the cases of $\nu < 3$ it diverges. For a parabolic dispersion of bosons, the calculated integral gives:

$$n_c(T) = \zeta\left(3/2\right)\left(\frac{mk_BT}{2\pi\hbar^2}\right)^{3/2}, \tag{1.34}$$

where $\zeta\left(3/2\right)$ is a Riemann Zeta function. Also, for a fixed density of particles there exists a finite temperature T_c:

$$T_c = \left(\frac{n}{\zeta(3/2)}\right)^{2/3}\frac{h^2}{2\pi mk_B}. \tag{1.35}$$

But what happens in the system when we exceed the n_c or when we cool our system below the T_c? It was proposed that extra particles would go to the lowest level which was not considered in 1.33. Indeed, when the chemical potential goes to zero, there is a divergence in eq. 1.31, so we can say that density of particles condensed in the ground state is:

$$n_0(T) = n(T) - n_c(T). \tag{1.36}$$

This process was called Bose-Einstein condensation of particles. So far as it is easier to manipulate the temperature of the gas than the number of particles, we will discuss generally T_c. For example, for the gas of rubidium atoms the critical temperature has the order of hundreds of nanoKelvins. The Bose-Einstein condensation at such extremely low temperatures was observed for the first time in 1995 by Eric Cornell and Carl Wieman at the University of Colorado at Boulder [2]. For this work, Cornell, Wieman, and Wolfgang Ketterle received the Nobel Prize in Physics in 2001.

For the systems with reduced dimensionality (2D, 1D, 0D) the integral 1.33 diverges and the logic described above is not valid anymore. However, real semiconductor nanostructures which provide 2(1,0)D systems have finite sizes. It means that in this case integral 1.33 converges as well, even for smaller dimensionalities, and the quasi-condensation is possible.

Also, the possibility of the low-temperature phase transition to the superfluid state of the 2D bosonic system was considered by Berezinskii, Kosterlitz and Thouless [27, 28] in the case of interacting bosons. The BKT transition was observed in a 2D gas of Rubidium atoms in 2006 [29].

As it could be seen in 1.35, T_c is inversely proportional to the mass of particles. The semiconductor systems provide numerous bosonic quasiparticles which are much lighter than atoms, what could simplify their condensation conditions. For example, the mass of an exciton is approximatively 10^5 times less than the mass of rubidium atom. Moreover, cavity polaritons could be 10^9 times lighter than atoms, which in theory leads to the room temperature values of T_c. Condensation of polaritons was first demonstrated very recently - in 2006 in the work of Kasprzak et. al. [30]. Fig. 1.8 shows the angle distribution of the cavity emission and its dispersion for different values of non-resonant pumping density. When the number of polaritons

exceeds the value of n_c, the phase transition occurs which provides sharp peaks both in angular distribution and in dispersion.

Also in 2012, the spontaneous coherence in a cold exciton gas was reported [31] what could be the evidence of the exciton condensation.

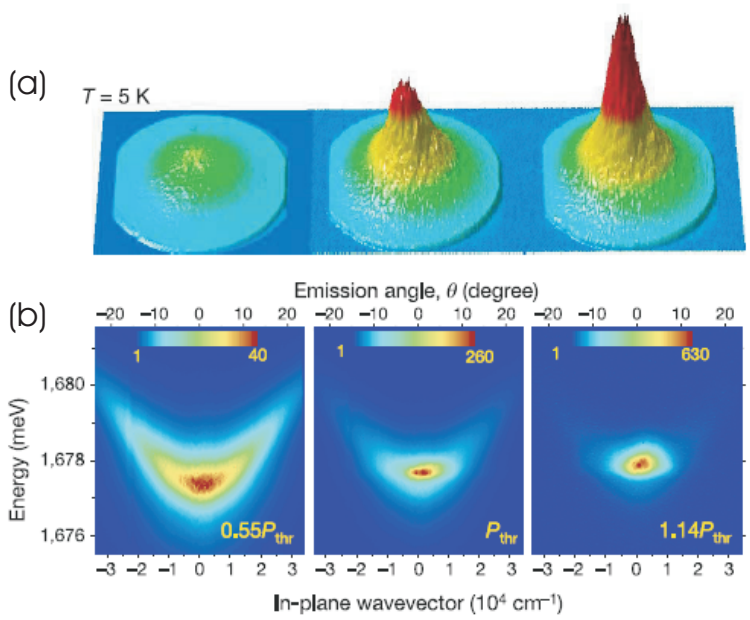

Figure 1.8: The angle distribution of the emission intensity (upper panels) and the dispersion of emission (lower panels) for different values of the density of excitation. Image is taken from [30]

1.3.2 Polariton scattering. Semiclassical Boltzmann equations

In classical statistics, the dynamics of the distribution function (the k-state population n_k) is typically described by the Boltzmann equations:

$$\frac{dn_k}{dt} = \sum_{k'} W_{k'\to k} n_{k'} - n_k \sum_{k'} W_{k\to k'}, \tag{1.37}$$

where the sums go over all other states different from k and $W_{k'\to k''}$ is a total scattering rate between k' and k'' states.

However, in our consideration the quantum properties of particles are very important. Uhlenbeck and Gropper in 1932 proposed a new concept of kinetic equations[32] which takes into account the quantum nature of particles. They are called semi-classical Boltzmann equations and have a form for bosons:

$$\frac{dn_k}{dt} = (1+n_k)\sum_{k'} W_{k'\to k} n_{k'} - n_k \sum_{k'} W_{k\to k'}(1+n_k), \tag{1.38}$$

and for fermions:

$$\frac{dn_k}{dt} = (1-n_k)\sum_{k'} W_{k'\to k} n_{k'} - n_k \sum_{k'} W_{k\to k'}(1-n_k). \tag{1.39}$$

Unlike the atoms, which could live almost infinitely long (there is a certain escape rate for atomic condensates as well, which is even used for their evaporative cooling) and therefore could be easily thermalized at any temperature, excitons and exciton-polaitons have finite lifetime. This is why, to keep the number of particles in the system constant one should have a permanent source of particles. In semiconductor nanostructures it could be obtained by a non-resonant (coherent or not) pumping of the high-energy states. Then, the quasiparticles could thermalize by scattering on phonons, if their lifetime is much longer than the effective times of scattering processes. We can introduce phenomenologically the pumping (P_k) and the lifetime (Γ_k) to 1.38:

$$\frac{dn_k}{dt} = P_k - n_k\Gamma_k + (1+n_k)\sum_{k'} W_{k'\to k} n_{k'} - n_k \sum_{k'} W_{k\to k'}(1+n_k). \tag{1.40}$$

There are few main mechanisms of polariton scattering: scattering on the structural disorder, polariton-phonon scattering and polariton-polariton scattering. In the processes of the first type, the propagating polaritons interact with the structural disorder of the system. However, this interaction can not change the absolute value of the polariton wave-vector and the scattering occurs on an elastic circle in reciprocal space. One could take this scattering into account by considering a cylindrically symmetrical distribution of polaritons, which is the main result of such scattering.

The second scattering mechanism - polariton-phonon scattering - consists of two parts: interaction with 2D optical and 3D acoustic phonons. Optical phonons carry relatively large energies, and they are responsible for the initial polariton relaxation. However, when polaritons relax to the energies below 20 meV (the activation energy of an LO phonon), this scattering process becomes inefficient. After that, polaritons could relax further by the interaction with acoustic phonons. This interaction is mediated by the deformation potential and involves relatively small amounts of energy.

Finally, polariton-polariton scattering can be very a efficient process of polariton thermalization, however, this process conserves the total energy of the polariton system. Scattering rate here depends strongly on polariton density. This process is responsible for an important non-linear optical effect called Optical Parametric Oscillator (OPO) observed first for polaritons by P. Savvidis et. al. in 2000 [33] and described theoretically by Ciuti et. al. in [34].

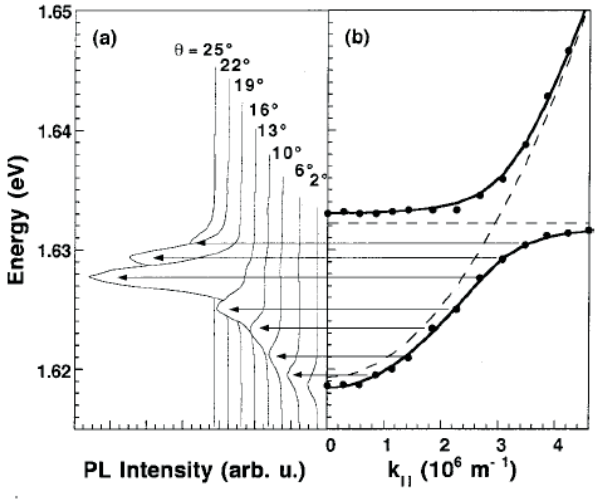

Figure 1.9: Experimental observation of the bottleneck effect. The highest intensity of emission is observed from the energies which correspond to the bottleneck region. Image is taken from [37]

As it was said, in order to obtain the condensation of polaritons in the ground state, polaritons should relax faster than they decay. However, due to the fact that most scattering goes via the excitonic part of the polariton and that polaritonic dispersion becomes very steep at small k-vectors, there is an effective deceleration of relaxation processes at the region called "bottleneck" [35, 36, 37]. Experimentally it can be observed by an enhanced intensity of cavity photoluminescence at certain k (fig. 1.9). In order to overcome the bottleneck effect, high densities of pumping or cavities with longer lifetimes and positive detuning between photonic and excitonic fractions are used.

The general behavior of polaritonic system is schematically illustrated on fig.1.10.

1.3.3 Bogoliubov theory and Gross-Pitaevskii equations

The ideal BEC consists of non-interacting bosons. However, real bosons are weakly-interacting. The Hamiltonian for the system of uniformely distributed weakly-interacting bosons could be written in second quantization terms as:

$$\hat{H} = \sum_k \frac{\hbar^2 k^2}{2m} \hat{a}_k^\dagger \hat{a}_k + \frac{\alpha}{2L^3} \sum_{k_1,k_2,q} \hat{a}_{k_1+q}^\dagger \hat{a}_{k_2-q}^\dagger \hat{a}_{k_1} \hat{a}_{k_2}, \tag{1.41}$$

where $\hat{a}_k, \hat{a}_k^\dagger$ are annihilation and creation operators for a particle with k wave-vector, α is an interaction constant and L is a size of a system.

We can separate the ground state and excited states in the Hamiltonian:

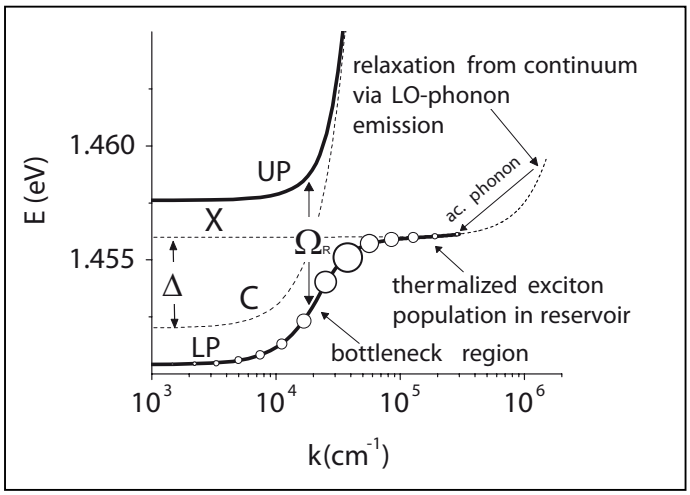

Figure 1.10: Scheme of the pumping and scattering processes for cavity polaritons. Image is taken from [38]

$$\hat{H} = \frac{\alpha}{2L^3}\hat{a}_0^\dagger\hat{a}_0^\dagger\hat{a}_0\hat{a}_0 + \sum_k \frac{\hbar^2k^2}{2m}\hat{a}_k^\dagger\hat{a}_k + \frac{\alpha}{2L^3}\sum_{k\neq 0}\left(4\hat{a}_0^\dagger\hat{a}_k^\dagger\hat{a}_0\hat{a}_k + \hat{a}_k^\dagger\hat{a}_{-k}^\dagger\hat{a}_0\hat{a}_0 + \hat{a}_0^\dagger\hat{a}_0^\dagger\hat{a}_k\hat{a}_{-k}\right). \tag{1.42}$$

Assuming that the total number of particles N is conserved and large, we can write the normalization relation $N = \hat{a}_0^\dagger\hat{a}_0 + \sum_{k\neq 0}\hat{a}_k^\dagger\hat{a}_k$. Finally, we get:

$$\hat{H} = \frac{1}{2}\alpha n N + \sum_k \frac{\hbar^2k^2}{2m}\hat{a}_k^\dagger\hat{a}_k + \frac{1}{2}\alpha n\sum_{k\neq 0}\left(2\hat{a}_k^\dagger\hat{a}_k + \hat{a}_k^\dagger\hat{a}_{-k}^\dagger + \hat{a}_k\hat{a}_{-k}\right). \tag{1.43}$$

This Hamiltonian could be diagonalized by Bogoliubov linear transformations[39]:

$$\begin{aligned}\hat{a}_k &= u_k\hat{b}_k + v_{-k}\hat{b}_{-k}^\dagger,\\ \hat{a}_k^\dagger &= u_k\hat{b}_k^\dagger + v_{-k}\hat{b}_{-k}.\end{aligned} \tag{1.44}$$

Two parameters u_k, v_{-k} can be written as:

$$u_k, v_{-k} = \pm\left(\frac{\hbar^2k^2/2m + \alpha n}{2\varepsilon(k)} \pm \frac{1}{2}\right)^{1/2}, \tag{1.45}$$

where the dispersion of excitation spectrum is:

$$\varepsilon(k) = \pm\left[\frac{\alpha n}{m}\hbar^2k^2 + \left(\frac{\hbar^2k^2}{2m}\right)^2\right]^{1/2}. \tag{1.46}$$

As one can see, there are two dispersion branches - with positive and negative values of energy. The dispersion is plotted on fig. 1.11.

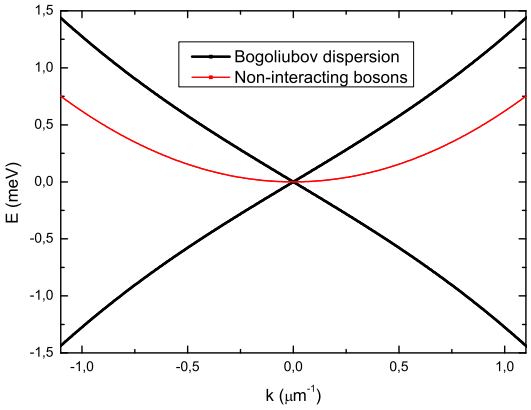

Figure 1.11: Black line shows positive and negative branches of Bogoliubov dispersion, when red line is the dispersion for non-interacting particles.

In new basis the Hamiltonian 1.43 has a simple form:

$$\hat{H} = E_0 + \sum_{k\neq 0} \varepsilon(k)\hat{b}_k^\dagger \hat{b}_k, \tag{1.47}$$

which is a Hamiltonian for a system of non-interacting quasi-particles, so-called *bogolons*, which could be considered as collective excitations. By this transformation, the ground state of bosons at zero temperature turned to a vacuum state for bogolons. The energy of the ground state E_0 in the lowest order calculations is equal to $\frac{1}{2}\alpha n N$. Bogoliubov excitation spectrum firstly was observed in 1999 in the work [40] on atomic BEC.

The dispersion law 1.46 for bogolons with small wave-vectors is linear by k (sound-like, fig.1.11). By this we can derive the effective sound velocity in the condensate:

$$c = \sqrt{\frac{\alpha n}{m}}. \tag{1.48}$$

In opposite case of large wave-vectors the dispersion becomes parabolic and has a free-particle form.

Interaction constant α for excitons and cavity polaritons is coming mainly from exciton-exciton exchange interaction. It is positive, which means repulsive interaction between particles, and can be written in a form [41]:

$$\alpha = 6E_b \mathrm{X}_C^2 a_B^2. \tag{1.49}$$

Here E_b is an exciton binding energy, X_C is the excitonic fraction of polariton and a_B is a Bohr radius.

As it was said, Bogoliubov theory considered an infinite homogeneous Bose gas. In 1961 Gross[42] and Pitaevskii[43] independently have extended the Bogoliubov

theory to the case of nonuniform condensate. The main idea was to describe by a classical field not only the ground state, but all other states in the system:

$$\psi(r,t) = \psi_0(r)e^{-i\mu t} + \sum_{k\neq 0} \psi_k e^{-i[k\cdot r-(\mu\pm\omega)t]}. \tag{1.50}$$

Putting 1.50 to the Heisenberg equation of motion one will get:

$$i\hbar\frac{d}{dt}\psi(r,t) = \left[-\frac{\hbar}{2m}\nabla^2 + \alpha|\psi(r,t)|^2\right]\psi(r,t). \tag{1.51}$$

This equation is called Gross-Pitaevskii equation and it is widely used to describe inhomogeneous coherent Bose gases. However, 1.53 does not take into account the decoherence and spontaneous scattering between states.

Finally, since we consider quasiparticles with finite lifetime τ, we can introduce phenomenologically the corresponding term to 1.53. Also, often the pumping term P is introduced into the equation which simulates the coherent quasi-resonant pumping. The final Gross-Pitaevskii equation could be written as:

$$i\hbar\frac{d}{dt}\psi(r,t) = \left[-\frac{\hbar}{2m}\nabla^2 + \alpha|\psi(r,t)|^2 - \frac{i\hbar}{2\tau}\right]\psi(r,t) + P. \tag{1.52}$$

Polaritons are formed by excitons and photons which total angular momentum projection on $\mathbf{Z}$ could take two values: ± 1. The polariton-polariton interaction is coming from their excitonic fractions and it was found to be spin-anisotropic[44, 45], notably co-polarized excitons interact strongly, and their interaction is repulsive, while polaritons with opposite spins are slightly mutually attracted. Because of that, it is reasonable to consider a two-component *spinor* polariton condensate. Let's designate $\sigma^{\pm}$ polarized states as the $\psi_{\pm}$ functions. We will discuss the nature of exciton-exciton interaction later, however, we will introduce two interaction constants: α_1 for a triplet state and α_2 for a singlet state. Taking into account TE-TM splitting (eq. 1.28) we can rewrite the Gross-Pitaevskii equation in a spinor form:

$$i\hbar\frac{\partial\psi_{\pm}}{\partial t} = -\frac{\hbar^2}{2m^*}\Delta\psi_{\pm} + \alpha_1|\psi_{\pm}|^2\psi_{\pm} + \alpha_2|\psi_{\mp}|^2\psi_{\pm} + \beta_{LT}(\partial_y \mp i\partial_x)^2\psi_{\mp} - \frac{i\hbar}{2\tau}\psi_{\pm} + P_{\pm}. \tag{1.53}$$

This is the most general form of the Gross-Pitaevskii equation that will be used throughout this thesis.

Bibliography

[1] A. Einstein, Quantentheorie des einatomigen idealen Gases, *Zweite Abhandlung, Sitzber Klg. Preuss. Akad. Wiss.* **1**, 3 (1925). (Cited on pages 1 and 14.)

[2] M. H. Anderson, J. R. Ensher, M. R. Matthews, C. E. Wieman, and E. A. Cornell, Observation of Bose-Einstein Condensation in a Dilute Atomic Vapor, *Science* **269**, 5221 (1995). (Cited on pages 1 and 15.)

[3] W. Friedrich, P. Knipping, M. Laue, Interferenz-Erscheinungen bei Rontgenstrahlen (Interference appearancesin X-rays), Proceedings of the Bavarian Academy of Sciences, *Sber. Bayer. Akad. Wiss.* (1912); reprinted in: *Annalen der Physik* **41** (1913). (Cited on page 1.)

[4] W.L. Bragg, The specular reflection of X-rays, *Nature* **90**, 410 (1912) (Cited on page 1.)

[5] W.L. Bragg, The diffraction of short electromagnetic waves by a crystal, *Proc. Cambridge Philos. Soc.* **17**, 43-57 (1913) (Cited on page 1.)

[6] W.L. Bragg, The structure of some crystals as indicated by their diffraction of X-rays, *Proc. Roy. Soc. Lond.* **89**, 248-277 (1913) (Cited on page 1.)

[7] Peter Y. Yu, Manuel Cardona, Fundamentals of Semiconductors, Springer, (2002) (Cited on pages 3 and 5.)

[8] F. Meier, B.P. Zakharchenya (eds.), Optical Orientation Modern Problems in Condensed Matter Science, North-Holland, Amsterdam, (1984) (Cited on pages 4 and 7.)

[9] N. W. Ashcroft and N. David Mermin, Solid State Physics, Harcourt, Orlando (1976) (Cited on page 5.)

[10] S. I. Pekar, The theory of electromagnetic waves in a crystal in which excitons are produced, *Zh. Eksp. Teor. Fiz.* **33**, 1022 (1957) (Cited on page 5.)

[11] J. Hopfield, Theory of the contribution of excitons to the complex dielectric constants of crystals, *Phys. Rev.* **112**, 1555 (1958) (Cited on page 5.)

[12] V. Agranovich, Dispersion of electromagnetic waves in crystals, *JEPT Lett.* **37**, 430 (1959) (Cited on page 5.)

[13] M. Dyakonov, Spin physics in semiconductors, Springer, (2008) (Cited on pages 6 and 7.)

[14] G. Dresselhaus, Spin-Orbit Coupling Effects in Zinc Blende Structures, *Phys. Rev.* **100**, 580 (1955) (Cited on page 7.)

[15] Y. Bychkov and E. I. Rashba, Oscillatory effects and the magnetic susceptibility of carriers in inversion layers, *J. Phys. C* **17**, 6039 (1984) (Cited on page 7.)

[16] A.N. Titkov, V.I. Safarov, G. Lampel, in *Proc. ICPS* **14**, Edinburgh (1978) (Cited on page 7.)

[17] Denis V. Bulaev and Daniel Loss, Spin Relaxation and Decoherence of Holes in Quantum Dots, *Phys. Rev. Lett.* **95**, 076805 (2005) (Cited on page 7.)

[18] O. Kyriienko, E. B. Magnusson, and I. A. Shelykh, Spin dynamics of cold exciton condensates, *Phys. Rev. B* **86**, 115324 (2012). (Cited on page 7.)

[19] E. I. Rashba and E. Ya. Sherman, Spin-Orbital Band Splitting in Symmetric Quantum Wells, *Phys. Lett. A* **129**, 35 (1988) (Cited on page 7.)

[20] M. Z. Maialle, E. A. de Andrada e Silva, and L. J. Sham, Exciton spin dynamics in quantum wells, *Phys. Rev. B* **47**, 15776 - 15788 (1993) (Cited on page 7.)

[21] A.I. Ekimov and A.A. Onushchenko, Quantum size effect in three-dimensional microscopic semiconductor crystals, *JETP Lett.* **34**, 345 (1981) (Cited on page 8.)

[22] Nanostructure optics, St-Petersburg, Nedra (2005) (Cited on page 8.)

[23] D. Lacombe, A. Ponchet, S. Frechengues, V. Drouot, N. Bertru, B. Lambert, and A. Le Corre, Formation of low-index facets in $Ga_0.2In_0.8As$ and InAs islands on a InP(113)B substrate, *Appl. Phys. Lett.* **74**, 1680 (1999) (Cited on page 8.)

[24] A. Kavokin and G. Malpuech, Cavity Polaritons, Elsevier, (2003). (Cited on pages 10 and 12.)

[25] C. Weisbuch, M. Nishioka, A. Ishikawa, and Y. Arakawa , Observation of the coupled exciton-photon mode splitting in a semiconductor quantum microcavity, *Phys. Rev. Lett.* **69**, 3314 (1992) (Cited on page 11.)

[26] S. N. Bose, Plancks Gesetz Lichtquantenhypothese, *Z. Phys* **26**, 178, (1924). (Cited on page 14.)

[27] V. L. Berezinskii, Violation of long range order in one-dimensional and two-dimensional systems with a continuous symmetry group, *Sov. Phys. JETP* **32**, 493 (1971). (Cited on page 15.)

[28] J. M. Kosterlitz, D. J. Thouless, Ordering, metastability and phase transitions in two-dimensional systems, *Journal of Physics C: Solid State Physics* **6**: 1181 (1973). (Cited on page 15.)

[29] Z. Hadzibabic, P. Krüger, M. Cheneau, B. Battelier and J. Dalibard, Berezinskii-Kosterlitz-Thouless crossover in a trapped atomic gas, *Nature* **441**, 1118 (2006). (Cited on page 15.)

[30] J. Kasprzak, M. Richard, S. Kundermann, A. Baas, P. Jeambrun, J. M. J. Keeling, F. M. Marchetti, M. H. Szymaska, R. André, J. L. Staehli, V. Savona, P. B. Littlewood, B. Deveaud, and Le Si Dang, Bose-Einstein condensation of exciton polaritons, *Nature* **443**, 409 (2006). (Cited on pages 15 and 16.)

[31] A.A. High and J. R. Leonard and A. T. Hammack and M. M. Fogler and L. V. Butov and A. V. Kavokin and K. L. Campman and A. C. Gossard, Spontaneous coherence in a cold exciton gas, *Nature* **483**, 584-588 (2012). (Cited on page 16.)

[32] G. E. Uhlenbeck, and L. Gropper, The equation of state of a non-ideal Einstein-Bose or Fermi-Dirac gas, *Phys. Rev.* **1**, 79 (1932). (Cited on page 16.)

[33] P. G. Savvidis, J. J. Baumberg, R. M. Stevenson, M. S. Skolnick, D. M. Whittaker, and J. S. Roberts, Angle-resonant stimulated polariton amplifier *Phys. Rev. Lett.* **84**, 1547 (2000). (Cited on page 17.)

[34] C. Ciuti, P. Schwendimann, B. Deveaud, and A. Quattropani, Theory of the angle-resonant polariton amplifier, *Phys. Rev. B* **62**, 4825(R)-4828(R) (2000). (Cited on page 17.)

[35] F. Tassone, C. Piermarocchia, V. Savona, A. Quattropani, and P. Schwendimann, Bottleneck effects in the relaxation and photoluminescence of microcavity polaritons, *Phys. Rev. B* **56**, 7554 (1997). (Cited on page 18.)

[36] A.I. Tartakovskii, M. Emam-Ismail, R. M. Stevenson, M. S. Skolnick, V. N. Astratov, D. M. Whittaker, J. J. Baumberg, and J. S. Roberts, Relaxation bottleneck and its suppression in semiconductor microcavities, *Phys. Rev. B* **62**, 2283(R)(2000). (Cited on page 18.)

[37] M. Müller, J. Markus, and A. Bleuse, Dynamics of the cavity polariton in CdTe-based semiconductor microcavities: Evidence for a relaxation edge, *Phys. Rev. B* **62** 16886 (2000). (Cited on page 18.)

[38] A. I. Tartakovskii, D. N. Krizhanovskii, G. Malpuech, M. Emam-Ismail, A. V. Chernenko, A. V. Kavokin, V. D. Kulakovskii, M. S. Skolnick, and J. S. Roberts, Giant enhancement of polariton relaxation in semiconductor microcavities by polariton-free carrier interaction: experimental evidence and theory, *Phys. Rev. B* **67**, 165302 (2003). (Cited on page 19.)

[39] N. N. Bogoliubov, On the theory of superfluidity, *J. Phys. USSR* **11**, 23 (1947). (Cited on page 19.)

[40] D. M. Stamper-Kurn, A. P. Chikkatur, A. Gorlitz, S. Inouye, S. Gupta, D. E. Pritchard, and W. Ketterle, Excitation of phonons in a bose-einstein condensate by light scatter- ing, *Phys. Rev. Lett.* **83**, 2876 (1999) (Cited on page 20.)

[41] F. Tassone, and Y. Yamamoto, Exciton-exciton scattering dynamics in a semiconductor microcavity and stimulated scattering into polaritons, *Phys. Rev. B* **59**, 10830 (1999). (Cited on page 20.)

[42] E. P. Gross, Structure of a quantized vortex in boson systems, *Novo Cimento* **20**, 454 (1961). (Cited on page 20.)

[43] L. P. Pitaevskii, Vortex Lines in an Imperfect Bose Gas, *Soviet Physics JETP* **13**, 451 (1961). (Cited on page 20.)

[44] C. Ciuti, V. Savona, C. Piermarocchi, A. Quattropani and P. Schwendimann, Role of the exchange of carriers in elastic exciton-exciton scattering in quantum wells, *Phys. Rev. B* **58**, 7926 (1998). (Cited on page 21.)

[45] M. Combescot and O. Betbeder-Matibet, Faraday rotation in photoexcited semiconductors: A composite-exciton many-body effect, *Phys. Rev. B* **74**, 125316 (2006). (Cited on page 21.)

Chapter 2

Coherent interactions between phonons and exciton or exciton-polariton condensates

Contents

The interactions between different quasiparticles in solids often lead to interesting effects and sometimes, in the case of strong interaction, could provide quasiparticles of a new type. For example, exciton-polaritons or cavity polaritons appear in the microcavities [1] as the elementary excitations formed by the coupling of excitons and photons. However, in the solids there is another type of collective excitations which is related to collective oscillations of the crystal lattice and which is usually described in terms of quasiparticles called *phonons*. Phonons can interact both with photons and with excitons.

The interaction between lattice oscillations and light has been studied for a long time, and it would be fare to say, that history of its investigation has its beginning in the works of Rayleigh[2, 3]. In spite of the fact, that in these works Rayleigh considered the elastic scattering of light by disordered media (gas) and not by a crystal, it was the first successful attempt to describe the scattering of electromagnetic waves by atoms.

Later, in the beginning of XX century the inelastic scattering was described and observed in two independent works. First - done by Raman - was performed in liquids[4]. The author has shown the appearance of additional spectral lines in the scattered light, which come from the vibrational and rotational excitations of molecules. At the same time, Landsberg and Mandelstam worked on the inelastic scattering by solids. Predicted theoretically by Mandelstam and Brillouin[5], this effect was finally observed and described in the work[6]. However, the effect occurred to be much stronger than it was expected. It has indicated the fundamental difference between solids and liquids, and revealed the necessity of individual theory of oscillations in solids.

If the frequency of the electro-magnetic wave, propagating in the crystal, is close to the exciton frequency, it is necessary to speak about exciton-polariton and consider the excitonic part as well. Carriers, composing the exciton, could effectively interact with lattice oscillations. Moreover, polaritons demonstrate efficient energy relaxation because of their excitonic part.

Because the exciton-phonon interaction is weak relatively to exciton-photon interaction, in general, it causes only Brillouin scattering. However, it was predicted by A. L. Ivanov et al.[7], that in a case of strong electro-magnetic wave, some sort of strong coupling between exciton-polaritons and phonons could occur, giving rise to new quasi-particle - *phonoriton*. Several experimental works have shown indirect evidence of this effect[8, 9], but because in the bulk both exciton-photon and exciton-phonon interactions are not so strong, directly the effect still was not observed.

The situation gets better with the reducing of the dimensionality. It was recently shown[10] that 2D cavity polaritons could demonstrate a significant reconstruction of their dispersion when interacting with a strong 2D surface acoustic wave. The theory of interaction between the 2D polaritons and a 2D acoustic wave was developed by A. L. Ivanov[11]. The phonon field has been treated as an external classical field, and its reduced dimensionality was obtained due to strong coherent external 2D pumping. However, it could be reduced also by embedding an acoustic cavity or an acoustic waveguide inside the optical cavity, like in [12]

In our work[13] we consider the interaction between a condensate of quantum well excitons or cavity exciton-polaritons and a coherent phonon field, possessing the same dimensionality. We develop a theory of interaction between phonons and bogolons (elementary excitations of the condensate) and we show that at some conditions the strong coupling regime could be obtained, resulting in a strong modification of the dispersion, and even in the appearance of a "roton instability" region.

This chapter will be organized as follows. In the first part I will describe the basics of phonons and of electron (exciton)-phonon interaction. Further, I will discuss the recent theoretical and experimental works performed on the strong acousto-polariton interaction in the systems with reduced dimensionality. And finally, I will explain the main idea of our work, introduce our theoretical model and describe the results that we have obtained.

2.1 Basics of exciton-phonon interaction

2.1.1 Phonons

Let us consider an infinite 1D lattice of equal atoms mutually bound by elastic force described by a coefficient C. One can write the following equation to describe the motion of n-th atom:

$$m\frac{\mathrm{d}^2u_n}{\mathrm{d}t^2} = -2Cu_n + C(u_{n+1} + u_{n-1}), \tag{2.1}$$

where u_n is the n-th atoms coordinate. This is a wave equation, so we can make a transformation from real coordinates u_n, which describe the position of each atom, to normal coordinates U_q, which describe different waves with different wavevectors:

$$u_n = \sum_q U_q e^{iqnd}. \tag{2.2}$$

Then, the wave equation will read:

$$m\frac{\mathrm{d}^2\,U_q}{\mathrm{d}\,t^2} = 2C(\cos\,qd - 1)U_q. \tag{2.3}$$

The solutions of this equation can be easily found:

$$U_q = A_q e^{i\omega_q t}, \qquad \omega_q = \sqrt{\frac{2C}{m}(1 - \cos qd)}. \tag{2.4}$$

So, the normal coordinates describe different vibrational modes, whose frequency obeys its own dispersion law. By this approach, one can treat these oscillations as a set of quasiparticles. This concept was first introduced by Igor Tamm in 1930 and the quasiparticles were called phonons by Yakov Frenkel.

Now, if we consider that 1D lattice is composed by 2 different types of atoms with masses $m_{1,2}$ with the spacing between two equal atoms a, we will obtain two different dispersion branches:

$$\omega_\pm^2 = C\left(\frac{1}{m_1} + \frac{1}{m_2}\right) \pm C\sqrt{\left(\frac{1}{m_1} + \frac{1}{m_2}\right)^2 - \frac{4\sin^2(qa/2)}{m_1 m_2}}. \tag{2.5}$$

For small values of wave-vector q we can write:

$$\omega_- = \sqrt{\frac{C}{2(m_1 + m_2)}}qa, \qquad \omega_+ = \sqrt{\frac{2C(m_1 + m_2)}{m_1 m_2}}. \tag{2.6}$$

The first dispersion branch is linear by q and the quasiparticles corresponding to this branch are called acoustic phonons. The second curve is nonzero for $q = 0$ and is called the dispersion branch of optical phonons. The schematic image of the two dispersion branches is shown at 2.1. Physically it means, that in the solids with an elementary cell containing more than one atom, a new type of phonons appears.

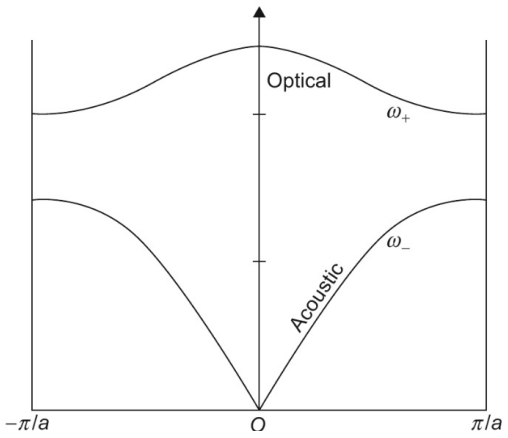

Figure 2.1: Optical and acoustic phonon dispersion branches. Image is taken from [14]

Moreover, these phonons could carry significant amounts of energy even with small wave-vectors.

Mandelstam and Landsberg in their experiment expected to observe the scattering of light by acoustic phonons, which should result in additional spectral lines close to the general line. However, they surprisingly obtained satellite lines situated quite far from the main one, which has been interpreted as an experimental evidence of the interaction with the optical phonons.

2.1.2 Exciton-phonon scattering

The common life cycle of an exciton or an exciton-polariton starts with its optical or electrical generation (electrons and holes are formed, and then they bind into excitons) at high-energy states, followed by its energy relaxation and decay. If the energy of hot excitons is high enough, the initial scattering process is mediated mainly by optical phonons. In each scattering act, quite large amounts of energy are exchanged - up to tens meV. The scattering is driven by so called Frohlich interaction, by the name of Herbert Frohlich - German-Brittish physicist, who described theoretically[15] the interaction between electrons and optical phonons in solids.

In the approximation of long wavelength optical phonons, one can consider the constant lattice oscillation frequency ω_{LO}. By this the energy of interaction between an electron and LO phonon with wave-vector $\mathbf{q}$ [15]:

$$E^{\mathbf{q}}_{e-LO} \sim \frac{4\pi e^2}{a^3 k\sqrt{2N}} \sin(\omega_{LO} t + \mathbf{kr}), \tag{2.7}$$

where the sum goes over all possible phonon states, e is a charge of an electron, a is a size of an unit cell and N is a number of unit cells in a crystal. The matrix element for the scattering of an electron from **k**-state to **k'**-state reads:

$$M_{kk'q} = \frac{2\pi e^2}{a^3 q\sqrt{2N}}\sqrt{\frac{\hbar([0,1]+n_q)}{2\mu\omega_{LO}}}. \tag{2.8}$$

Here n_q is a number of q-phonons and $\mu = \frac{m_+ m_-}{m_+ + m_-}$ - the reduced mass of the unit cell, composed of positive and negative ions with masses m_+ and m_-. $[0,1]$ corresponds to the emission or the absorption of the phonon.

For a 2D exciton confined in a quantum well with S and L dimensions, the corresponding matrix element would be:

$$M^{LO}_{kk'q} = \frac{-e}{q}\sqrt{\frac{\hbar\omega_{LO}([0,1]+n_q)}{2SL}\left(\frac{1}{\varepsilon_\infty}-\frac{1}{\varepsilon_s}\right)} = \frac{M^{LO}_0}{q\sqrt{SL}}. \tag{2.9}$$

Here, $\varepsilon_{\infty,s}$ are dielectric constants for high and low frequencies.

However, it was shown [16, 17], that in a QW one should consider also "slab" or confined LO modes. The wave-vector of phonon becomes quantized in z-direction and it takes values $q_z^\nu = \nu\pi/L$ where ν is an integer. However, the overlap integral between phonon and exciton wave-function quickly vanishes with ν. Considering only first confined mode for LO-phonon, one can write [17, 18]:

$$M^{LO}_{kk'q} = \frac{M^{LO}_0}{\sqrt{|q_{||}|^2 + (\pi/L)^2}\sqrt{SL}}. \tag{2.10}$$

When the exciton relaxes to the lower energy states, its energy is not sufficient any more to excite optical phonons and the scattering on long wavelength acoustic phonons comes to the fore. Longitudinal acoustic oscillations of the crystal lattice effectively modulate the size of its unit cells, what in its turn changes the energy of electronic bands. The energy shift is linear by the phonon amplitude and is called deformation potential. The matrix element of electron (hole)-acoustic phonon interaction reads [18]:

$$M^{LA}_{kk'q} = D_{e,h}\sqrt{\frac{\hbar q([0,1]+n_q)}{2\rho c_s V}}I(k,k',q). \tag{2.11}$$

Here $D_{e,h}$ is a coefficient of the deformation potential for the electrons (holes), ρ is the density, c_s is the speed of sound, V is the volume of crystal (normalization volume) and $I(k,k',q)$ is the overlap integral between the wavefunctions of the electrons (holes) and the phonons.

In a case of 2D carriers coupled to 3D phonon gas, the wave-vector conservation law applies to in-plane wave-vectors only. The value of q_z - z-component of emitted or absorpted phonons wave-vector could take any value, while the in-plane $q_{||}$ is defined by initial and final states of the carrier, by the momentum conservation law.

Besides the interaction with LA-phonons in some materials there is an effective mechanism of interaction with TA-phonons, mediated by piezoelectricity. The matrix element of this interaction is proportional to $q^{3/2}$. Piezoelectric phonons could be considered as an induced electric field inside the semiconductor, they strongly

affect the motion of charged carriers but they do not affect the width of the band gap, and their influence on the excitonic behavior is not so strong. That is why in my studies I was interested only in the LA-phonons.

2.1.3 Phonoritons

The first attempt to describe strong coupling regime between acoustic oscillations and an electromagnetic wave propagating in solid was done by A. L. Ivanov and L. V. Keldysh in 1982 [7, 19]. Authors considered a strong electromagnetic wave with a frequency close to the exciton resonant frequency. If the number of polaritons in the system is high enough, the scattering processes on phonons become much faster than polariton decay. Because the phonon dispersion is linear, the interaction couples the initial state **k** with two final states **k'**, **k"**: anti-Stokes (**k'** = **k**+**q**) which is followed by an absorption of a phonon and Stokes (**k"** = **k** + **q'**),followed by an emission of a phonon. In the work [7], the authors have analyzed only the case of anti-Stokes scattering. They have described the modification of the dispersion in the regions where the phonon and polariton dispersion curves cross each other (fig. 2.2).

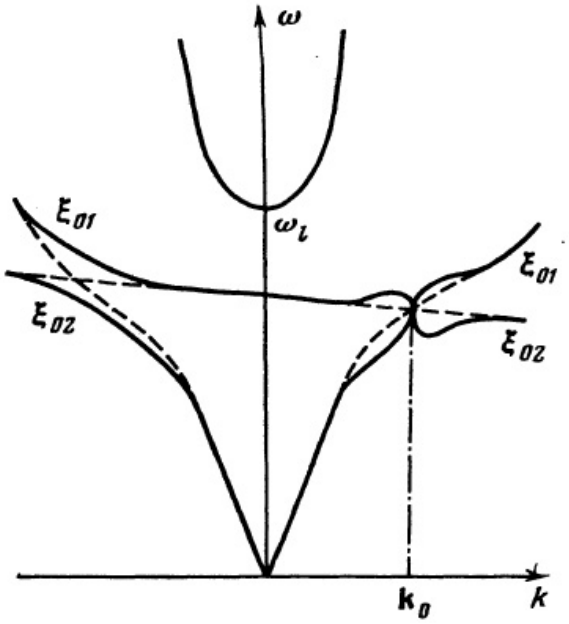

Figure 2.2: Dashed lines - pure polaritonic and acoustic dispersions. Solid lines - the renormalized phonoriton dispersion. Image is taken from [7]

In terms of second quantization operators a_k, b_k, c_k for excitons, photons and phonons respectively, the Hamiltonian reads:

$$H = \sum_k \hbar \left[\omega_k^{ex} a_k^\dagger a_k + \omega_k b_k^\dagger b_k + i\frac{\Omega_c}{2}(a_k^\dagger b_k - a_k b_k^\dagger)\right] + \sum_q \hbar\Omega_q c_q^\dagger c_q + \sum_{i,j,k,q}\left[iM'_{i,j}(k-q)a_k^\dagger a_q(c_{k-q} + c_{q-k}^\dagger) + c.c.\right]. \tag{2.12}$$

Here ω_k is the energy of the photon: $\omega_k = c|k|/\hbar$, and ω_k^{ex} is the energy of the exciton with momentum k:$\omega_k^{ex} = \omega_0^{ex} + \hbar k^2/2m_e x$ where $m_e x$ is the effective mass of exciton, Ω_p is the phonon frequency. The interaction between oscillators is described in the following terms: Ω_c denotes the photon-exciton interaction and $M(k-q)$ is the matrix element of exciton-phonon interaction.

Now, if we write the exciton-photon part in the polariton basis, we can obtain the standard polariton dispersion $\omega(k)$. Considering strong pumping close to the exciton resonance at k_0, we can take into account the scattering into two final states. This renormalizes the polariton dispersion:

$$\omega_{1,2}^{\pm}(k) = \tfrac{1}{2}[\omega(k) \pm \Omega_{k_0-k} - \omega_{k_0}] + (-)\tfrac{1}{2}\sqrt{[\omega_{1,2}(k) \mp \Omega_{k_0-k} - \omega_{k_0}]^2 \pm \Psi_{ex}(k)Q^2}, \tag{2.13}$$

$$Q = \sqrt{VN_0}M(k-k_0). \tag{2.14}$$

Here $\pm$ states anti-Stokes $(-)$ and Stokes $(+)$ scattering processes, $\Psi_{ex}(k)$ - the excitonic fraction of the polariton, V is the volume and N_0 is the number of polaritons. Thanks to the exciton-phonon interaction, two new gaps appear. They are proportional to the square root of the intensity of the pumping laser and to the strength of the exiton-phonon interaction. However, because the interaction is quite weak, the direct observation of the gaps in spectra seems to be very complicated. However, there were reports on indirect observation of phonoritons [8, 9], obtained by polariton-LO phonon anti-Stokes scattering. In the first work [8], the authors analyzed the transmission spectra of CdS under strong external pumping. They found strong increasing of the transmission spectra at the position where the phonoriton gap should occur (fig.2.3). Also Brodin, Kadan, and Matskosov'[9] observed a dip in photoluminescence spectra of HgI_2.

Finally, the LA-phonoriton was observed in a Cu_2O bulk crystal in the presence of a coherent orthoexcitonic polariton by stimulated two-photon emission spectroscopy[20].

2.2 Exciton-phonon interaction in 2D

Lifetime of cavity polaritons is significantly larger than that of bulk polaritons. This fact allows to obtain large amount of polaritons even at moderate pump intensities, which in its turn simplifies, in theory, the production of strong coupling between phonons and polaritons. However, 2D polaritons couple with a 3D phonon bath, which produces nothing but incoherent scattering of polaritons. To obtain renormalization of polaritonic dispersion, one should reduce the dimensionality of phonons as

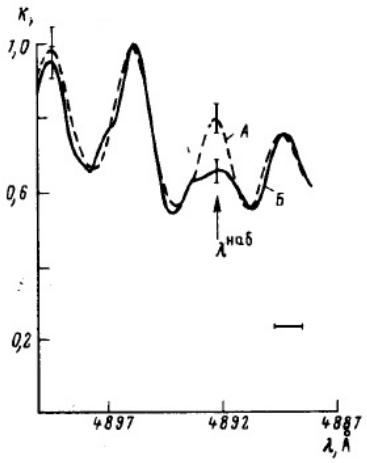

Figure 2.3: The transmission coefficient K of CdS vs wavelength λ with (solid line) and without (dashed line) strong external pumping. Image is taken from [8]

well. There are two ways for this: either confine acoustic oscillations in a 2D acoustic cavity or waveguide, or consider externally pumped strong *surface acoustic wave* (SAW), which could be considered as a macroscopically occupied coherent phonon state. This section is devoted to the discussion of different works on the subject of coupling between 2D excitons or cavity polaritons and 2D phonons.

2.2.1 SAW

Despite the fact that the surface waves in liquids and even in solids (seismic waves) have been common throughout history, it was Rayleigh, who first described in 1885 the surface acoustic waves in elastic solids [21]. He developed the theory, describing the oscillating motion of surface atoms. However, the massive experimental studies of solid SAW have started in the 60s by the work of White and Voltmer [22], who invented the thin-film interdigital transducer (IDT). IDT consists of two interlocking comb-shaped metallic coatings applied to the surface of a piezoelectric material (fig. 2.4). Applying voltage to the thin film, one can create and manipulate the surface acoustic wave, and vice versa - IDT could detect propagating SAW.

Such structure could be used for analogue electrical filters, correlators, transformers, etc. Presently, the SAWs are widely used in radio- and telecommunications, and in microelectronics. Also, SAWs could be implemented in sensors of numerous types.

And of course, surface acoustic waves are good objects to study the acousto-optical interaction in semiconductor nanostructures, as far as they could provide micrometer-scale periodical potential. For example, in 1997 Rocke et al. proposed [24] to use the SAW to dissociate the photogenerated excitons and by this, to separate holes and electrons in space. They observed strong increasing of radiative

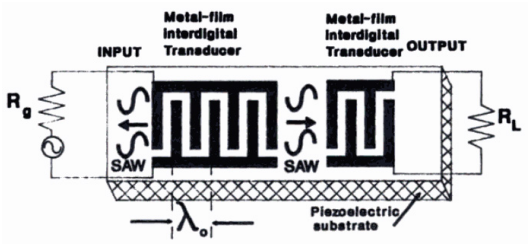

Figure 2.4: Schematic representation of an IDT. Image is taken from [23]

lifetime of the system as well as spatial transportation of carriers.

With the rise of the interest to the optical confinement, numerous works were done on acoustically induced optical and polariton superlattices. It has begun with the studies of the waveguided light diffraction on the surface acoustic waves [25, 26]. Later in 2005, M. M. de Lima et al. demonstrated a formation of an optical superlattice driven by a surface acoustic wave [27] in optical microcavities. The SAW periodically modulates the dielectric constant in the medium, which folds the optical in-plane dispersion at the Bragg vector. The authors have shown the splitting of the dip in the cavity reflection spectra into two dips (fig. 2.5)

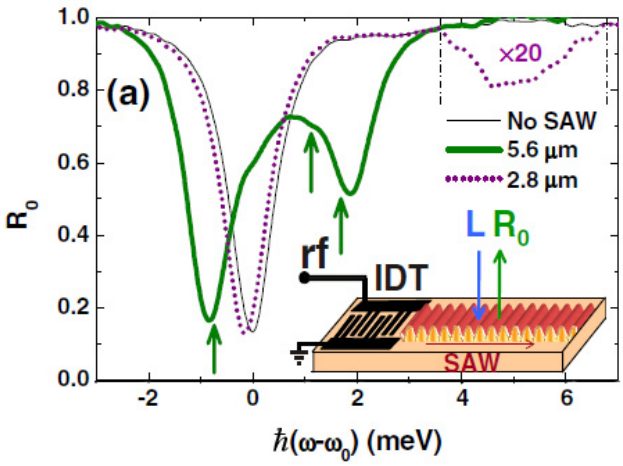

Figure 2.5: Normal incidence reflectivity of the cavity in the absence of a SAW (thin line) and under SAWs (green and dotted line). Image is taken from [27]

The theory of polaritons in the presence of a strong surface acoustic wave was developed in works [11, 28] by A. Ivanov et al. The authors wrote the equations for two coupled oscillators - electromagnetic E and polarization P (exciton) wave propagating in plane of the structure:

$$\begin{aligned}\left[\frac{\partial^2}{\partial x^2}+\frac{\partial^2}{\partial z^2}-\frac{\varepsilon_b(z)}{c^2}\frac{\partial^2}{\partial t^2}\right]E&=\frac{4\pi}{c^2}\frac{\partial^2}{\partial t^2}P+J_{ext},\\ \left[\frac{\partial^2}{\partial t^2}+2\gamma_x\frac{\partial}{\partial t}+\omega_T^2-\frac{\hbar\omega_T}{M_X}\frac{\partial^2}{\partial x^2}-4m_k^x\omega_T\cos(\Omega_k^{ac}t-kx)\right]P&=\Omega_{x-\gamma}^2E.\end{aligned} \tag{2.15}$$

Here $\hbar\omega_T$ and M_x are the energy and the in-plane mass of the exciton, $\Omega_{x-\gamma}$ is the matrix element of the exciton-photon interaction, $2\gamma_x$ is the rate of incoherent exciton scattering, J_{ext} - the external optical pumping and ε_b is the dielectric constant. Acoustic wave propagating in x-direction is presented as an external periodic potential for the exciton part only and is characterized by the frequency Ω_k^{ac}, wave-vector k and exciton-phonon coupling coefficient m_k^x, which comes from the deformation and the piezoelectric potentials.

The authors have predicted the formation of mini-Brillouin bands as well as the reconstruction of reflectivity spectra (fig. 2.6). It was predicted that the energy gaps produced by the SAW in polariton spectra could reach the values of several meV.

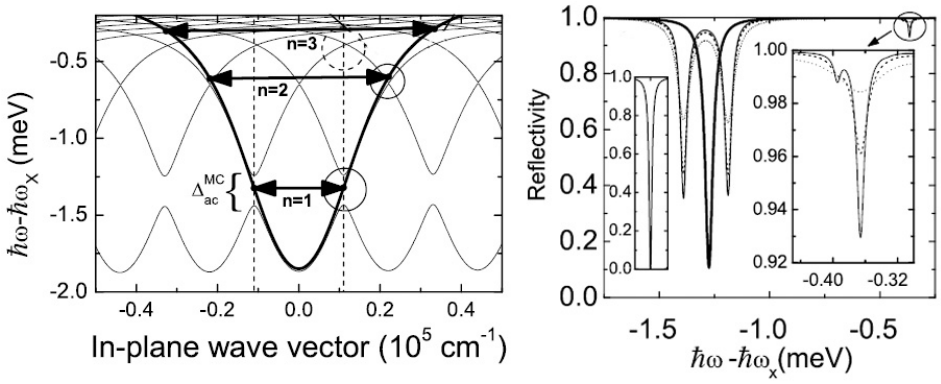

Figure 2.6: Left panel shows the initial (bold solid line) and renormalized by SAW (thin lines) polariton dispersions. Right panel shows the reflection spectra with (thin lines) and without (bold lines) the SAW. The inset shows the reflection dip for $n = 3$ SAW-phonon transition. Image is taken from [28]

The idea of utilization of a SAW as a superlattice potential for cavity polaritons was developed experimentally in the work [29], where authors observed the folding of polariton dispersion. Also, the authors have followed the reduction of polariton dimensionality from 2D to 1D, which manifested in the formation of the number of polariton stripes. These stripes appeared to be weakly coupled, and the diffraction experiments demonstrated coherency in their reemission under optical excitation. In the work [30], the dimensionality of polaritons was reduced to 0D by two surface acoustic waves propagating in orthogonal directions (fig. 2.7).

The works on coupling between coherent acoustic field and polariton condensates appeared very recently [10, 30]. Authors considered condensation of polaritons in 1D and 0D acoustically driven lattices. The coherency between condensates in neighbor potential wells was studied. Also, it was shown, that localization of polaritons results in two effects: 1) the reduction of the condensate formation threshold pump intensity, 2) with the increasing of polariton density, the SAW potential could be effectively screened by polariton-polariton repulsive interaction.

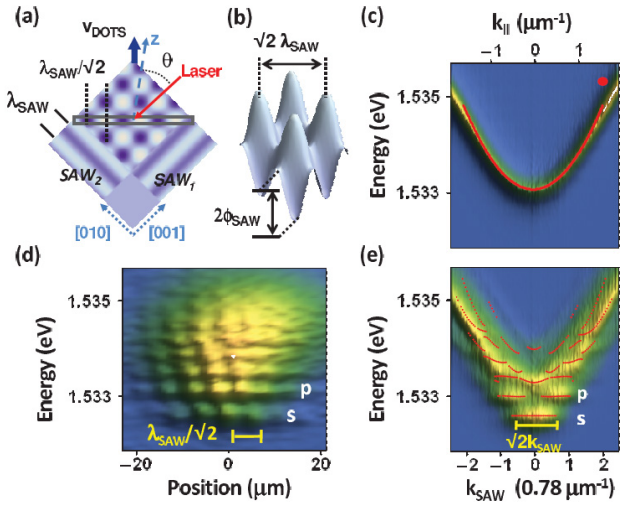

Figure 2.7: (a),(b) SAW square lattice potential. (c),(e) Angular resolved PL spectra maps the planar dispersion of the photon-like polaritons with (e) and without (c) SAW. (d) Spatially resolved spectra below threshold. Image is taken from [30]

.

2.2.2 Acoustic cavities and waveguides

Since phonons are acoustic waves, it is natural to confine them in waveguides. Waveguides usually consist of one central and two boundary layers with acoustic refraction coefficients n_1 and n_2 respectively. If we take the z-axis as the growth axis and consider an acoustic wave propagating in x direction with an in-plane wave-vector $q_{||}$ inside a waveguide, we can write the following equations for its amplitude inside the waveguide[31]:

$$\phi = \phi_0 \cos(\kappa z), \tag{2.16}$$

and in side layers:

$$\phi = \phi_0 \cos(\kappa d) e^{-\gamma(|z|-d)}. \tag{2.17}$$

We consider a waveguide width $2d$ and we count z from the middle of the waveguide. The parameters κ and γ are coupled via the following equations:

$$\begin{aligned} &\tan \kappa d = \frac{\gamma}{\kappa}, \\ &\gamma^2 n_1^2 = \left(n_1^2 - n_2^2\right) q_{||}^2 - n_2^2 \kappa^2. \end{aligned} \tag{2.18}$$

Also, acoustic waves could be confined in acoustic microcavity instead of a waveguide. Recently, the optical generation and detection of coherent acoustic phonons was studied [12, 32]. In these works, the acoustic microcavity was embedded in an optical microcavity, as shown at fig.2.8

The idea of acoustic cavity is the same as for light cavity. However, acoustic wavelengths under study were smaller than optic ones, and it requires the acoustic

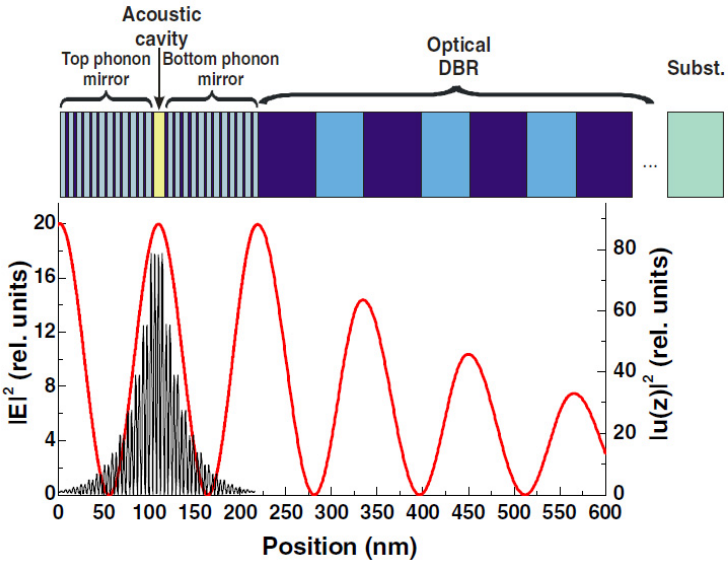

Figure 2.8: Top: scheme of acoustic cavity embedded in the optical cavity. Lower panel - spatial distribution of the light (red curve) and sound (black curve) wave intensities. Image is taken from [12]

.

cavity to be embedded inside the optical. In their latest work [33], authors have constructed a single cavity both for phonons and photons, so they had identical stopbands for both types of excitations. In this work they reported observation of the strong coupling regime between subterahertz phonons and near-infrared light.

2.3 Coherent interactions between phonons and exciton or exciton-polariton condensates

In our work [13] we consider the interaction between a condensate of quantum well excitons or cavity exciton polaritons and a coherent phonon field possessing the same dimensionality [two (2D) or one dimension (1D)]. If the phonons are not confined to the same dimensionality, they play the role of an incoherent reservoir providing exciton or exciton-polariton relaxation, which is not the case we would like to consider here in order to obtain strong coupling. In the phonon-photon or phonon-exciton coherent interaction models developed previously [11, 28] the phonon field has usually been treated as an external potential. This approach is valid under strong external pumping, whereas the model we develop can be used both for the external pumping case and for the case when phonons are created by the excitons themselves.

2.3.1 Formalism

We treat our system as consisting of three interacting classical fields: complex fields $\psi_\pm$ corresponding to right and left circular polarized excitons or exciton-polaritons and a real vector field of the lattice displacements $\mathbf{u}$ corresponding to phonons. The energy of polariton or exciton system is measured from the minimum of the dispersion curve. The model Lagrangian of the system, that accounts for only longitudinal acoustic waves (i.e. assuming shear modulus to be zero) reads:

$$\begin{aligned}\mathcal{L} = \frac{i\hbar}{2}\sum_{s=\pm}\left(\psi_s\partial_t\psi_s^* - \psi_s^*\partial_t\psi_s\right) - \frac{\hbar^2}{2m}\sum_{s=\pm}\left(\nabla\psi_s\right)\left(\nabla\psi_s^*\right) + \\ \frac{1}{2}\left\{\rho\left(\partial_t\mathbf{u}\right)^2 - Y\left[\left(\partial_x u_x\right)^2 + \left(\partial_y u_y\right)^2\right]\right\} - \\ -\frac{\alpha_1}{2}\sum_{s=\pm}|\psi_s|^4 - \alpha_2|\psi_+|^2|\psi_-|^2 - g\mathrm{div}(\mathbf{u})\sum_{s=\pm}|\psi_s|^2.\end{aligned} \tag{2.19}$$

The first line corresponds to free polaritons described by means of their macroscopic wavefunctions ψ_s and acoustic phonons described in terms of the lattice displacement field $\mathbf{u} = (\mathbf{u_x}, \mathbf{u_y})$. The second line to their mutual interactions: the term with α_1 describes the interactions of the polaritons of the same circular polarization, term with α_2- the interactions of the polaritons of the opposite circular polarization, term with g- polariton-coherent phonon interaction. For the moment, we neglect the wavevector dependence of this interaction and g should be considered as a constant determined by the deformation potential. m is an effective mass of cavity polaritons and ρ and Y are the density and the bulk elastic modulus, determining the velocity $c_s = \sqrt{Y/\rho}$ of the longitudinal acoustic wave for zero shear modulus.

The equations of motion for the considered fields are Lagrange equations (ψ_s and ψ_s^* should be considered as independent functions):

$$\frac{\partial}{\partial t}\left(\frac{\partial\mathcal{L}}{\partial(\partial_t\psi_s)}\right) + \sum_{i=x,y}\frac{\partial}{\partial x_i}\left(\frac{\partial\mathcal{L}}{\partial(\partial_{x_i}\psi_s)}\right) - \left(\frac{\partial\mathcal{L}}{\partial\psi_s}\right) = 0, \tag{2.20}$$

$$\frac{\partial}{\partial t}\left(\frac{\partial\mathcal{L}}{\partial(\partial_t u_i)}\right) + \sum_{i=x,y}\frac{\partial}{\partial x_i}\left(\frac{\partial\mathcal{L}}{\partial(\partial_{x_i} u_i)}\right) - \left(\frac{\partial\mathcal{L}}{\partial u_i}\right) = 0. \tag{2.21}$$

This gives:

$$i\hbar\frac{\partial\psi_s}{\partial t} = -\frac{\hbar^2}{2m}\nabla^2\psi_s + \left(\alpha_1|\psi_s|^2 + \alpha_2|\psi_{-s}|^2\right)\psi_s + g\mathrm{div}(\mathbf{u})\psi_s, \tag{2.22}$$

$$\rho\frac{\partial^2\mathbf{u}}{\partial t^2} = Y\nabla^2\mathbf{u} + g\nabla\left[\sum_{s=\pm}|\psi_s|^2\right]. \tag{2.23}$$

Taking the divergence of the second equation and introducing a scalar phonon field

$$\phi = \mathrm{div}(\mathbf{u}), \tag{2.24}$$

one gets

$$i\hbar\frac{\partial\psi_s}{\partial t} = -\frac{\hbar^2}{2m}\nabla^2\psi_s + \left(\alpha_1|\psi_s|^2 + \alpha_2|\psi_{-s}|^2\right)\psi_s + g\phi\psi_s, \tag{2.25}$$

$$\rho\frac{\partial^2\phi}{\partial t^2} = \nabla^2\left[Y\phi + g\sum_{s=\pm}|\psi_s|^2\right]. \tag{2.26}$$

These equations describe the motion and interaction of two fields: polarization and acoustic. However, both field could escape and could be introduced to the system, so one have to introduce phenomenologically the terms corresponding to the resonant pumping of the polariton and phonon modes (P_ψ ans P_ϕ respectively) and the finite lifetime of the polaritons and phonons described by terms containing γ_ψ and γ_ϕ respectively. Finally we get:

$$i\hbar\frac{\partial\psi_s}{\partial t} = -\frac{\hbar^2}{2m}\nabla^2\psi_s + \left(\alpha_1|\psi_s|^2 + \alpha_2|\psi_{-s}|^2\right)\psi_s + g\phi\psi_s - i\gamma_\psi\psi_s + P_\psi(\mathbf{r},t), \tag{2.27}$$

$$\rho\frac{\partial^2\phi}{\partial t^2} = \nabla^2\left[Y\phi + g\sum_{s=\pm}|\psi_s|^2\right] - \frac{\rho\gamma_\phi}{\hbar}\frac{\partial\phi}{\partial t} + P_{ph}(\mathbf{r},t). \tag{2.28}$$

2.3.2 Analytical solution

In this section we calculate analytically the dispersion of excitations of coupled exciton or exciton-polariton and phonon modes with a k-independent interaction g. For simplicity, we neglect here the spin of the polaritons, as our main goal here is to investigate the effects of spin- independent polariton- phonon coherent coupling. Then, one has the system of the equations for two coupled fields:

$$i\hbar\frac{\partial\psi}{\partial t} = -i\gamma_\psi - \frac{\hbar^2}{2m}\nabla^2\psi + \alpha|\psi|^2\psi + g\phi\psi + P(\mathbf{r},t), \tag{2.29}$$

$$\rho\frac{\partial^2\phi}{\partial t^2} = \nabla^2\left[Y\phi + g|\psi|^2\right] - \frac{\rho\gamma_\phi}{\hbar}\frac{\partial\phi}{\partial t} + P_{ph}(\mathbf{r},t). \tag{2.30}$$

Terms $g\phi\psi$ and $g|\psi|^2$ describe the coupling and, therefore, the scattering between two coherent fields: exciton-polariton and acoustic. However, these equations could not express the loss of coherency usually accompanied to the scattering processes.

Now, consider a spatially homogeneous resonant pump of the polaritonic field under normal incidence, $P = P_0e^{-i\omega_0 t}, P_{ph} = 0$. Then, introducing $\psi = \Psi e^{-i\omega_0 t}$ one gets

$$i\hbar\frac{\partial\Psi}{\partial t} = -(\hbar\omega_0 + i\gamma_\psi)\Psi - \frac{\hbar^2}{2m}\nabla^2\Psi + \alpha|\Psi|^2\Psi + g\phi\Psi + P_0, \tag{2.31}$$

$$\rho\frac{\partial^2\phi}{\partial t^2} = \nabla^2\left[Y\phi + g|\Psi|^2\right] - \frac{\rho\gamma_\phi}{\hbar}\frac{\partial\phi}{\partial t}. \tag{2.32}$$

Looking for a spatially homogeneous stationary solution Ψ_0, ϕ_0 one gets

$$-\left(\omega_0 + i\gamma_\psi\right)\Psi_0 + \alpha|\Psi_0|^2\Psi_0 + g\phi_0\Psi_0 + P_0 = 0, \tag{2.33}$$

$$Y\phi_0 + g|\Psi_0|^2 = F. \tag{2.34}$$

Equation 2.32 is an equation for a longitudinal acoustic wave and $Y\phi_0 + g|\Psi_0|^2$ is the stress tensor in the presence of polaritons. In case of stationary homogeneous solution this stress tensor must be equal to the external hydrostatic pressure that we denote by F. In this model F results only in constant shift of exciton energy, that is chosen as reference point in the following calculations. Thus in what follows we assume F to be zero.

$$\phi_0 = -g|\Psi_0|^2/Y, \tag{2.35}$$

and for the determination of the polariton field one has:

$$-\left(\omega_0 + i\gamma_\psi\right)\Psi_0 + \left(\alpha - \frac{g^2}{Y}\right)|\Psi_0|^2\Psi_0 + P_0 = 0. \tag{2.36}$$

This is the same equation as for the case with polariton-polariton interactions but with a renormalized polariton-polariton interaction constant,

$$\tilde{\alpha} = \alpha - \frac{g^2}{Y}. \tag{2.37}$$

One sees, that since the correction to the interaction constant is negative, polariton-polariton interactions mediated by acoustic phonons are attractive. This is not surprising, as similar interactions for the electrons give the famous attractive BCS potential.

Let us now calculate the dispersion of the weak elementary excitations. Following a standard procedure, one represents the solutions in the following form

$$\Psi = \Psi_0 + Ae^{i(\mathbf{kr}-\omega t)} + B^*e^{-i(\mathbf{kr}-\omega^* t)}, \tag{2.38}$$

$$\phi = \phi_0 + Ce^{i(\mathbf{kr}-\omega t)} + C^*e^{-i(\mathbf{kr}-\omega^* t)}, \tag{2.39}$$

which should be then put into Eqs. 2.31,2.32. Considering deviations from equilibrium being small, one should then carry out the procedure of linearization, i.e. in the resulting equations keep only the terms linear in A,B,C.

$$\alpha|\Psi|^2\Psi = \alpha\left(\Psi_0 + Ae^{i(\mathbf{kr}-\omega t)} + B^*e^{-i(\mathbf{kr}-\omega^* t)}\right)^2\left(\Psi_0^* + A^*e^{-i(\mathbf{kr}-\omega t)} + Be^{i(\mathbf{kr}-\omega^* t)}\right) \approx$$
$$\approx \alpha\left\{|\Psi_0|^2\Psi_0 + \left(2A|\Psi_0|^2 + B\Psi_0^2\right)e^{i(\mathbf{kr}-\omega t)} + \left(2B^*|\Psi_0|^2 + A^*\Psi_0^2\right)e^{-i(\mathbf{kr}-\omega^* t)}\right\},$$

$$g\Psi\phi \approx g\left\{\Psi_0\phi_0 + (\phi_0 A + \Psi_0 C)\,e^{i(\mathbf{kr}-\omega t)} + (\phi_0 B^* + \Psi_0 C^*)\,e^{-i(\mathbf{kr}-\omega^* t)}\right\},$$

$$g\nabla^2|\Psi|^2 = g\nabla^2\left(\Psi_0 + Ae^{i(\mathbf{kr}-\omega t)} + B^*e^{-i(\mathbf{kr}-\omega^* t)}\right)\left(\Psi_0^* + A^*e^{-i(\mathbf{kr}-\omega t)} + Be^{i(\mathbf{kr}-\omega^* t)}\right) \approx$$
$$= -gk^2\left[(\Psi_0^* A + \Psi_0 B)\,e^{i(\mathbf{kr}-\omega t)} + (\Psi_0 A^* + \Psi_0^* B^*)\,e^{-i(\mathbf{kr}-\omega^* t)}\right].$$

The system of equations for determination of the small amplitudes A,B,C reads:

$$\begin{pmatrix} -\hbar\omega - 2\alpha|\Psi_0|^2 + \theta + g\phi_0 & \alpha\Psi_0^2 & g\Psi_0 \\ \alpha\Psi_0^{*2} & \hbar\omega + 2\alpha|\Psi_0|^2 + \theta + g\phi_0 & g\Psi_0^* \\ -gk^2\Psi_0^* & -gk^2\Psi_0 & \rho\omega^2 - Yk^2 + i\frac{\rho\gamma_\phi}{\hbar} \end{pmatrix}\begin{pmatrix} A \\ B \\ C \end{pmatrix} = 0,$$

where $\theta = -(\hbar\omega_0 + i\gamma_\psi) + \frac{\hbar^2k^2}{2m}$. And thus the dispersions of the elementary excitations can be determined from the following equation:

$$\begin{vmatrix} -\hbar\omega + \left(2\alpha - \frac{g^2}{Y}\right)|\Psi_0|^2 + \theta & \alpha\Psi_0^2 & g\Psi_0 \\ \alpha\Psi_0^{*2} & \hbar\omega + \left(2\alpha - \frac{g^2}{Y}\right)|\Psi_0|^2 + \theta & g\Psi_0^* \\ -gk^2\Psi_0^* & -gk^2\Psi_0 & \rho\omega^2 - Yk^2 + i\frac{\rho\gamma_\phi}{\hbar} \end{vmatrix} = 0,$$

where we used the relation 2.35 between the amplitudes of the excitonic and phonon fields.

The consideration of the incoherent continous pump of the polariton system accompanied by the onset of the polariton BEC should be made in a different way. In this case, one can assume that in a stationary regime the finite lifetime of the polaritons is compensated by the pump, and calculations can be done in the same way as for particles with infinite lifetime with no external coherent pumping (i.e. one puts $P = 0, \gamma_\phi = \gamma_\psi = 0$). Besides, the energy of the macroscopically occupied mode is not pinned by the frequency of the resonant pump ω_0 but is given by the chemical potential of the system $\mu = \left(\alpha - \frac{g^2}{Y}\right)|\Psi_0|^2$. In this case, the dispersions of the elementary excitations read

$$\begin{vmatrix} -\hbar\omega + \alpha n + \frac{\hbar^2k^2}{2m} & \alpha n & g\sqrt{n} \\ \alpha n & \hbar\omega + \alpha n + \frac{\hbar^2k^2}{2m} & g\sqrt{n} \\ -gk^2\sqrt{n} & -gk^2\sqrt{n} & \rho\omega^2 - Yk^2 \end{vmatrix} = 0, \qquad (2.40)$$

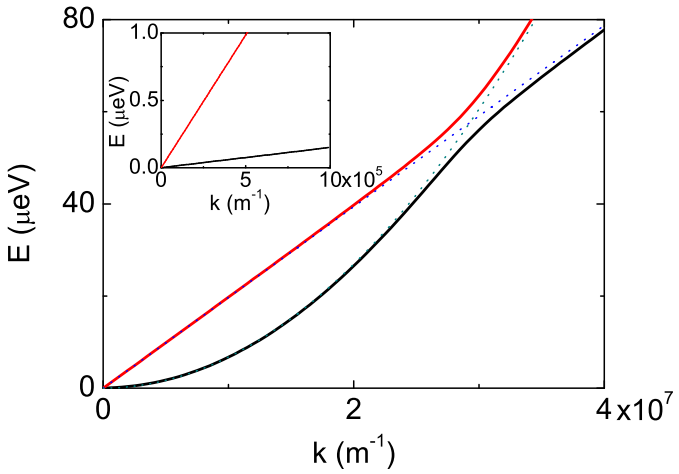

Figure 2.9: Dispersion of the elementary excitations of an exciton condensate strongly coupled with the phonon field. Dashed lines show the original excitations, solid lines show the renormalized dispersions. Inset: same dispersions for the small k-vectors

which gives a following equation for $\omega(k)$, the dispersion of the new quasiparticles in the strongly-coupled system of bogolons (BEC elementary excitations)[34] and phonons:

$$\begin{aligned}\left(\rho\omega^2 - Yk^2\right)\left(E_0(k)^2 + 2\alpha n E_0(k) - (\hbar\omega)^2\right) + \\ +2g^2k^2nE_0(k) = 0,\end{aligned} \tag{2.41}$$

or

$$\begin{aligned}-\left(\hbar^2\rho\right)\omega^4 + \left[\rho E_0(k)\left(E_0(k) + 2\alpha n\right) + Y\hbar^2k^2\right]\omega^2 + \\ +k^2E_0(k)\left[2g^2n - Y\left(E_0(k) + 2\alpha n\right)\right] = 0,\end{aligned} \tag{2.42}$$

with $E_0(k) = \frac{\hbar^2k^2}{2m}$. This equation gives rise to two solutions, close to the original dispersions in the low-k limit and showing the typical anticrossing at higher wavevectors. As expected, in the region of small k the dispersions are linear,

$$\omega_{1,2} = v_{1,2}k, \tag{2.43}$$

where

$$v_{1,2} = \sqrt{\frac{1}{2\rho}\left[\frac{\rho\alpha n}{m} + Y \pm \sqrt{\left(\frac{\rho\alpha n}{m} - Y\right)^2 + \frac{4\rho g^2 n}{m}}\right]}. \tag{2.44}$$

Figure 2.9 shows the dispersions calculated with the use of this equation (solid lines) in comparison with the original dispersions at zero exciton-phonon coupling $g = 0$. The inset demonstrates the linear character of the dispersions near zero. Here and below we consider only exciton condensates, although the theory developed applies to both exciton and exciton-polaritons (the latter in the parabolic approximation). The material parameters used are those of GaAs, as in [32, 35]. Since the dispersion of phonons is not steep at all compared to that of polaritons, the anticrossing of the two dispersions takes place at relatively small wave vectors (10^3 m^{-1}). For excitons the situation is much more favorable, because their energy grows slower with k than that of polaritons, and thus the anticrossing takes place at much larger k (10^7 m^{-1}). In order to demonstrate the effects linked with the presence of the condensate we have to choose its density carefully, so that the speed of sound in the condensate $c = \sqrt{\alpha_1 n/m}$ lies below that of phonons, otherwise the branches will not anticross.

2.3.3 Wavevector dependence

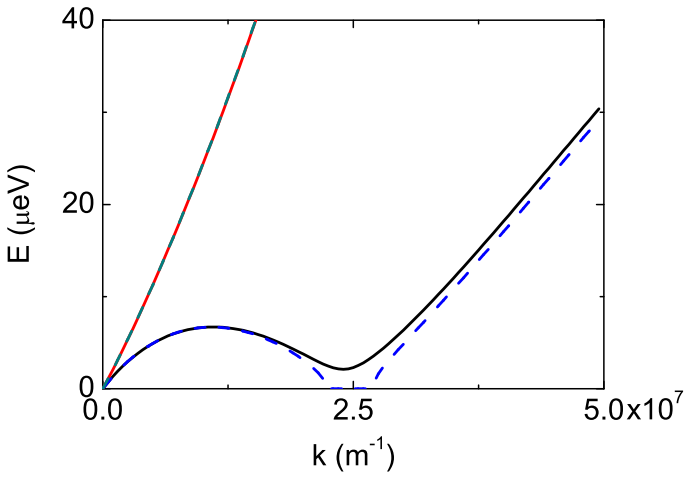

Figure 2.10: Dispersion of the excitations in the exciton condensate coupled with waveguided phonon mode. The wavevector dependence of interactions is taken into account. Solid lines correspond to the stable situation with an additional valley appearing in the dispersion, whereas dashed lines show the unstable case with imaginary dispersion.

In order to obtain an analytical solution for the dispersions of excitations, we had to assume that the interactions between excitons and phonons were independent on the wavevector. However, in realistic systems this is not the case: $g(k)$ first increases with wavevector and then drops down to zero exponentially due to the overlap integrals between the exciton wavefunction and the amplitude of the acoustic wave. We will calculate this dependence for the structure placed in an acoustic waveguide.

The matrix element of exciton-acoustic phonon interaction is[18]:

$$M^{ac}(\vec{q}) = \sqrt{\frac{\hbar q}{2\rho c_s SL}} G(\vec{q}_{||}, q_z), \tag{2.45}$$

where S, L - dimensions of the QW, $\vec{q}$ - acoustic wave vector. One can represent the function $G(\vec{q}_{||}, q_z)$ as:

$$G(\vec{q}_{||}, q_z) = D_e I_e^{||}(\vec{q}_{||}) I_e^{\perp}(q_z) + D_h I_h^{||}(\vec{q}_{||}) I_h^{\perp}(q_z). \tag{2.46}$$

D_e, D_h - are the deformation coefficients for electrons and holes and $I_e^{\perp}(q_z)$, $I_h^{\perp}(q_z)$, $I_e^{\perp}(\vec{q}_{||})$, $I_h^{\perp}(\vec{q}_{||})$ are the overlap integrals between the phonon and exciton mode.

In order to calculate these integrals, we have to obtain the distribution of the amplitude of the guided phonon wave inside the waveguide. Taking into account that QW thickness is much less than the thickness of waveguide, we can assume that the amplitude of the acoustic field is constant over the QW in the z direction. This value can be found from the waveguide equations 2.16 - 2.18:

$$\phi_0 = \frac{1}{2(\frac{\sin \kappa d}{\kappa} + \frac{n_1 \cos \kappa d}{\sqrt{[n_1^2 - n_2^2]q_{||}^2 - n_2^2 \kappa^2}})}. \tag{2.47}$$

Putting the value of ϕ_0 into the overlap integrals, we can obtain the final value of $g(q_{||})$:

$$g(q_{||}) = \phi_0(q_{||}) \sqrt{\frac{\hbar q}{2\rho c_s SL}} \left(D_e \left[1 + \left(\frac{m_e q_{||} a_b^{2D}}{2(m_e + m_h)} \right)^2 \right]^{-3/2} + \right.$$
$$\left. + D_h \left[1 + \left(\frac{m_h q_{||} a_b^{2D}}{2(m_e + m_h)} \right)^2 \right]^{-3/2} \right) . \tag{2.48}$$

First, we have calculated the dispersion of the excitations numerically, in order to compare the result with the analytical solution found above. The results of these calculations are shown in figure 2.10 (solid lines). One can see that if the maximum of the $q_{||}$-dependent exciton-phonon interactions coincides with the crossing of the original branches, the interactions can lead to a much larger splitting and even to the appearance of a valley on the dispersion, similar to the "roton minimum" [36, 37] (but of course, with a completely different origin). The wave-vector dependence of the factor g is composed of two parts: one which is dominant at small values of wave-vectors is increasing with $q_{||}$ and other is decreasing with $q_{||}$ at large values of $q_{||}$. Its maximum g obtains when the factor $(q_{||} a_b^{2D})$ becomes comparable to 1, and so in order to obtain the maximum of g near the point of crossing of the original branches, we considered quite large excitons. In our calculation we took $a_b^{2D} = 100nm$. The

width of the acoustic waveguide d was taken equal to $5\mu m$. Other parameters were taken as table values for GaAs.

Modulating the strength of acousto-exciton interaction, for example, changing the density of the condensate, we can tune the depth of the dip in the dispersion. Moreover, it could be moved towards the zero values of the energy. Dashed lines in the figure 2.10 correspond to the extreme case, when the dispersion of the excitations becomes imaginary and the system becomes unstable against any small perturbation in this wave-vector region.

We have next studied the behavior of the system characterized by such interactions between bogolons and phonons. An anticrossing between two quantum levels can give rise to so-called Rabi oscillations, which take place if only one of the original levels is excited initially. We demonstrate them in our system by solving numerically the equations for the exciton condensate order parameter and for the displacement field (2.32), assuming a homogeneous condensate and a propagating acoustic wave in the x direction as the initial conditions. The system is homogeneous in the y direction and thus the problem is reduced to 1D.

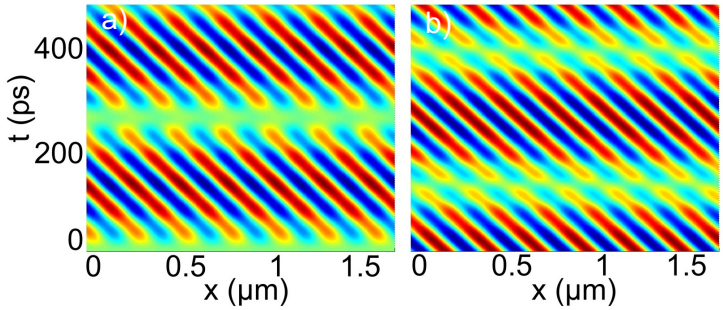

Figure 2.11: Rabi oscillations between the excitations of the exciton condensate (bogolons) and phonons: the amplitude of the propagating waves in each component oscillates in time, as expected. Panel (a) shows the condensate density as a function of coordinate and time, panel (b) shows the amplitude of the acoustic wave.

Figure 2.11 obtained this way demonstrates the Rabi oscillations between the two types of propagating waves: the bogolons (panel a) and the phonons (panel b). Initially, the exciton condensate is homogeneous (no bogolons), whereas the phonon field contains a single monochromatic propagating wave. This situation corresponds to an excited atom in an empty cavity in original Rabi oscillations. After 150 ps, the amplitude of the oscillations of the acoustic wave drops to zero, whereas the condensate density exhibits a running wave. This corresponds to the atom being in the ground state and a photon in the cavity mode, if one continues the analogy with Rabi oscillations. After about 300 ps, the acoustic wave becomes strong again while the bogolons disappear completely, which corresponds to one period of Rabi oscillations.

Finally, we have simulated the unstable situation corresponding to the dashed lines in figure 2.11. An excitation is created in the phonon field with its wavevector

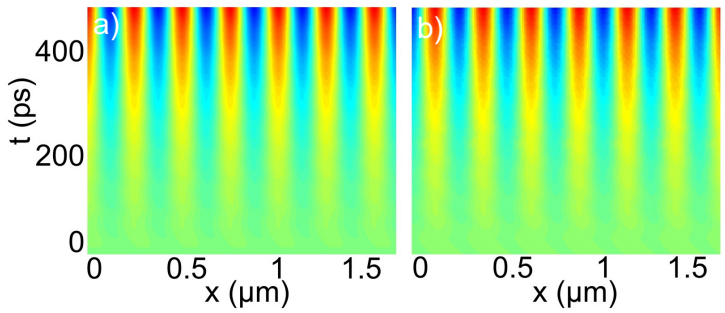

Figure 2.12: Exponential growth of a weak excitation in the unstable case. Panel (a) shows the evolution of the condensate density over time, panel (b) shows the amplitude of the acoustic wave over time.

in the region with imaginary dispersion of excitations (flat real part). Figure 2.12 shows the results of our simulations: the small initial perturbation (a monochromatic wave) grows over time, but does not propagate in space, as expected from the flat real part and positive imaginary part of the dispersion (see 2.11). The perturbations grow in both components (condensate and phonon field, panels (a) and (b)). This interesting effect cannot be described with the previous models (such as ref.[11]), because they do not allow to take into account the effect produced by excitons or photons on the acoustic field itself. Of course such behavior is reasonable until the perturbations amplitude on the condensate surface is small and our model is valid. With the increasing of the amplitude, the system would undergo to the strong nonlinear regime. In order to describe further behavior of the system more complex theory is needed.

2.3.4 Conclusions

In this chapter, we have studied the interaction of QW excitons and cavity exciton-polaritons (condensed or uncondensed) with a coherent phonon field (guided acoustic mode). We have found an analytical solution and studied the renormalized dispersion of excitations in different situations. We have shown that it is possible to obtain strong-coupling regime between the two types of excitation and the anti-crossing between two branches could appear. We have shown that as it follows from the strong-coupling one could obtain the Rabi oscillations between bogolons and phonons. Moreover, in the case of the excitons with large Bohr radius, the strong-coupling effect interfering with the wave-vector dependence of the acousto-exciton interaction, could lead to the appearance of a valley in the dispersion at $k \neq 0$. If the lower dispersion branch touches 0, the system becomes unstable against any small perturbation in the corresponding wave-vector range, the condensate becomes strongly disturbed and the approximation of small perturbations is not more valid. We have performed numerical simulations to demonstrate the Rabi oscillations between bogolons and phonons in the stable regime and the exponential growth of the

perturbations in the unstable regime.

Bibliography

[1] A.V. Kavokin, J.J. Baumberg, G. Malpuech and F.P. Laussy, Microcavities, Oxford University Press, (2007). (Cited on page 27.)

[2] J. Strutt, On the light from the sky, its polarization and colour, *Philosophical Magazine 4*, **41**, 107-120, 274-279, (1871). (Cited on page 27.)

[3] J. Strutt, On the scattering of light by small particles, *Philosophical Magazine 4*, **41**, 447-454, (1871). (Cited on page 27.)

[4] C.V. Raman, A new radiation, *Ind. J. Phys.*, **2**, 387 (1928). (Cited on page 28.)

[5] L. Brillouin, *Ann. Phys.* **17**, 88 (1922). (Cited on page 28.)

[6] L.I. Mandelstam, *Zh. Russ. Fiz-Khim.* **58**, 381 (1926). (Cited on page 28.)

[7] A. L. Ivanov and L. V. Keldysh, Restructuring of polariton and phonon spectra of a semiconductor in the presence of a strong electromagnetic wave, *JETP*, **57**, 234 (1983). (Cited on pages 28 and 32.)

[8] G. S. Vygovskii, G. P.Golubev, E. A. Zhukov, A. A. Fomichev and M. A. Yaskin, *JETP Lett*, **42**, 164 (1985). (Cited on pages 28, 33 and 34.)

[9] M. S. Brodin, V. N Kadan, and M. G. Matsko, *Sov. Phys. Solid State*, **30**, 735 (1988). (Cited on pages 28 and 33.)

[10] E. A. Cerda-Mendez, D. N. Krizhanovskii, M. Wouters, R. Bradley, K. Biermann, K. Guda, R. Hey, P. V. Santos, D. Sarkar, and M. S. Skolnick, Polariton Condensation in Dynamic Acoustic Lattices, *Phys. Rev. Lett.* **105**, 116402 (2010). (Cited on pages 28 and 36.)

[11] A. L. Ivanov, P. B. Littlewood, Acoustically Induced Stark Effect for Excitons in Intrinsic Semiconductors, *Phys. Rev. Lett.* **87**, 136403 (2001) (Cited on pages 28, 35, 38 and 47.)

[12] N. D. Lanzillotti-Kimura, A. Fainstein, A. Huynh, B. Perrin, B. Jusserand, A. Miard, and A. Lemaitre, Coherent Generation of Acoustic Phonons in an Optical Microcavity, Phys. Rev. Lett. 99, 217405 (2007). (Cited on pages 28, 37 and 38.)

[13] D. V. Vishnevsky, D. D. Solnyshkov, G. Malpuech, N. A. Gippius and I. A. Shelykh, Coherent interactions between phonons and exciton or exciton-polariton condensates, *Phys. Rev. B* **84**, 035312 (2011) (Cited on pages 28 and 38.)

[14] Prasanta Kumar Misra, Physics of Condensed Matter, Academic Press. (2010). (Cited on page 30.)

[15] H. Frohlich, *Proc. Roy. Soc. A* **160**, 230 (1937) (Cited on page 30.)

[16] J. K. Jain and S. Das Sarma , Role of discrete slab phonons in carrier relaxation in semiconductor quantum wells, *Phys. Rev. Lett.* **62**, 2305 (1989). (Cited on page 31.)

[17] B. K. Ridley , Electron scattering by confined LO polar phonons in a quantum well, *Phys. Rev. B* **39**, 5282 (1989). (Cited on page 31.)

[18] A. Kavokin and G. Malpuech, Cavity Polaritons, Elsevier, (2003). (Cited on pages 31 and 45.)

[19] Bing Shen Wang and Joseph L. Birman, Theory of phonoritons and experiments to determine phonoriton dispersion and spectrum, *Phys. Rev. B* **42**, 9609 (1990). (Cited on page 32.)

[20] L. Hanke, D. Frohlich, A. L. Ivanov, P. B. Littlewood, and H. Stolz, LA Phonoritons in Cu_2O, *Phys. Rev. Lett.* **83**, 4365 (1999). (Cited on page 33.)

[21] Lord Rayleigh, On Waves Propagated along the Plane Surface of an Elastic Solid, *Proc. London Math. Soc.*, **1-17** , (1): 4-11 (1885). (Cited on page 34.)

[22] R. M. White and F. M. Voltmer, Direct piezoelectric coupling to surface elastic waves, *Appl. Phys. Lett.* **7**, pp. 314-316 (1965). (Cited on page 34.)

[23] C. Campbell, Surface acoustic wave devices for mobile and wireless communications, Elsevier, (1998). (Cited on page 35.)

[24] C. Rocke, S. Zimmermann, A. Wixforth, J. P. Kotthaus, G. Bohm and G. Weimann , Acoustically Driven Storage of Light in a Quantum Well, *Phys. Rev. Lett.* **78**, 4099-4102 (1997). (Cited on page 34.)

[25] L. Kuhn, M. L. Dakss, P. F. Heidrich, and B. A. Scott, Deflection of an optical guided wave by a surface acoustic wave, *Appl. Phys. Lett.* **17**, 265 (1970). (Cited on page 35.)

[26] D. Ciplys, R. Rimeika, M. S. Shur, R. Gaska, J. Deng, J. W. Yang, and M. A. Khan, Acousto-optic diffraction of blue and red light in GaN, *Appl. Phys. Lett.* **80**, 1701 (2002). (Cited on page 35.)

[27] M. M. de Lima, Jr., R. Hey, P. V. Santos, and A. Cantarero, Phonon-Induced Optical Superlattice, *Phys. Rev. Lett.* **94**, 126805 (2005). (Cited on page 35.)

[28] Kikuo Cho, Kazunori Okumoto, N. I. Nikolaev, and A. L. Ivanov, Bragg Diffraction of Microcavity Polaritons by a Surface Acoustic Wave, *Phys. Rev. Lett.* **94**, 226406 (2005) (Cited on pages 35, 36 and 38.)

[29] M. M. de Lima, Jr, M. van der Poel, P. V. Santos, and J. M. Hvam , Phonon-Induced Polariton Superlattices, *Phys. Rev. Lett.* **97**, 045501 (2006). (Cited on page 36.)

[30] Edgar A. Cerda-Mendez, Dmitry N. Krizhanovskii, Klaus Biermann, Rudolf Hey, Maurice S. Skolnick, and Paulo V. Santos, Dynamic exciton-polariton macroscopic coherent phases in a tunable dot lattice, *Phys. Rev. B* **86**, 100301(R) (2012). (Cited on pages 36 and 37.)

[31] D. Markuse, Light Transmission Optics, 1972 (Cited on page 37.)

[32] N. D. Lanzillotti-Kimura, A. Fainstein, B. Perrin, and B. Jusserand, Theory of coherent generation and detection of THz acoustic phonons using optical microcavities, *Phys. Rev. B* **84**, 064307 (2011). (Cited on pages 37 and 44.)

[33] A. Fainstein, N. D. Lanzillotti-Kimura, B. Jusserand, and B. Perrin, Strong Optical-Mechanical Coupling in a Vertical GaAs/AlAs Microcavity for Subterahertz Phonons and Near-Infrared Light, *Phys. Rev. Lett.* **110**, 037403 (2013). (Cited on page 38.)

[34] S. Utsunomiya, L. Tian, G. Roumpos, C. W. Lai1, N. Kumada, T. Fujisawa, M. Kuwata-Gonokami, A. Loffler, S. Hofling, A. Forchel and Y. Yamamoto, Observation of Bogoliubov excitations in exciton-polariton condensates, *Nature Physics* **4**, 700 (2008) (Cited on page 43.)

[35] Esther Wertz, Lydie Ferrier, Dmitry D. Solnyshkov, Pascale Senellart, Daniele Bajoni, Audrey Miard, Aristide Lemaitre, Guillaume Malpuech, and Jacqueline Bloch, Spontaneous formation of a polariton condensate in a planar GaAs microcavity, *Appl. Phys. Lett.* **95**, 051108 (2009). (Cited on page 44.)

[36] L. D. Landau, On the theory of superfluidity of helium II, *J. Phys. USSR* **11**, 91 (1947). (Cited on page 45.)

[37] Ivan A. Shelykh, Thomas Taylor, and Alexey V. Kavokin, Rotons in a Hybrid Bose-Fermi System, *Phys. Rev. Lett.* **105**, 140402 (2010) (Cited on page 45.)

Chapter 3

QD lasing

Contents

The key effect that is exploited in the laser (light amplification by stimulated emission of radiation) technologies is the *stimulated emission* which was predicted theoretically in the work of Albert Einstein[1] in 1916. It was experimentally proved more than 10 years later in the work of R. Ladenburg and H. Kopfermann on "negative dispersion" of the electrically excited neon [2]. However, because it was difficult to fulfill two requirements of the optical generation - the population inversion and the positive feedback - the first laser appeared just in 1960.

Since that time, more than 50 years has passed and all this time laser technologies were continuously developing. The main direction of the research was to decrease the value of the threshold current and to increase working temperatures up to room values.

In semiconductor structures it has been achieving by the consecutive reduction of the dimensionality of carriers up to a total confinement of carriers in quantum dots. The procedure of confinement gave good results and quantum dots now are the most promising objects for the semiconductor lasers. However, because of their size nonhomogeneity, only small fraction of the dots in the ensemble usually participates in the lasing. Recently, a work has been published by C. Bruggemann et al. [3] in which authors significantly amplified the emission of the quantum dots laser "shaking" it by an acoustic pulse.

In this chapter I discuss the semiconductor lasers. In the first part I describe the history of their investigation and their general properties. Then I will speak about

quantum dot lasers and the work of Bruggemann. Finally, I present our work [4] in which we have tried to develop a simple theoretical model describing the acoustic modulation of the lasing in the system of quantum dots coupled to a microcavity. By this model we simulate the experiment and explain its features. Also, we propose to use the surface acoustic waves in order to obtain different lasing patterns.

3.1 Lasers

3.1.1 History of the laser invention

As it was mentioned, the key equations for the laser physics were written by Albert Einstein in 1916 [1] in his work performed on the statistical equilibrium between molecules and thermal radiation with the spatial spectral energy density $\rho(\omega)$. He considered two energy levels of the molecule E_1 and E_2 and the frequency of transition $\omega_0 = (E_2 - E_1)/\hbar$. Then, the kinetics of the population $N_{1,2}$ of states could be described by formulas:

$$\frac{\partial N_2}{\partial t} = -\frac{\partial N_1}{\partial t} = B_{12}\rho(\omega_0)N_1 - B_{21}\rho(\omega_0)N_2 - A_{21}N_2. \tag{3.1}$$

Here $B_{12,21}$ are the Einstein coefficients describing the probability of absorption and stimulated emission processes and A_{21} shows the probability of the spontaneous emission. The need of the constant B_{21} and of the stimulated emission process has come from the combination of the Boltzmann distribution law and the Planck's formula for the spectral density. The equation shows that probability for the molecule to change its state followed by a photon emission is proportional to the intensity of light already present at the corresponding frequency.

If we will consider the equilibrium case, then we could write the expression:

$$\frac{N_2}{N_1} = \frac{B_{12}\rho(\omega_0)}{B_{21}\rho(\omega_0) + A_{21}}. \tag{3.2}$$

On the other hand, in the case of thermal equilibrium, this relation could be described by Boltzmann formula:

$$\frac{N_2}{N_1} = \exp\left[-\frac{\hbar\omega_0}{kT}\right]. \tag{3.3}$$

Also the spectral density $\rho(\omega)$ of the electromagnetic wave obeys the Planck law:

$$\rho(\omega_0) = \frac{\omega_0^2}{\pi^2 c^3}\frac{\hbar\omega_0}{e^{\frac{\hbar\omega_0}{kT}} - 1}. \tag{3.4}$$

By this one could derive the relations between Einstein coefficients, notably:

$$\mathrm{B_{21}}{=}\mathrm{B_{12}} = \frac{\pi^2 c^3}{\hbar\omega_0^3} \cdot A_{21}. \tag{3.5}$$

Theory of the stimulated emission was developed further by P. Dirac in 1920s in the framework of quantum mechanics. The first indirect experimental proof of

the theory was done by R. Ladenburg and H. Kopfermann in 1928[2]. Authors considered the dependence of the change of the refractive index of neon gas on the magnitude of the electrical current inside the gas. The formulas give that for the frequency of electromagnetic wave equal to the frequency of the transition between states j and k the changes of the refractive index should be proportional to the product:

$$f_{kj} N_j \frac{g_k}{g_j} \left(1 - \frac{N_k}{N_j} \frac{g_j}{g_k}\right), \tag{3.6}$$

where $N_{k,j}$ is the population of j and k states, $g_{k,j}$ are the degeneracy value of these states and f_{kj} is the oscillator strength of the transition. According to this equation, the refractive index depends on the relation N_k/N_j which is almost zero when the number of excited atoms is small. However, when this value is not negligible it causes strong changes in the value 3.6.

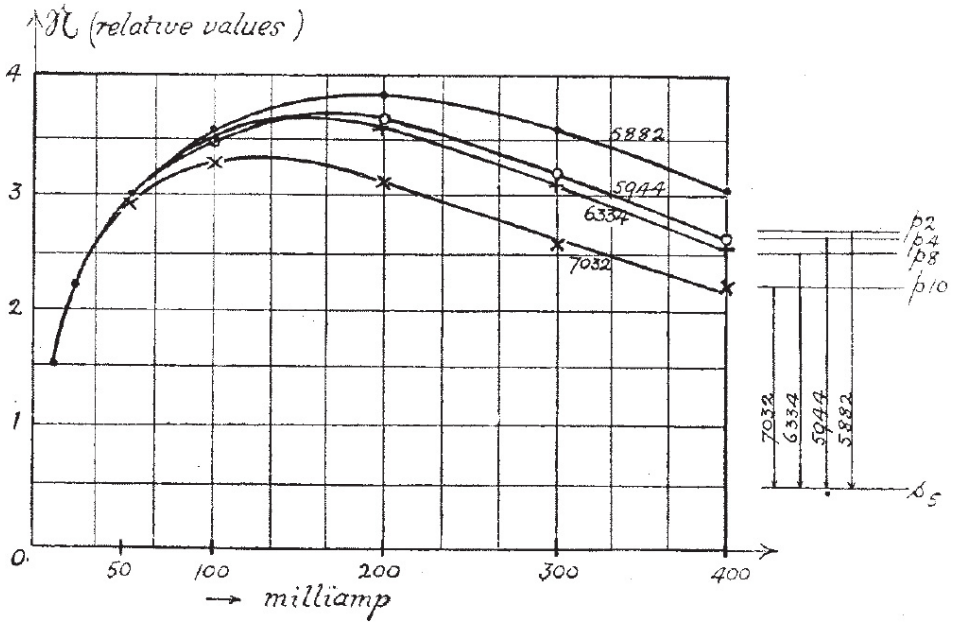

Figure 3.1: The refractive index of the neon gas for different transitions vs the electrical current. Image was taken from [2]

In the work [2] authors observed the changes in the refractive index of the neon gas changing the population of the excited atoms (fig. 3.1). They considered the anomalous dispersions for different transitions and found that for strong electric current, the differences between these values for different transitions changed with the value of current. It has shown that the refractive index of the neon did depend on the occupation numbers of excited states.

From the principles of quantum mechanics the electromagnetic wave, provided by the fact that stimulated emission should be coherent with the initial electromagnetic wave, the stimulated emission should amplify the wave. However, the real

amplification can occur only when the number of stimulated emission processes is larger than the number of the absorption processes. As far as $B_{12} = B_{21}$, it could happen when the number of excited particles is larger than the number of particles in the ground state $N_2 > N_1$. This case is called the *population inversion* and it is the general criterion to obtain the amplification properties of the medium.

Moreover, the lasers should not just amplify but also generate the electromagnetic wave what gives the second key requirement for the laser construction - the *positive feedback* of the system. In other words, each photon, appeared in the system, should stimulate at least one additional emission process *before it leaves the system*. Thus, there were two requirements, which one should satisfy in order to obtain a laser, and it happened to be a difficult task.

However, both problems were solved almost simultaneously in 1953-1955 by two groups of radiospectroscopists who realized the concept of *maser* - microwave amplification by stimulated emission of radiation. The problem of the population inversion has been solved in two different ways. First, the group of Ch. H. Townes by the application of the inhomogeneous electric field spatially separated the beam of excited ammonia atoms from atoms in the ground state. The spatial region containing mostly excited atoms had population inversion by definition, and could amplify the microwaves. However, this scheme could provide not continuous but only pulsed output[5].

Two years later, Soviet scientists A. Prokhorov and N. Basov proposed to consider a three energy level system, where the ground state energy E_0 and two exited states energies $E_{1,2}$ ($E_2 > E_1$) were under consideration [6]. In such scheme, the optical pumping with the frequency $\omega_p = (E_2 - E_0)/\hbar$ provides the transitions from 0 to 2 state and then excited particles relax to the state 1. By this, it is possible to obtain the population inversion either between two excited states (2 and 1) or between excited and ground states (1 and 0). Depending on what process is considered, the electromagnetic wave with the frequency equal to $(E_2 - E_1)/\hbar$ or to $(E_1 - E_0)/\hbar$ could be amplified.

The positive feedback in the maser was realized by the volume resonator where the microwave was confined. And this was one of the main reasons, why masers were constructed before lasers - the size of resonator should be comparable to the wavelength of the electromagnetic wave under consideration. Optical range of spectra demands the resonator to be very small, what was technologically impossible in the 1950s. On the other hand, the microwave resonators were quite common objects in the radio physics.

In 1958 Prokhorov proposed to use a pair of plane parallel mirrors as a resonator [7]. In such system, called an open resonator, the wavelength was much less than the size of the resonator, but the conditions for the positive feedback were obtained.

Finally, in 1960 the first laser was reported by T. H. Maiman [8]. He considered a $1cm$ ruby crystal coated on two parallel faces with silver. The energy scheme of the processes is illustrated in fig. 3.2. When the crystal was irradiated by the 5500 A light, the chromium atoms were excited to $^4F_2$ states and then quickly relaxed to ^2E states. This state spontaneously emitted a doublet of 6943A and 6929A. Under a

very intense excitation, the population inversion between ^2E and the ground states has been reached what resulted in a strong reconstruction of the emitting spectrum (fig. 3.2 (a),(b)).

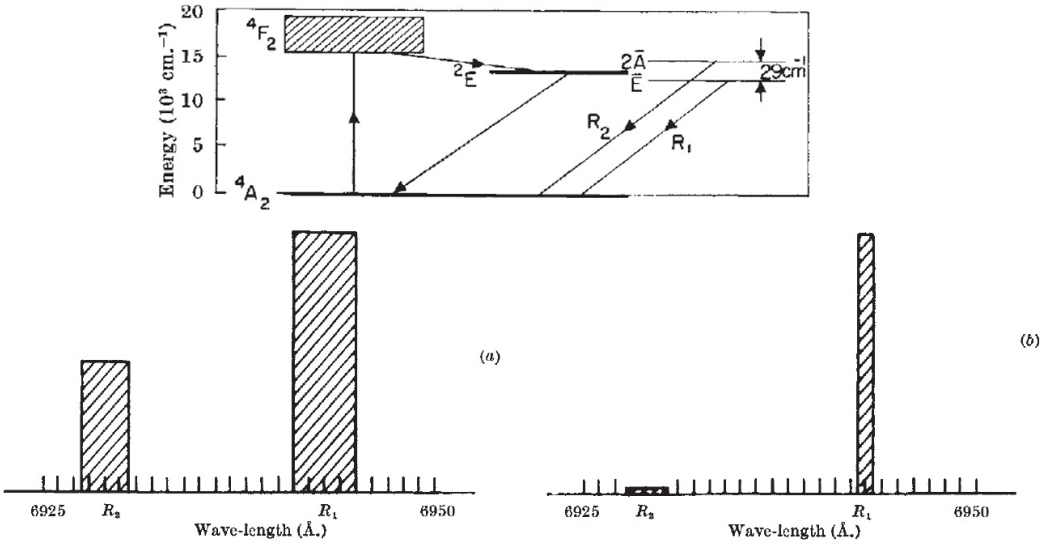

Figure 3.2: Upper panel - the energy diagram of the ruby. Lower panel - the emission spectra for (a) low excitation spectra, (b) high excitation spectra. Image was taken from [8]

3.1.2 Semiconductor lasers

The appearance of the first lasers has revealed the enormously large potential of this technology. The new types of the active medium have been intensively investigated. In 1959 Basov et al. have proposed to use semiconductors as the active medium for the electromagnetic wave amplification [9]. The idea was to use n-(p-) doped semiconductors where the donors (acceptors) could be effectively ionized by a strong electrical pulse and thus one could get the population inversion between donor (acceptor) level and the bottom of the conduction (valence) band.

The idea was developed further by the same group and in 1961 they proposed to use the p-n junction in order to obtain the negative temperature distribution of carriers [10]. Application of the forward electrical bias to the p-n junction injects holes and electrons from opposite sides of the p-n junction into the depletion region where the population inversion between the conduction and the valence band occurs. This work has led the beginning to the laser diode technology which is widely used nowadays.

The first diode laser was created by Hall et al. in 1962 [11]. Authors have constructed the GaAs p-n junction inside the cavity. They changed the applied voltage and they observed abrupt decreasing of the spectral width of the diode

luminescence after the current through the p-n junction has exceeded a threshold value.

There are two key parameters, which define the efficiency of the laser - the value of the threshold current and the maximum value of the temperature, at which laser could work. Because of the broad thermal energy distribution of free carries, only a small amount of them, namely electrons (holes) in the ground state of the conduction (valence) band (resonant with the confined optical wave frequency) participate in the lasing. Thus one need both small temperatures and high current in the structure in order to maximize the quantity of carriers in the ground state and to obtain the lasing regime. First semiconductor lasers required very high currents ($J_{th} = 8500 A/cm^2$), what limited laser operations to short pulses, and very low working temperatures ($T \approx 70K$).

Further evolution of the laser technologies was marked by the attempts to reduce the threshold current for room working temperatures. In 1963 two groups, one of Zh. Alferov and another of H. Kroemer, independently proposed to use *double heterostructure* (DHS) to realize the p-i-n junction laser [12, 13]. Because of heterotransitions, the potential barriers for carriers are much higher than for the same homostructures, what provides a better confinement and much larger values of density of carriers. In 1969 the group of Alferov reported the continuous room temperature operation of the first laser based on GaAs/AlGaAs planar DHS[14]. The idea of DHS has been evolved to the production of quantum wells, where the motion of carriers is strongly confined and quantized in one direction.

Semiconductor lasers were made for a long time in such a way, that the light was confined between two parallel facets. Also the light emission had been effectuating from the open edge of the structure. Thus the quality factor of such structures was very low, the photon interacted with the active medium for a short time, so the positive feedback was quite weak. The situation has significantly changed when the active medium was embedded into an optical microcavity, consisting of two Bragg mirrors, and the so-called *vertical-cavity surface-emitting laser* or VCSEL was invented. The first VCSEL was presented in 1979 by Soda et al. [15], however, first device for CW operation at room temperature was reported just in 1988[16]. In such structures, the light is emitted normally to the structures surface, and the quality factor of cavities could be extremely high (up to tens of thousands) what significantly increases the strength of the light-matter interaction inside.

3.1.3 Quantum dots lasers

The confinement of carrier motion in just one direction in planar DHS has shown the great enhancement of the laser properties. In 1982, Arakawa and Sakaki have performed a work [17], considering the further carrier confinement. They have written simple expressions for the threshold currents for the case of 2D- and 0D-carriers (cases of quantum wells and quantum dots respectively):

$$\begin{aligned} J_{th}^{2D} &\approx \frac{ed}{\eta}\frac{m_c}{\pi\hbar^2 L_z} p_0 B^{2D} kT \ln\left(\frac{m_v kT}{p_0 \pi\hbar^2 L_z}\right), \\ J_{th}^{0D} &= \frac{ed}{\eta}\left(\frac{a^{0D}V}{A^{0D}} + \frac{1}{V} - p_0\right) p_0 B^{0D}. \end{aligned} \tag{3.7}$$

Here d is the active layer thickness, $m_{c,v}$ are the electron and hole effective mass, $B^{0,2D}$ is the constant representing the probability of dipole transitions, L_z and V are the dimensional constants of QW and QD, η is the quantum efficiency and p_0 is the fixed hole concentration.

According to this expression, the temperature dependence of the threshold current vanishes with the total confinement of carriers. This prediction has stimulated the intensive investigation of $0D$ systems, but first QD lasers showing the predicted properties were produced more than ten years later [18, 19]. Since the carriers in such structures could occupy only discrete energy levels, quantum dots indeed demonstrated a better temperature dependence of their properties than quantum well systems. However, because of their size inhomogeneity, the luminescence spectrum of the quantum dots ensemble is inhomogeneously broadened.

Theory of lasing in quantum dot system was developed in numerous works [20, 21, 22, 23], but most explicitly it was considered by Asryan and Suris [24, 25] and Grundmann and Bimberg [26]. The energy dependence of the gain $g_0(E)$ reduced to one QD may be written as:

$$g_0(E) = \frac{8}{3}\frac{\pi^2 e^2}{\hbar c\sqrt{\varepsilon}}\frac{P^2}{V_0 E}\left(f_e + f_h - 1\right)\sum_{\Lambda}\delta\left(E - E_\Lambda\right). \tag{3.8}$$

Here P is the Kane's parameter, V_0 is the quantum dot volume, $f_{e,h}$ are the probabilities of occupation of the electron and hole level in the quantum dot, which are described by the Fermi-Dirac distribution functions, and the summation goes over all energy levels Λ in the dot.

In order to take into account the inhomogeneous distribution of quantum dots, one should average this value over the ensemble. The probability of the dot to have a size a with respect to their average size $\bar{a}$ is usually taken by the normal distribution:

$$w\left(\frac{a-\bar{a}}{\bar{a}}\right) = \frac{1}{\sqrt{2\pi}\delta}\exp\left[-\frac{1}{2\delta^2}\left(\frac{a-\bar{a}}{\bar{a}}\right)^2\right], \tag{3.9}$$

where the parameter δ describes the width of the distribution.

In general, depending on the values of the two parameters - the temperature and the width of the inhomogeneous distribution - there could be two regimes. In the first, the time of the thermal escape for the carrier trapped in a dot is larger than the time of radiative decay. In such systems, all quantum dots are populated homogeneously and the gain is proportional to their size distribution. In other case, when the time of the thermal escape is much shorter than the radiative lifetime, the carrier migration between dots could be achieved and a quasi-equilibrium distribution is established. In this case, the dots with lower energies of ground states are

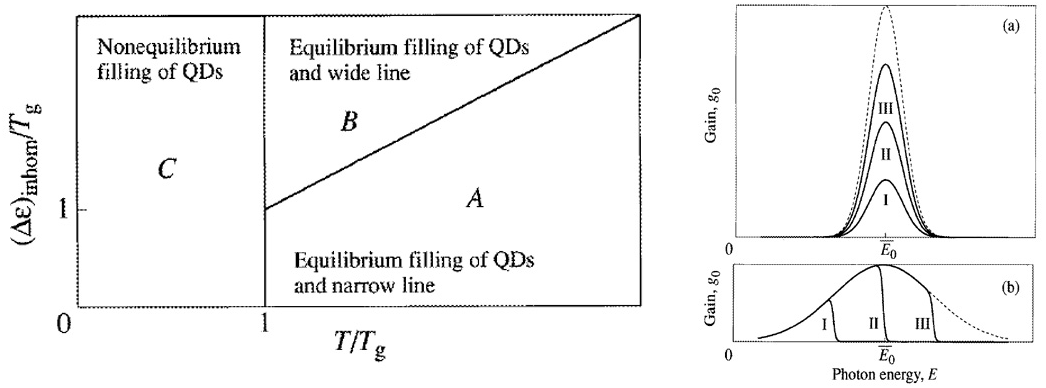

Figure 3.3: Left panel - The diagram presenting different cases of filling of carrier levels in QDs on temperature and QD size fluctuations. Right panel - the gain spectra for (a) low temperatures or narrow QD distribution (regions A and C in the left panel), (b) high temperatures and broad QD line (region B in the left panel). Image was taken from [24]

more likely populated. This leads to strong renormalization of the gain spectra (fig 3.3)

Like the system of quantum wells, the quantum dot arrays have been recently successfully embedded in optical microcavities in order to provide quantum dot VCSELs [27]. Because of the high Q-factor of microcavities, these cavities demonstrate very narrow PL spectra, and thus only a small fraction of quantum dots is coupled to the cavity mode.

3.2 Acoustic modulation of the lasing of QDs in MC

Recently, an attempt was made to involve into the lasing process all quantum dots which lie away from the cavity resonance by a short acoustic pulse [3]. This led to the amplification of the emission intensity up to 50 times. However, some strange behavior of the system was observed.

In this section, I will describe the experimental work [3] and our work [4] where we apply the simple theoretical model which describes an ensemble of quantum dots in the optical microcavity. We consider quantum dots as a number of two-level systems, so the evolution of the QDs population can be described by the von Neumann equation. For the electromagnetic field of the microcavity we can use a resonant mode approximation [29, 30, 31], and get a system of two coupled equations which gives us a behavior of the system.

In first part of the work we described in more details the model we use and its possibilities and limitations. We have shown several results that could be obtained with this model. And after that we introduced the acousto-optic interaction to our system to describe theoretically the experimental results and to explain the strange

behavior[3]. In the final part of the paper we discuss a proposal of implementation of the surface acoustic waves to this system and describe the effects of dynamical lasing pattern formation.

3.2.1 Shaking quantum dots by ultrafast acoustic pulses

In 2012, C. Bruggemann et al. have reported the work [3] where the lasing regime of InGaAs/GaAs quantum dots array coupled to the microcavity was studied. Quantum dots were pumped optically with the high-energy laser and both normal and side photoluminescence were analyzed. Fig. 3.4 (a) shows the normalized photoluminescence spectra. The side view PL represents all quantum dots and the shape of its spectra repeats the inhomogeneous normal distribution of quantum dots, when the normal PL comes generally from the dots coupled to cavity, and thus, this spectra is more or less equal to the narrow cavity spectra. It is clear, that the cavity resonance is shifted with respect to the maximum of the quantum dots distribution. However, one can tune the cavity resonance exciting different locations of the cavity. Fig. 3.4 (b) shows the transition between absorption-generation regimes which occurs at some threshold values of the excitation densities P, W_{th}. These transitions are followed by abrupt strong amplification of the emission intensity.

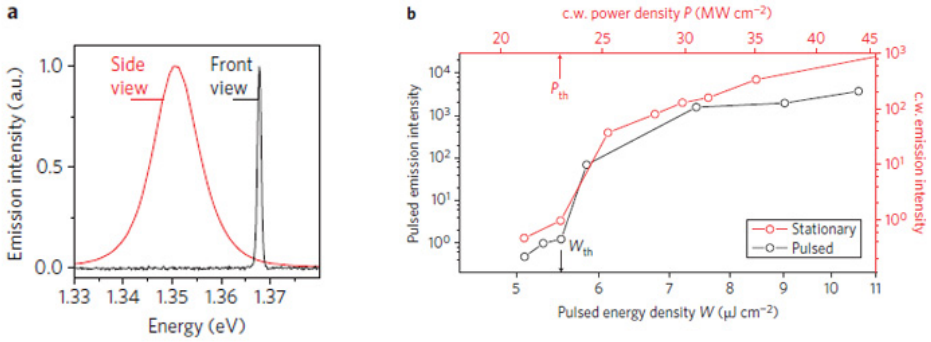

Figure 3.4: (a) Photoluminescence spectra. Emission was collected either normal to the cavity from its front (black curve) or parallel to the cavity from the side (red curve). (b) Emission intensity vs excitation density for pulsed (black curve) and cw (red curve) excitation. Image was taken from [3]

To the backside of the sample, the thin aluminium film was attached. This film was heated by very short strong laser pulses and this introduced short strain pulses into the substrate. The injected strain pulse (its temporal shape is plotted on fig. 3.5 (b)) has reached the QD layer after being distorted by the first Bragg mirror (fig. 3.5 (c)) This pulse shook quantum dots and after passing the second Bragg mirror it was reflected from the samples surface and returned back (fig. 3.5 (d)). Thus, the quantum dots have experienced two strain pulses - incident and reflected. The scheme of the experiment is illustrated at fig. 3.5 (a).

The main idea of the experiment was to involve in the lasing process those

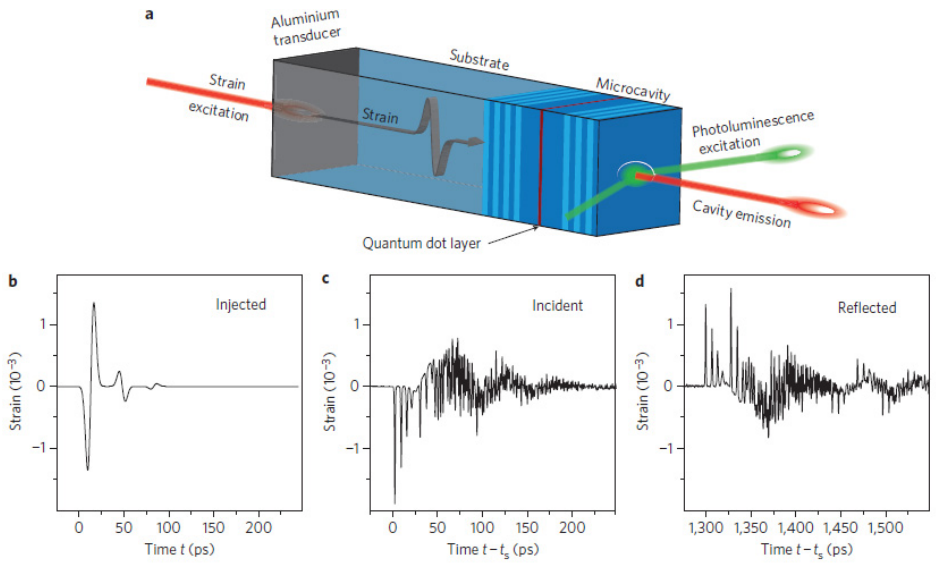

Figure 3.5: (a) Experimental set-up and the scheme of the experiment. (b)-(d) Temporal evolution of strain pulses: initially injected from the aluminium film at t_0 (b), in the quantum-dot layer, arriving from the substrate at $t = t_{ts}$ (c), and in the quantum-dot layer after reflection from the open surface of the microcavity (d). Image was taken from [3]

quantum dots whose ground state energies lie not in resonance with the cavity mode. The strain pulse arriving to the quantum dot array and shifting the lattice constant, changes the energy values of the quantum dots. Roughly speaking, it is shaking the whole quantum dot energy distribution along the energy axis. A lot of quantum dots with population inversion, lying outside of the cavity resonance, are moved to it and are involved in the generation process.

In order to observe the amplification coming from the shaking, authors have recorded the time resolved relation between two emission intensities - with and without strain pulses (fig. 3.6). Two high peaks of amplification were observed coming respectively from the incident and the reflected strain pulses. What was surprising, is that amplification coming from the reflected pulse appeared to be larger than from the incident one. But anyway, acoustic shaking of quantum dots allowed to amplify the intensity of the emission up to 50 times.

3.2.2 Theoretical model

Quantum dots

We use the density matrix formalism in a scalar approximation[32, 33], where each dot can be described by its own 2x2 density matrix ρ. The dynamics of the system is given by von Neumannn equation:

$$i\hbar\dot{\rho} = [\hat{H}\rho]. \tag{3.10}$$

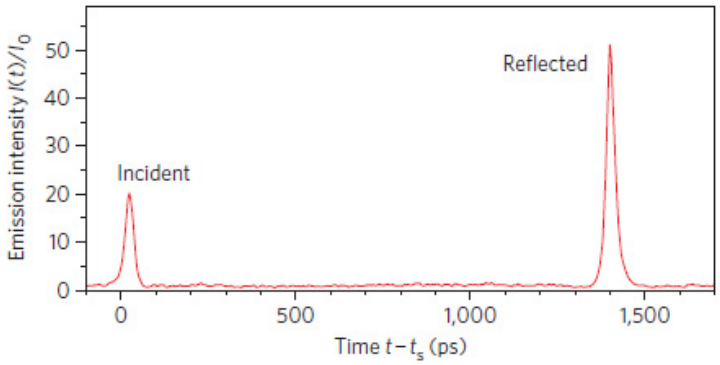

Figure 3.6: The time resolved normalized photoluminescence intensity. Two peaks represent the amplification of the emission intensity by the incident and the reflected strain pulses. Image was taken from [3]

Diagonal elements of ρ give the probabilities to find quantum dot in the ground state or in the excited state and the non-diagonal ones describe the correlations between the ground and excited states, that are responsible for the magnitude of the quantum dot polarization. In fact, the Hamiltonian and the density matrix depend on the in-plane dot position. However, for the electromagnetic wave propagating in the z-direction (that is the subject of our study, see the beginning of the next section for details) the field is homogeneous through x and y, and it is constant over all the dots. Thus under this condition the quantum dot density matrix does not depend on the dot position but just on the dot type. Since we neglect all the interactions between the dots except the interaction with the electromagnetic field the dynamics of each dot depends only on the local electromagnetic field and the resonant dot transition energy. The inhomogeneous broadening of the dots over the spectrum is accounted for by the spectral density function of the dots $n_x(E^j)$, with the dot optical transition energy E^j.

Another approximation of the model is that we consider only two types of interaction with the quantum dots: first, the interaction of quantum dot with the resonant electromagnetic field of the cavity that is explicitly included in the Hamiltonian. The second is the external pumping and relaxation of quantum dots, that is introduced as additional phenomenological terms in the equation for the density matrix of j-th type of quantum dots:

$$i\hbar\dot{\rho}^j = [\hat{H}^j\rho^j] + P^j. \tag{3.11}$$

The Hamiltonian of the j-th type of quantum dot with its resonant energy E^j can be written in the following form:

$$\hat{H} = \begin{pmatrix} 0 & (i\mathcal{E}_0 d^j)^* \\ i\mathcal{E}_0 d^j & E^j \end{pmatrix}, \tag{3.12}$$

where d^j is the matrix element of the dipole moment between the ground and

excited states of j-th quantum dot, $\mathcal{E}_0$ - the amplitude of the cavity electromagnetic field on the quantum dot layer, E^j - the energy of the first exciton state in the QD. The dipole matrix element of the dot can be expressed via the matrix element of the interband currents of the dot $d^j = \frac{J_0^j}{\omega_0^j}$. Its value is defined only by the quantum dot structure and we take it as a parameter in our model. Finally, $\omega_0^j = E_j/\hbar$ is the frequency of QD optical transition.

The last term in Eq.(3.11), responsible for external pumping and relaxation in QDs reads:

$$P^j = \begin{pmatrix} -(\rho_{22}^{st} - \rho_{22}^j)\gamma_1 & -\rho_{12}^j\gamma_2 \\ -\rho_{21}^j\gamma_2 & (\rho_{22}^{st} - \rho_{22}^j)\gamma_1 \end{pmatrix}. \tag{3.13}$$

The experiment [3] was performed at low temperatures ($5K$) and the quantum dots were annealed. Thus, we can consider that there is no quasi-equilibrium distribution of the carriers and all quantum dots are populated equally. Because of that, we could write the phenomenological pump term independent of the dot size like 3.13.

If one neglects the interaction with the cavity mode, the nonresonant pumping drives the system into the stationary state with $\rho_{22}^j = \rho_{22}^{st}$ within the characteristic relaxation time $1/\gamma_1$. As a first approximation, we assume that ρ_{22}^{st} is the same for all types of quantum dots and the non-diagonal elements relax to zero with characteristic time $1/\gamma_2$. All these values are taken as parameters of the model. In order to describe the spontaneous emission in QDs ensemble we add a white noise to the off-diagonal elements of Hamiltonian (5.19).

Another important parameter describing the quantum dots is their inhomogeneous spectral density distribution n_{xE}. We take it as a Gaussian distribution over energy:

$$n_{xE}^j = n_0 e^{-\frac{(E^j - E_{QD})^2}{\Delta E_{QD}^2}}. \tag{3.14}$$

Here E_{QD} is the center of QD energetic distribution and ΔE_{QD} is its width.

Equations for electromagnetic wave

Electromagnetic field dynamics in the microcavity with the optically pumped QDs is a rather complicated problem. In this paper we study the modification of the lasing thresholds by the deformation pulse and are interested in not very strong deviation of the pump intensity from the threshold one. Because of inevitable inhomogeneity of the QD spatial distribution there are always the preferential spots where the lasing starts first due to optimal gain conditions. These spots being of finite size, feed all the cavity modes but are most efficient for the modes slowly propagating along the cavity i.e. the modes with in-plane wave vector close to zero[34]. Thus, in what follows we will treat only the normal cavity mode as the one that starts first to emit the coherent light. It should be understood that this assumption becomes invalid for the pump strongly above the threshold value.

The dynamics of the electromagnetic field $\mathcal{E}_0$ of the normal cavity mode acting on the QDs can be found from the following oscillator-like equation:

$$i\hbar\frac{d}{dt}\mathcal{E}_0 = \hbar\omega_c\mathcal{E}_0 + \beta_J J_x. \tag{3.15}$$

Here $\hbar\omega_c = Re(\hbar\omega_c) - i\gamma_c$ is the resonant photon energy of the microcavity for zero inplane wavevector. The imaginary part of cavity resonance γ_c results from the finite cavity lifetime. The second term $\beta_J J_x$ comes from the interaction with the resonant polarization J_x induced in QDs layer and coherent with the cavity electromagnetic field $\mathcal{E}_0$. This polarization can be written as

$$J_x = \sum_j J_0^j n_{xE}^j \rho_{21}^j. \tag{3.16}$$

For monochromatic wave with frequency ω we can solve Eq.(3.11), find the ρ_{21}^j and substitute it into Eq.(3.16) to get:

$$J_x = \mathcal{E}_0 \sum_j \frac{(J_0^j)^2}{\omega_0^j} n_{xE}^j \frac{1-2\rho_{22}^j}{\hbar(\omega-\omega_0^j)-i\gamma_2}. \tag{3.17}$$

In case of zero (or small) broadening of the QDs ensemble ($\omega_0^j = \omega_0$ the same for all quantum dots) this equation gives the standard polariton splitting equation for homogeneous exciton line.

$$\hbar(\omega-\omega_c)\hbar(\omega-\omega_0+i\gamma_2) = \beta_J \sum_j \frac{(J_0^j)^2(1-2\rho_{22}^j)}{\omega_0} n_{xE}^j. \tag{3.18}$$

For the opposite case of the broad QDs energy spectra that is the subject of our study we can calculate the modification of the imaginary part of the cavity resonance due to pumped QDs as

$$g_c^{eff} = Im[(\hbar\omega_c + \beta_J \sum_j (J_0^j)^2 \Big/ \omega_0 n_{xE}^j \frac{1-2\rho_{22}^j}{\hbar\omega_c - H_{22}^j - i\gamma_2})]. \tag{3.19}$$

If $g_c^{eff} = -\gamma_c^{eff} < 0$ then the amplitude of electromagnetic field will decay with time $\hbar/\gamma_c^{eff}$ and the system is in the absorption regime. In the case, when this parameter is positive, the amplitude of the field grows and it means that the system is in the generation regime. Thus, analyzing γ_c^{eff} we could analyze the generation-absorption transitions. Fig. 3.7 shows the dependence of γ_c^{eff} on the detuning between cavity resonance and the center of quantum dot distribution for three values of ρ_{22}.

From this figure it becomes clear that lasing threshold (pumping power for which the imaginary part becomes positive) depends on the detuning.

Acousto-optical interaction

Acoustic vibrations locally modify the lattice structure of semiconductor, increasing or decreasing the lattice constant. This fact could give rise to two effects: 1) changes in the energy of quantum dot states [35]. In this case energy of QD

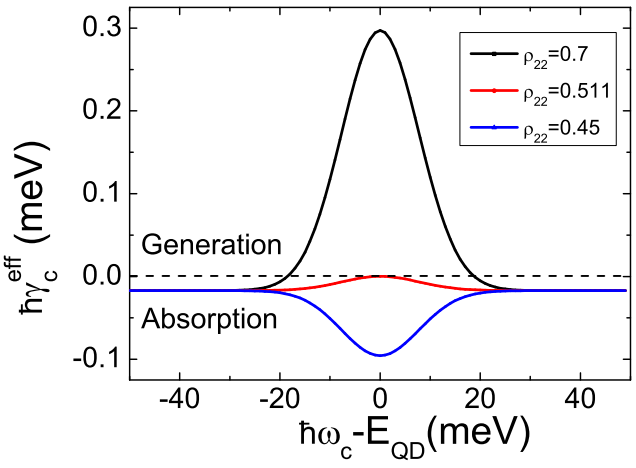

Figure 3.7: Absorption coefficient dependence on detuning for different values of pumping.

transition is shifted by a value which in the first approximation is linear by the amplitude of deformation. The compression of the lattice decreases the lattice constant increasing the energy of the band gap whereas the tension causes the redshift. 2) The second impact of the acoustical deformation is the modification of the microcavity resonant energy [28] due to the deformation in the Bragg mirrors and in the central cavity zone. However, the magnitude of this effect is negligible compared to the first one and in what follows we consider that the acoustic wave is coupled with excitons in QDs only. The resulting modification of the quantum dot Hamiltonian reads:

$$H_{22}^{j}(t) = E^{j} + E_{strain}(t). \tag{3.20}$$

Here $E_{strain}(t)$ is the energy shift of exciton levels caused by the strain. The quations (3.11 - 3.20) describe the behavior and the interactions between all three components: quantum dots, electromagnetic wave and acoustic vibrations.

3.2.3 Implementation of the model

Let us first consider the time evolution of our model system without any strain pulse We take $\rho_{22}^{j} = \rho_{22}^{st} = 0.7$ at a starting point and we consider the detuning $\delta = \hbar\omega_c - E_{QD} = 12meV$ which corresponds to slightly above lasing threshold regime. The results of the calculations are shown in Fig. 3.8. The black curve shows the time evolution of the photoluminescence intensity, and the red dotted curve shows ρ_{22} for quantum dots that are in the resonance with the microcavity. One can see that both electric field and the occupation ρ_{22} oscillate in time with the same frequency but shifted in a phase by $\frac{\pi}{4}$. These oscillations show periodical transitions of the system from lasing to absorption regime and vice versa. This

effect comes from the assumption of system's homogeneity, while for a realistic non-homogeneous case we should average in time the intensity coming from different lasing spots.

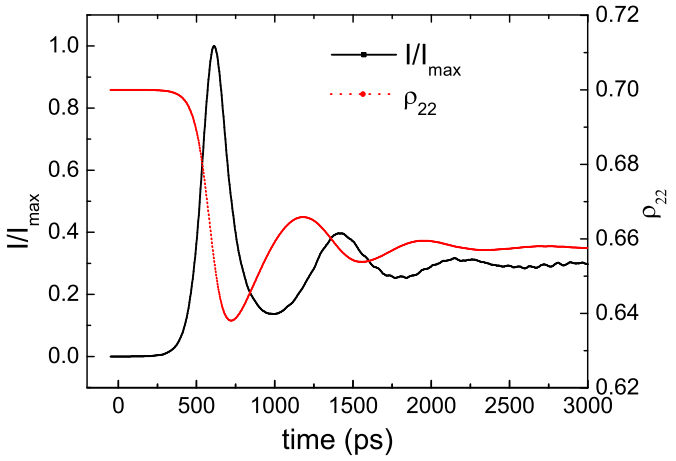

Figure 3.8: Black curve - relation of photoluminescence intensity to its maximum value versus time. Red dotted curve - time evolution of ρ_{22}

The typical time dependencies of the electromagnetic field intensities for different detunings $\delta = \hbar\omega_c - E_{QD}$ are shown on Fig. 3.9. The black curve shows the case when the cavity resonance coincides with the QD distribution maximum. The red and blue ones are for the detunings slightly above and slightly below lasing threshold respectively. The electromagnetic radiation in the absorption regime is spontaneous and it is a narrow-band noise with a small amplitude.

The application of the acoustic pulse changes drastically the dynamics of the microcavity emission and absorption.

First, we took acoustic vibrations in a form of model harmonic oscillations. We put the detuning $\delta = \hbar\omega_c - E_{QD} = 12meV$, that corresponds to slightly above lasing threshold case. The amplitude of vibrations we took equal to $1meV$ and we calculated several curves for different frequencies of oscillations. The results for 100, 50 and $20GHz$ are shown on Fig. 3.10. From this picture, one can see that even small vibrations can strongly amplify the signal from microcavity. This effect comes from the fact that in the presence of vibrations in the system, more quantum dots are involved in lasing process. The characteristic time of microcavity light coupling to the resonant QDs is proportional to the dots density. The amplification of the cavity field depends on the vibration frequency. When these vibrations are too frequent, the quantum dots just do not have time to respond to the external field.

In order to compare the results of our approach with the experimental work [3], we took their strain pulses and put them into our model. The profile of the strain pulse is shown in Fig. 3.11 (a). Incident strain pulse comes in the moment of approximately $750ps$. Its starts from compressive deformation that increases the

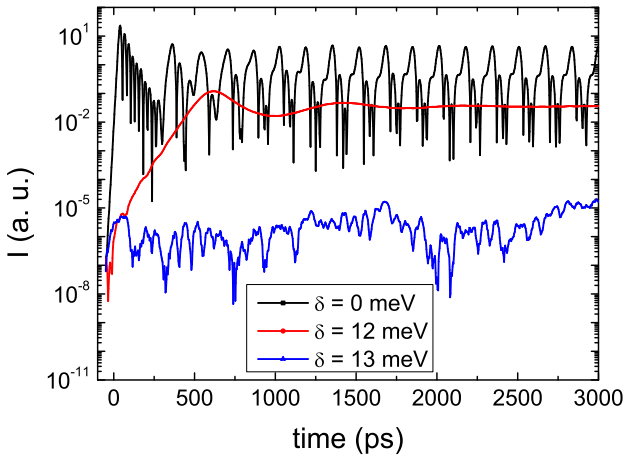

Figure 3.9: Intensities of electromagnetic fields calculated for different values of detunings.

gap and the energy of QDs excitons. At the moment of 2100ps the pulse reflected from the surface comes which starts with a decompression part. In the experimental work [3], authors surprisingly observed that the amplification of the luminescence intensity from the reflected pulse is much stronger that from the incident one. To check whether it is possible to obtain this effect within our model, we put the real strain profile in our code and calculate the time evolution of the electromagnetic field amplitude. One can see it on fig. 3.11 (b). Indeed, the effect in question was successfully reproduced.

We propose the following explanation of the physics of this effect. One can notice that between two pulses there still remain small vibrations in the system. Their amplitude is not larger than $1meV$ but as we have shown in the beginning of this section, even such small oscillations could strongly modify the electromagnetic field in the cavity. From Fig. 3.11 (b) it is clear that between pulses the amplitude of the field is much larger than before the incident pulse. So, the initial conditions are "better" for amplification before the second pulse than before the first one when the amplification factor of the reflected pulse could be less than of the incident.

To check our assumptions we cut the vibrations between two pulses and put the new strain profile in our model. One can see it in Fig. 3.12 (a). In the figure 3.12 (b) we show the ratio between the intensity in the presence of acoustic pulses ($I_{ac}(t)$) and the average intensity without them (I_0) for two cases: with (black curve) and without (red curve) the interpulse vibrations.

It is clear that the real amplification from the reflected strain pulse is less than from the incident.

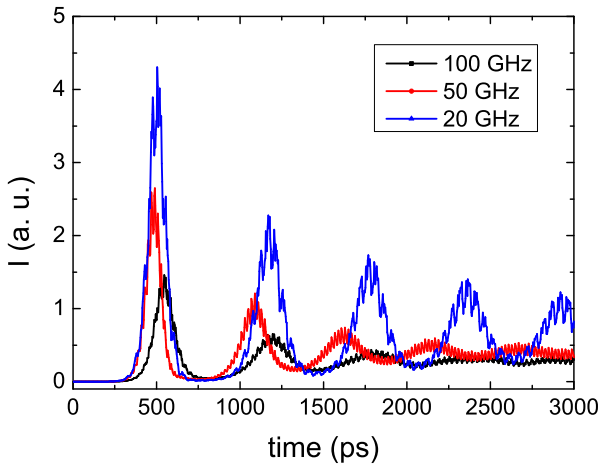

Figure 3.10: Intensities of electromagnetic fields calculated for different frequencies of harmonic acoustic vibrations.

3.2.4 Modulation of the lasing by surface standing acoustic waves

In previous sections we considered interactions with an acoustic shock wave propagating in the transverse (relative to the layer of QDs) direction. In this section we want to discuss another case - the case of surface acoustic waves (SAW). SAW are acoustic waves created piezoelectrically on the surfaces of the structures and propagating in planar directions. Because of their long wavelengths, they produce slowly changing in time (quasistationary for excitons in most planar systems) periodic potential. Recently SAW were used in the studies of polariton condensates [36, 37, 38], and of the photoluminescence from quantum wells [39] etc. We propose to implement SAW to obtain different lasing patterns in the ensemble of quantum dots coupled to a microcavity. If we consider two counterpropagating acoustic waves in the XY-plane with the same amplitude, we could obtain a standing SAW (SSAW). Furthermore, we can produce two-dimensional SSAW by the interference between two orthogonaly propagating one-dimensional SSAW. The E_{strain} in this case will be a function of planar coordinates and time and can be written in the form:

$$E_{strain}(x, y, t) = A_{SAW} \sin(k_x x) \sin(k_y y) \sin(\omega_{SAW} t). \tag{3.21}$$

Here A_{SAW} is the amplitude of exciton energy shift by SAW (several meV in order), k_x, k_y - wave-vectors of $x-$ and $y-$SAW, ω_{SAW} - frequency of SAW.

It was shown that for the same pump intensity, the transition to the lasing regime strongly depends on the relative position between the cavity resonance and quantum dots distribution maximum. So, for a given pump power there is threshold value of detuning δ_{th} such that when $|\delta| \leq \delta_{th}$ there is a gain in the system. And it is clear that using strain provided by planar acoustic waves we can obtain some regions of cavity where conditions of lasing would be satisfied and in others would not. So we

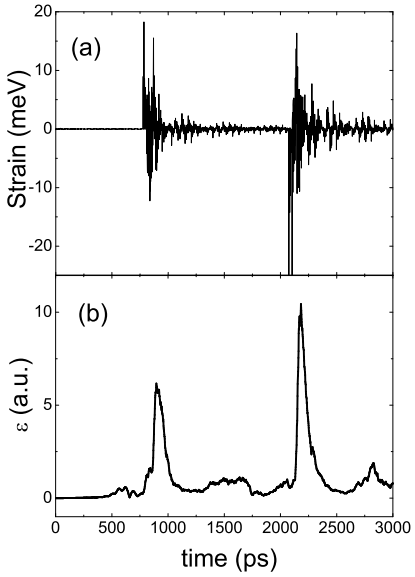

Figure 3.11: (a) Temporal profile of real strain. (b) Evolution of the electromagnetic fields amplitude in MC.

could observe patterns of bright spots. To derive the dependence of lasing intensity on planar coordinates we have considered a simple model based on a pair of kinetic equations:

$$\frac{dN_{ph}}{dt} = wN_x(2\rho_{22} - 1)N_{ph} - \frac{N_{ph}}{\tau_c}, \tag{3.22}$$

$$N_x\frac{d\rho_{22}}{dt} = P - wN_x(2\rho_{22} - 1)N_{ph} - \frac{N_x\rho_{22}}{\tau_{QD}}. \tag{3.23}$$

First equation describes the number of photons (N_{ph}) in the system and the second one - the number of excited quantum dots ($N_x\rho_{22}$). w - is a probability for the photon to be captured by a free quantum dot, τ_c - the lifetime of the photon in the MC, while τ_{QD} is a non-radiative lifetime of an excited quantum dot. P is the term describing the pump and in general case it should be proportional to the number of free quantum dots: $P = pN_x(1 - \rho_{22})$. Here we consider only quantum dots which participate in lasing, in other words whose frequency of transition is equal to the MC frequency:

$$N_x(x, y, t) \sim n_0 exp(-\frac{(E_{mc} - E_{QD} + E_{strain}(x, y, t))^2}{\Delta E_{QD}^2}). \tag{3.24}$$

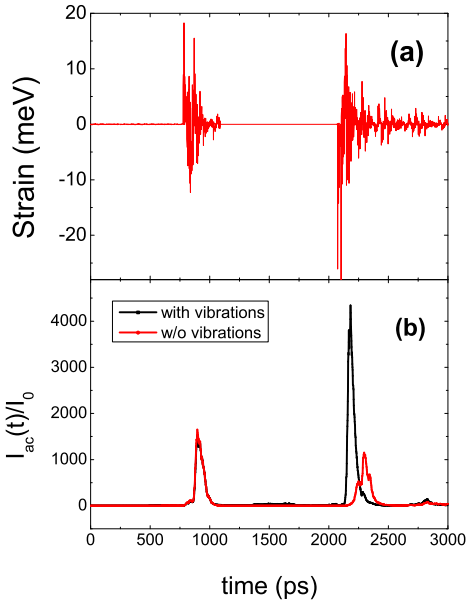

Figure 3.12: (a) Temporal profile of real strain without interpulse vibrations. (b) Amplification of the PL intensities with (black curve) and without (red curve) vibrations.

In the regions which are in the absorption regime, we can take $N_{ph} = 0$. In other regions, we could derive N_{ph} finding stationary solutions of Eqs.(3.22-3.23):

$$N_{ph} = \tau_c \frac{p\tau_{QD} - 1}{2\tau_{QD}} N_x - \frac{p\tau_{QD} + 1}{2w\tau_{QD}}. \tag{3.25}$$

From this equation, the conditions for lasing could be derived. First, the pump should be strong enough so that the prefactor before N_x needs to be positive: $p\tau_{QD} \geq 1$. Second, even with strong pumping it is necessary to have enough quantum dots to make N_{ph} positive, so $\tau_c(\frac{p\tau_{QD}-1}{2\tau_{QD}})N_x \geq \frac{p\tau_{QD}+1}{2w\tau_{QD}}$.

On Fig. 3.13 we plotted the solutions of Eqs. (3.24-3.25) for different moments of time. We consider the pump corresponding to the threshold detuning $\delta_{th} = 10meV$, and the detuning of the unstrained system we took to be slightly larger than that. A_{SAW} we took equal to $5meV$.

Now let us consider weaker pumping to obtain threshold detuning δ_{th} smaller than double strain amplitude. If we start with absolute value of detuning δ slightly larger than δ_{th} then the strain could be so high that $|\delta|$ will cross the threshold value twice. In this case one can obtain holes in bright spots of photoluminescence as it is shown on fig. 3.14.

We have tried to show that surface acoustic waves are quite handy objects to

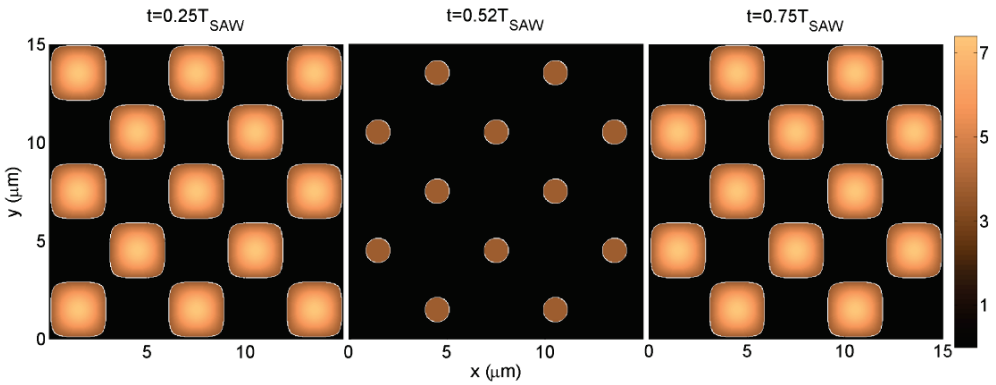

Figure 3.13: Evolution of photoluminescence in time. Snapshots are taken for the values of time 0.25, 0.52 and 0.75 of the SAW period T_{SAW}

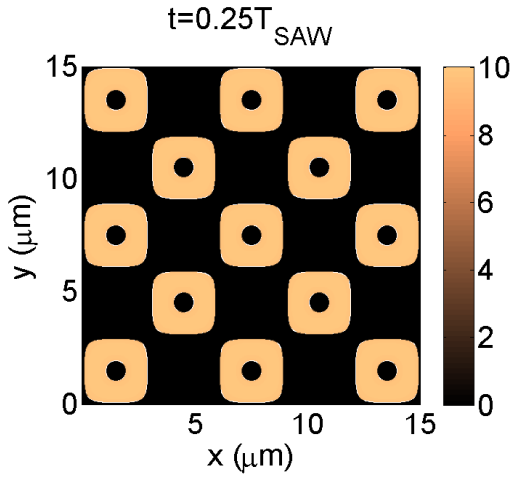

Figure 3.14: Snapshop of PL for $\delta \approx \delta_{th} = 2meV$ and $A_{SAW} = 5meV$

form the radiation patterns in the system of quantum dots. Tuning the parameters of the waves one can obtain on the same system very different radiation structures: standing spots, circles, running stripes or spots, etc. It seems that it is possible to provide the optical lattices this way. For example, irradiating the on-chip atomic Bose-Einstein condensates by such structures one could create the periodical potential. Unfortunately, the light coming from different isolated spots is not coherent. However, if the initial detuning δ is slightly less than δ_{th} one will obtain the set of spots connected by little bridges at the corners and this could increase the coherency across different spots and hence this could decrease the spreading of the radiation beams.

3.2.5 Conclusion

We started this chapter with the discussion of the history of laser technology. We have shown that there are two key parameters for the semiconductor lasers - the threshold current and the working temperature. Then we discussed the quantum dots lasers, its advantages and imperfections. Finally I described the work in which we have developed a simple theoretical model of light-matter interaction in the system of quantum dots coupled to microcavity in the presence of acoustic deformations. We have described the effect of acoustically driven amplification of the lasing regime in the system. Moreover, we successfully reproduced experimental effects obtained in [3]. In the final section of our work we proposed an application of surface acoustic waves to modify lasing patterns of the system.

Bibliography

[1] Einstein A, Strahlungs-emission und -absorption nach der Quantentheorie, *Verhandlungen der Deutschen Physikalischen Gesellschaft* **18** 318-323 (1916). (Cited on pages 53 and 54.)

[2] H. Kopfermann and R. Ladenburg, Experimental Proof of 'Negative Dispersion', *Nature* **122** 438-439 (1928). (Cited on pages 53 and 55.)

[3] C. Bruggemann, A. V. Akimov, A. V. Scherbakov, M. Bombeck, C. Schneider, S. Hofling, A. Forchel, D. R. Yakovlev and M. Bayer, Laser mode feeding by shaking quantum dots in a planar microcavity, *Nature Photonics* **6** (2012). (Cited on pages 53, 60, 61, 62, 63, 64, 67, 68 and 73.)

[4] D. V. Vishnevsky, N. A. Gippius, Acoustic control of the lasing threshold in QDs ensemble coupled to an optical microcavity , *arXiv:1210.3199* (2012). (Cited on pages 54 and 60.)

[5] C. Towns,Production of coherent radiation by atoms and molecules, *Nobel Lecture*, (1964). (Cited on page 56.)

[6] Basov N.G., Prokhorov A. M., About possible methods for obtaining active molecules for a molecular oscillator, *Sov.Phys. JETP* **1**, 184 (1955). (Cited on page 56.)

[7] Prokhorov A. M., Molecular amplifier and generator for submillimeter waves, *Sov.Phys. JETP* **7**, 1140 (1958). (Cited on page 56.)

[8] Maiman T. H., Stimulated Optical Radiation in Ruby, *Nature* **187** 493 (1960). (Cited on pages 56 and 57.)

[9] Basov N. G., Vul B. M., Popov Yu. M., Quantum-mechanical semiconductor generators and amplifiers of electromagnetic oscillations, *Sov.Phys. JETP* **10**, 416 (1960). (Cited on page 57.)

[10] Basov N. G., Krokhin O. N., Popov Yu. M., Production of negative-temperature states in p-n junctions of degenerate semiconductors, *Sov.Phys. JETP* **13**, 1320 (1961). (Cited on page 57.)

[11] R. N. Hall, G. E. Fenner, J. D. Kingsley, T. J. Soltys, and R. O. Carlson, Coherent Light Emission From GaAs Junctions, *Phys. Rev. Lett.* **9**, 366 (1962). (Cited on page 57.)

[12] Zh. I. Alferov, P. F. Kazarinov, Certificate of authorship 181737, priority date of 30 March 1963. (Cited on page 58.)

[13] Kroemer H., *Proc. IEEE* **51** 1782 (1963). (Cited on page 58.)

[14] Zh. I. Alferov, V. M. Andreev, E. L. Portnoi, and M. K. Trukan, *Sov. Phys. Semicond.* **3**, 1107 (1969). (Cited on page 58.)

[15] Soda Haruhisa, Iga Ken-ichi, Kitahara Chiyuki, Suematsu Yasuharu, GaInAsP/InP Surface Emitting Injection Lasers, *Japanese Journal of Applied Physics* **18**, 12 (1979). (Cited on page 58.)

[16] Koyama Fumio et al., Room temperature cw operation of GaAs vertical cavity surface emitting laser, *Trans. IEICE* **E71**, 11 (1988). (Cited on page 58.)

[17] Y. Arakawa and H. Sakaki, Multidimensional quantum well laser and temperature dependence of its threshold current, *Appl. Phys. Lett.* **40**, 939 (1982). (Cited on page 58.)

[18] N. N. Ledentsov, V. M. Ustinov, A. Yu. Egorov, A. E. Zhukov, M. V. Maximov, I. G. Tabatadze, and P. S. Kop'ev, *Semiconductors* **28**, 832 (1994). (Cited on page 59.)

[19] N. Kirstaedter, N. N. Ledentsov, M. Grundmann, D. Bimberg, V. M. Ustinov, S. S. Ruvimov, M. V. Maximov, P. S. KopŠev, Zh. I. Alferov, U. Richter, P. Werner, U. Gosele, and J. Heydenreich, Low threshold, large T_0 injection laser emission from (InGa)As quantum dots, *Electron. Lett.* **30**, 1416 (1994). (Cited on page 59.)

[20] Asada M., Miyamoto Y. and Suematsu Y., *IEEE J. Quantum Electron.* **22**, 1915 (1986). (Cited on page 59.)

[21] Vahala K. J., *IEEE J. Quantum Electron.* **24**, 523 (1988). (Cited on page 59.)

[22] Miyamoto Y., Miyake Y., Asada M. and Suematsu Y., *IEEE J. Quantum Electron.* **25**, 2001 (1989). (Cited on page 59.)

[23] Yan R. H., Corzine S. W., Coldren L. A. and Suemune I., *IEEE J. Quantum Electron.* **26**, 213 (1990). (Cited on page 59.)

[24] L. V. Asryan and R. A. Suris, Inhomogeneous line broadening and the threshold current density of a semiconductor quantum dot laser *Semicond. Sci. Technol.* **11**, 554 (1996). (Cited on pages 59 and 60.)

[25] L. V. Asryan and R. A. Suris, Charge Neutrality Violation in Quantum-Dot Lasers, *IEEE J. Sel. Top. Quantum Electron.* **3**, 148 (1997). (Cited on page 59.)

[26] M. Grundmann and D. Bimberg, Gain and threshold of quantum dot lasers: theory and comparison to experiments, *Jpn. J. Appl. Phys.* **36**, 4181 (1997). (Cited on page 59.)

[27] Lott J. A., Ledentsov N. N., Ustinov V. M., Maleev N.A., Zhukov A.E., Kovsh A.R., Maximov M.V., Volovik B.V., Alferov Zh.I., Bimberg D., InAs-InGaAs quantum dot VCSELs on GaAs substrates emitting at 1.3μm, *Electron. Lett.* **36**, 1384 (2000). (Cited on page 60.)

[28] T. Berstermann, A. V. Scherbakov, A. V. Akimov, D. R. Yakovlev, N. A. Gippius, B. A. Glavin, I. Sagnes, J. Bloch, and M. Bayer, Terahertz polariton sidebands generated by ultrafast strain pulses in an optical semiconductor microcavity, *Phys. Rev. B* **80**, 075301 (2009). (Cited on page 66.)

[29] N. A. Gippius, T. Weiss, S. G. Tikhodeev, and H. Giessen, Resonant mode coupling of optical resonances in stacked nanostructures, *Optics Express* **18**, 7569 (2010). (Cited on page 60.)

[30] N. A. Gippius, S. G. Tikhodeev, V. D. Kulakovskii, D. N. Krizhanovskii, and A. I. Tartakovskii, Nonlinear dynamics of polariton scattering in semiconductor microcavity: Bistability vs. stimulated scattering , *Europhysics Letters* **67**, 997 (2004). (Cited on page 60.)

[31] N. A. Gippius and S. G. Tikhodeev, Multiple-polariton scattering in a semiconductor microcavity, *Journal of Physics: Condensed Matter* **16**, S3653 (2004). (Cited on page 60.)

[32] D. N. Krizhanovskii, G. Dasbach, A. A. Dremin, V. D. Kulakovskii, N. A. Gippius, M. Bayer, A. Forchel, *Solid State Communications*, **119**, 435 (2001) (Cited on page 62.)

[33] V. D. Kulakovskii, D. N. Krizhanovskii, G. Dasbach, A. A. Dremin, N. A. Gippius, M. Bayer, and A. Forchel, *Phys. Stat. Sol. (a)* **190**, 421 (2002) (Cited on page 62.)

[34] G. Ramon, U. Mizrahi, N. Akopian, S. Braitbart, D. Gershoni, T. L. Reinecke, B. D. Gerardot, and P. M. Petroff, Emission characteristics of quantum dots in planar microcavities, *Phys. Rev. B* **73**, 205330 (2006). (Cited on page 64.)

[35] J. Bardeen and W. Shockley, Deformation Potentials and Mobilities in Non-Polar Crystals, *Phys. Rev.* **80**, 72 (1950). (Cited on page 65.)

[36] E. A. Cerda-Mendez, D. N. Krizhanovskii, M. Wouters, R. Bradley, K. Biermann, K. Guda, R. Hey, P.V. Santos, D. Sarkar, and M. S. Skolnick, Polariton Condensation in Dynamic Acoustic Lattices, *Phys. Rev. Lett.* **105**, 116402 (2010). (Cited on page 69.)

[37] E. A. Cerda-Mendez, D. N. Krizhanovskii, K. Biermann, R. Hey, M. S. Skolnick and P. V. Santos, Wavefunction of polariton condensates in a tunable acoustic lattice, *New J. Phys.* **14**, 075011 (2012). (Cited on page 69.)

[38] Vishnevsky D. V., Solnyshkov D. D., Malpuech G., Gippius N. A. and Shelykh I. A., Coherent interactions between phonons and exciton or exciton-polariton condensates, *Phys. Rev. B* **84**, 035312 (2011). (Cited on page 69.)

[39] Tetsuomi Sogawa, Haruki Sanada, Hideki Gotoh, Hiroshi Yamaguchi, and Paulo V. Santos, Dynamic control of photoluminescence polarization properties in

GaAs/AlAs quantum wells by surface acoustic waves, *Phys. Rev. B* **86**, 035311 (2012). (Cited on page 69.)

Chapter 4

Non-linear optical effects. Polariton multistability

Contents

If the polarization of the medium has a non-linear response on the field of the incident light, the non-linear optical (NLO) effects could occur. However, generally, one needs high intensities of light to observe NLO effects, so they were discovered only in 1960s with the developing of laser technologies. In 1961 Franken et. al. performed a work [1], where they irradiated the crystalline quartz by a strong laser beam and they observed the formation of second harmonics in the transmitted light. This work has begun the intensive investigation of non-linear optical properties of different materials.

NLO effects could be qualitatively divided in two groups: parametric, where the quantum state of the medium is not changed by the interaction with light, and non-parametric, where the medium state is changed. The parametric processes are instantaneous.

Optical microcavities allow to obtain significant values of the electric field inside, and cavity polaritons mutual interactions via their excitonic fraction show a strong non-linear behavior. All this simplifies the observation of NLO effects. Also, a well-defined relation between the polariton state and the angle of incident or emitted light helps to manipulate, detect and analyse the non-linear processes. A lot of effects, like parametric oscillations and amplifications [2, 3, 4] and optical bi-(multi-)stabilities [5, 6] were observed. However, recent experiments on polariton multistability [6] have shown the necessity to reconsider the polariton-polariton interaction schemes.

In this chapter, I will first present a general discussion of the non-linear optical effects. Then I will discuss the bistability and multistability in the polaritonic system. I will demonstrate the contradiction between the theoretical expectations and the experimental data. And after all, I will describe our work [7], where we consider the scattering of polaritons from ground to upper states. This process has been always treated as negligible and has been ignored. In our work we have shown that in some cases such scattering could lead to the formation of the respectively dense excitonic reservoir, which could effectively renormalize the polariton-polariton interactions.

4.1 NLO

4.1.1 Additional harmonics

In general, the polarization of the medium $\mathbf{P}$ could be expressed in terms of the external electric field $\mathbf{E}$ in the following way:

$$P_i = \chi^{(1)}_{ij} E_j + \chi^{(2)}_{ijk} E_j E_k + \chi^{(3)}_{ijkl} E_j E_k E_l + ... \tag{4.1}$$

Here $\chi^{(n)}$ is the n-th order tensor of susceptibility.

Let us consider the quadratic by $\mathbf{E}$ part of the polarization vector and let us call it $\mathbf{P}^{(2)}$. Then $\mathbf{P}^{(2)}$ would be a linear function of the components of the 6×6 symmetric tensor $\mathbf{EE}$. The symmetry of the medium imposes certain restrictions on the coefficients $\chi^{(2)}$, which are, in fact, the same as for the piezoelectrical tensor. Thus, there is no $\mathbf{P}^{(2)}$ in isotropic materials or in materials containing a center of inversion. However, for example, in crystalline quartz one could write the following expressions for the components of $\mathbf{P}^{(2)}$:

$$\begin{aligned} P^{(2)}_x &= \alpha(E_x^2 - E_y^2) + \beta E_y E_z, \\ P^{(2)}_y &= -\beta E_x E_z - 2\alpha E_x E_y, \\ P^{(2)}_z &= 0. \end{aligned} \tag{4.2}$$

Here α and β are some coefficients. So, if the incident electromagnetic wave can be described by harmonic oscillations with frequency ω, it provokes the double ω oscillations of the medium polarization. The polarization wave in its turn could be considered as the generator of an electromagnetic wave, so new harmonics could

appear in the spectrum of the crystal. This process is called second-harmonics generation (SHG).

In 1961 Franken et. al. observed SHG in the crystal of quartz under strong laser pumping [1]. The image of the photographic plate is shown on fig. 4.1.

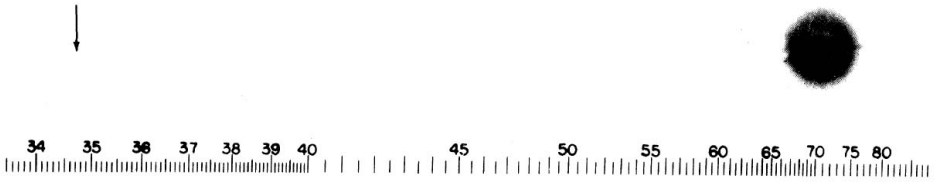

Figure 4.1: The reproduction of the photographic plate from the Franken experiment [1]. The wavelength scale is in the units of 100 Å. The spot at 6943 Å indicates the incident light, while the arrow indicates the position of the second harmonics at 3472 Å. Unfortunately, the spot itself has disappeared during editorial process. The story says that it was considered by the editor as a speck of dirt and was removed from the publication [8].

Thanks to that SHG could be observed only in certain materials and to SHG polarization anisotropy, nowadays it is widely used in biological and medical science for high-resolution optical microscopy. Also the second-harmonic generation process is used to obtain green lasers from the infrared source.

In general, the intensity I_n of the n-th harmonic is proportional to[9]:

$$I_n \sim \frac{n}{c^{n-1}\lambda^{n+1}} \left|\chi^{(n)}\right|^2 I_1^n, \tag{4.3}$$

where c is the velocity of light in vacuum, λ and I_1 are the wavelength and power of incident light. Observation of higher harmonics becomes a very hard task. However, the higher harmonics from third [10] up to fifteenth [9] were obtained in different materials. Moreover, when the light interacts with electron-nuclear plasma, the expression 4.3 is not valid anymore and High Harmonic Generation (HHG) could be obtained. The first HHG was observed in solids in 1977 [11] and in 1987 in gases [12]. The later work [13] has shown a surprising result: the intensities of high harmonics stopped to decrease with the number n and formed a plateau. The intensities of harmonics remained constant over hundreds of eV.

If two electromagnetic waves with different frequencies ω_1 and ω_2 are propagating in the non-linear medium, the additional harmonics could appear, whose frequency ω_3 would be the sum $\omega_1+\omega_2$. This process is called sum-frequency generation (SFG). SFG occurs efficiently, if the condition of phase-matching is satisfied, notably, the wave vector of the third wave should be the sum of the wave vectors of two initial waves: $\mathbf{k}_3 = \mathbf{k}_1 + \mathbf{k}_2$. Obviously, the SHG is the special case of the SFG.

4.1.2 Optical parametric amplification

Besides the formation of new harmonics by the interaction between two photons, in non-linear medium there could be an opposite process - parametric scattering of one photon followed by the generation of two new photons, what gives rise to two new additional harmonics, whose frequencies are lower than the frequency of pumping. Such effects were predicted theoretically in the beginning of 60s in works of Louisell et al.[14, 15, 16]. New harmonics are usually called *signal* (commonly the harmonic of higher frequency) and *idler* or s and i for brevity. Once signal and idler photons are produced, they could stimulate the scattering processes further. If the pump is strong enough, the scattering becomes avalanche-like and and strong amplification of s and i amplitudes could be obtained.

The frequencies and the wave vectors of these harmonics are defined by the phase matching conditions:

$$\begin{aligned} \omega_p &= \omega_s + \omega_i, \\ \mathbf{k}_p &= \mathbf{k}_s + \mathbf{k}_i. \end{aligned} \tag{4.4}$$

The solution of these equations strongly depends on the medium properties namely its dispersion. Thus, changing the conditions for the medium, one can tune the frequencies of harmonics. The tunable optical parametric fluorescence was first observed in works [17] where the temperature of the crystal was changed and [18] where the crystal position was changed. The results are presented on figure 4.2.

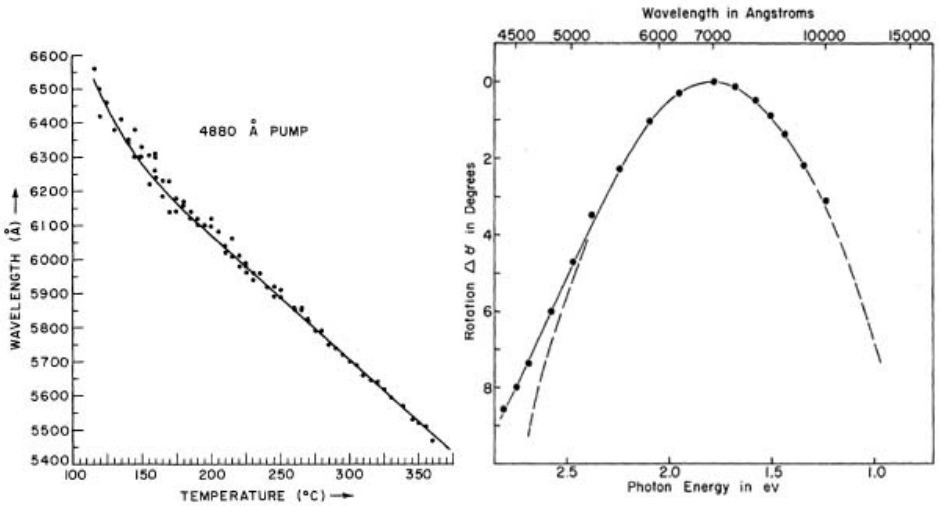

Figure 4.2: Left panel: dependence of the signal wavelength on the temperature taken form [17]. Right panel: relation between the angle of the crystal orientation and the wavelength of the signal taken from [18].

As it was shown, the authors have succeeded in the tuning of the signal wavelength from 4000 to 16000 Å. The effect of optical parametric amplification (OPA)

has a great application in the technologies of tunable lasers, where the most famous Ti:sapphire laser is completely based on the OPA.

4.1.3 Optical phase conjugation

As it was stated in previous chapter, the light propagating in the medium could scatter by the Mandelstam-Brillouin mechanism, and the frequency of light is changed most significantly when the backscattering occurs. So three waves are coupled in the medium: incident electromagnetic wave with frequency w_0 and wave vector $\mathbf{k}_0$, scattered electromagnetic wave w_s, $\mathbf{k}_s$ and acoustic wave $w_{ac} = w_0 - w_s$, $\mathbf{k}_{ac} = \mathbf{k}_0 - \mathbf{k}_s$. At moderate light intensities the probability of the scattering is not very high and the medium remains almost transparent for the light. However, it was shown[19], that after some threshold intensity, the stimulated scattering process takes place and the intensities of both scattered light and acoustic wave increase significantly. Because of stimulated Brillouin scattering (SBS), the medium becomes opaque and almost all light is reflected backwards.

In 1972 Zel'dovich et al. performed an experience on SBS and they have discovered an interesting effect [20]. They distorted the red laser pulse by the plate of a frosted glass and then they turned it to the tube filled by the methane gas. Thanks to the stimulated Brillouin scattering, the light was reflected backwards. Surprisingly, when the reflected beam passed the glass plate again it appeared to be almost undistorted. One could write the following wave equation for the reflected wave $E_s(r_\perp, z) = e^{-ik_s z}\varepsilon_s(r_\perp, z)$:

$$\frac{\partial \varepsilon_s}{\partial z} + \frac{i}{2k_s}\Delta_\perp \varepsilon_s + \frac{1}{2} g\left(r_\perp, z\right) \varepsilon_s = 0, \tag{4.5}$$

where the gain $g\left(r_\perp, z\right)$ is defined by the local intensity of the incident light $g\left(r_\perp, z\right) \sim \left|E_0\left(r_\perp, z\right)\right|^2$. This equation is conjugated to the wave equation describing the incident electromagnetic wave:

$$\frac{\partial \varepsilon_0}{\partial z} - \frac{i}{2k_0}\Delta_\perp \varepsilon_0 = 0. \tag{4.6}$$

Thanks to this, the reflected wave field is complex conjugated to laser field: $E_s\left(r_\perp, z_0\right) \sim E_0^*\left(r_\perp, z_0\right)$. One can consider, that scattering process reverses in time the laser pulse and because of that, when it goes through the frosted glass plate for the second time, it experiences the same changes but back in time. Finally, it arrives to the source, almost undistorted. This effect was called the effect of *phase conjugation* or *wavefront reversal*.

Phase conjugation effect could be obtained also by a four wave mixing (FWM) technique [21, 22]. The semiconductor sample is illuminated by two pump and one probe beams. If the j-th wave could be expressed as $E_j(\mathbf{r}, t) = \frac{1}{2}E_j(\mathbf{r})e^{i(\omega_j t - \mathbf{k}_j \mathbf{r})} + c.c.$, then the polarization term of the third order would be:

$$P_{\mathrm{NL}} = \chi^{(3)}(E_1 + E_2 + E_3)^3; \tag{4.7}$$

this could give rise to different additional harmonics of frequencies $\omega = \pm\omega_1 \pm \omega_2 \pm \omega_3$. The same could be written for their wave-vectors. However, if we consider that $\omega_1 = \omega_2 = \omega_3$ and $\mathbf{k}_1 = -\mathbf{k}_2$, then because of phase-matching conditions, the new (signal) wave will effectively appear with a frequency $\omega_s = \omega_{1,2,3}$ and the wave-vector $\mathbf{k}_s = -\mathbf{k}_3$. Thus, as opposed to normal mirrors, where only the component of wave vector normal to the plane of the mirrors changes its sign, in phase conjugating mirrors, all three components change their sign and the reflected beam becomes parallel to the incident one. However, the frequency does not change its sign, and this makes the reflected wave "reversed in time" with respect to the incident.

4.2 NLO in optical microcavities

Confining the electromagnetic wave in the cavity allows to obtain significant intensities of the field inside, even with moderate pump intensities. By the coupling with quantum well excitons, cavity photons form polaritons, which interact with each other by their excitonic fraction. There is no center of inversion in GaAs, so the non-linear effects coming from the second order of the field amplitude should exist. However, all these effects usually couple the initial waves with waves twice higher or twice smaller in frequency which are not in cavity resonance and they decay rapidly. Thus, non-linearities for cavity polaritons are usually described by the third order of the field amplitude, and the wave equations can be written in the form of nonlinear Schroedinger equation.

4.2.1 Optical parametric oscillator

The key feature of cavity polaritons is the definite relation between the in-plane wave-vector and the angle of emission. This fact simplifies the creation and detection of certain polariton states. In 2000, a seminal work on angle-resonant stimulated polariton amplifier[2] has been published. It was a pulsed pump-probe experiment, where the pump pulse excited polaritons resonantly at some angle θ_p, and a probe pulse was directed normally to the plane. The scheme of the process is illustrated at the fig.4.3 (b).

In other words, two polariton states were populated: one at at some wave-vector $\mathbf{k}_p$ and one in the bottom of the dispersion curve, with zero wave vector. It was shown, that when $\theta_p = 16.5°$ in the presence of the pump pulse, the intensity of the normally reflected light increases by two orders of magnitude with respect to the case when the pumping is switched off.

Authors claimed, that this experiment was the evidence of the stimulated scattering process of two "pump" photons, one of which was scattered to the ground probe state, and another to a state with $\mathbf{k}_s = 2\mathbf{k}_p$. This effect is similar to the optical parametric amplification effect in the bulk discussed in 4.1.2.

The same year there was another work done by R. M. Stevenson et al [3]. Authors pumped continuously the microcavity containing three InGaAs quantum wells at

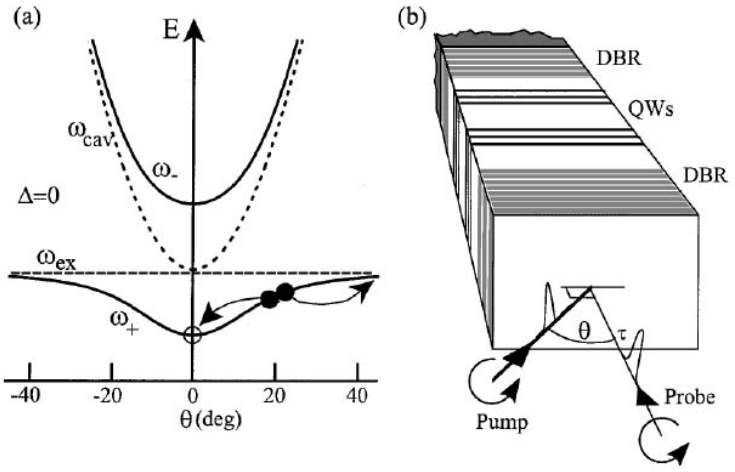

Figure 4.3: (a) Cavity polariton dispersion. Closed (open) circles point the pumped (probed) states. (b) Scheme of the sample and the geometry of the experiment. Image was taken from [2].

some nonzero angle. When the excitation intensity exceeded some threshold value, strong redistribution of polariton occupancies occurred, notably, a strong polariton population at two specific wave vectors (0 and $3.9 \times 10^4 cm^{-1}$) was observed (fig. 4.4).

The mechanism of formation of signal and idler states in this work is similar to the previous one. Two polaritons could be scattered by each other to two specific states, defined by the momentum and energy conservation law and the obtained s- and i-states could further stimulate the scattering. At some point, the stimulated scattering process becomes faster than the polariton lifetime and the population of two additional states increases abruptly.

Theory of the kinetics of three coupled states was developed by Ciuti et al. in the work [4]. The main result was that the kinetics of the signal state with k wave-vector is proportional to:

$$\frac{d}{dt}N_k(t) \sim E_k^{\text{int}} P_{k_p}^2 e^{-i2\omega_p t} \left\langle p_k^\dagger(t) p_{k_{idler}}^\dagger(t) \right\rangle , \tag{4.8}$$

where E_k^{int} is the energy of polariton-polariton interaction, P_{k_p} is the pump-induced polarization, ω_p is the pump frequency, $\left\langle p_k^\dagger(t) p_{k_{idler}}^\dagger(t) \right\rangle$ is the anomalous quantum correlation between signal ($p_k^\dagger(t)$ is the signal polariton creation operator) and idler ($p_{k_{idler}}^\dagger(t)$ is the idler polariton creation operator), whose kinetics in its turn is proportional to:

$$\frac{d}{dt}\left\langle p_k^\dagger(t) p_{k_{idler}}^\dagger(t) \right\rangle \sim E_k^{\text{int}} P_{k_p}^{*2} e^{i2\omega_p t} \left[1 + N_k(t) + N_{k_{idler}}(t)\right] . \tag{4.9}$$

These equations show, that besides spontaneous, there is a stimulated scattering due to the signal and idler states. In works [2] - [4] the four polariton states were

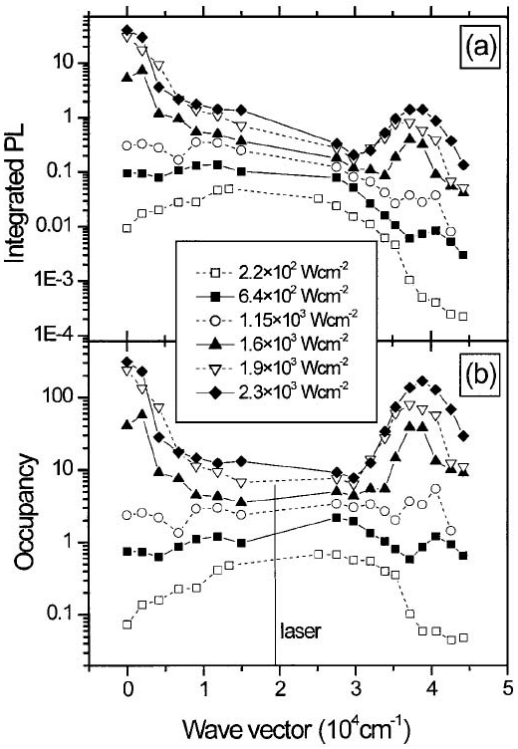

Figure 4.4: (a) Integrated PL intensities vs wave-vector for different excitation intensities. (b) Occupancy of the polariton states calculated taking into account the photonic fraction of the polariton. Image was taken from [3].

coupled by the interactions (two of them are identical), so the effect was similar to the four wave mixing in the bulk, considering two identical pump beams. However, such stimulated polariton-polariton scattering is called usually the *optical parametric oscillator* (OPO). Nevertheless, the standard four wave mixing effect was also observed for cavity polaritons [23, 24].

4.2.2 Bistability

In 2004, the optical bistability effect in microcavity was observed by Baas et al. [5]. Authors considered the optical parametric oscillator and the energy of pumping was detuned with respect to the resonance. The hysteresis in the dependence of the signal emission intensity vs the excitation intensity was traced (fig. 4.5).

Mathematically, the bistability effect could be described by the solution of following coupled equations for three (pump, signal and idler) states:

$$\begin{aligned}
\frac{dp_s}{dt} &= -\left[\gamma_s + iE_{LP}(k_s) + 2i\alpha_s|p_p|^2\right] p_s + E_{\text{int}} p_i^* p_p^2, \\
\frac{dp_p}{dt} &= -\left[\gamma_p + iE_{LP}(k_p) + 2i\alpha_p|p_p|^2\right] p_p - 2E_{\text{int}} p_p^* p_s p_i - C_p\sqrt{2\gamma_a} A_p^{in}, \\
\frac{dp_i}{dt} &= -\left[\gamma_i + iE_{LP}(k_i) + 2i\alpha_i|p_p|^2\right] p_i + E_{\text{int}} p_s^* p_p^2.
\end{aligned} \tag{4.10}$$

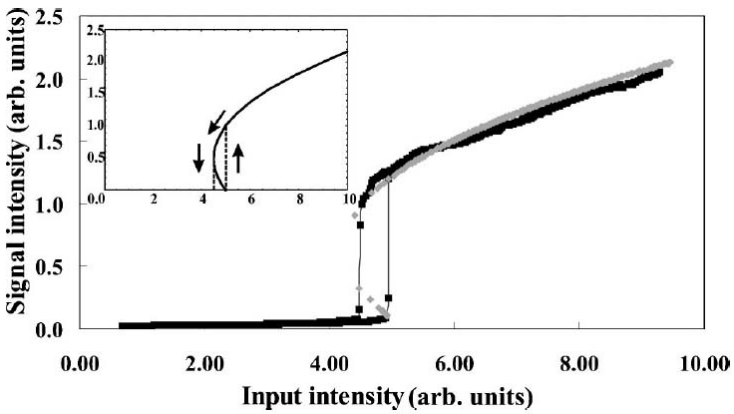

Figure 4.5: Hysteresis loop in the dependence of the emission intensity of signal on external pump intensity. Grey curve is the theoretical fitting. Image was taken from [5].

Here γ_j is the linewidth of the j-th mode, $E_{LP}(k)$ is the bare lower branch of polariton dispersion, α_j is the nonlinear coupling constant between j-th mode with the pump mode, E_{int} is the interaction energy. Term $C_p\sqrt{2\gamma_a}A_p^{in}$ describes the coherent resonant pumping in the p-state. In the stationary regime, the solution gives the following dependence between the excitation intensity P_p^{in} and intensity of the signal emission P_s:

$$\left|\bar{P}_p^{in}\right|^2 = (1+\Delta^2)\left|\bar{P}_s\right|^4 + 2(1-\Delta_p\Delta)\left|\bar{P}_s\right|^2 + 1 + \Delta_p^2, \tag{4.11}$$

where $\bar{P}_{p,s}^{in} = P_{p,s}^{in}(1+\Delta^2)^{-1/4}$, and Δ and Δ_p are the detunings of signal and pump mode normalized to their half width at half maximum. The equation 4.11 gives the condition for the bistability existence: $\Delta_p\Delta > 1$. In this case there is a region where the P_s has three solutions with a single P_p^{in} and the curve P_s vs P_p^{in} becomes hysteresis like, as it is shown by the grey curve in fig. 4.5.

The population of these states depends strongly on the detuning of the laser - the far it is from the resonance, the less efficient is the pumping. However, the resonant frequencies of the states could be tuned because of the exciton-exciton repulsive interaction - the stronger state is populated, the higher is its frequency. When the pump intensity is strong enough, it could move the frequency of the state close to the laser level, the population process will get the avalanche form and it will increase abruptly. This is the physical meaning of the bistability effect.

The experiment on bistability considered the unpolarized polariton states, and it has shown that the polariton-polariton interaction is generally repulsive. However, polaritons are bosons with non-zero angular momentum, whose projection on the chosen axis could be either plus either minus one. The strong spin anisotropy of the polariton-polariton interaction gives rise to a set of multistability effects which have been recently predicted [25, 26] and observed [6]. However, before the description of these effects, we should discuss more thoroughly the nature of spin-anisotropic

polariton-polariton interaction.

4.2.3 Polariton-polariton interaction

The major contribution to the interaction between unpolarized excitons comes from the triplet state. The theory of co-polarized 2D exciton-exciton interaction was developed in [27]. Authors considered the scattering of two excitons with wave-vectors **K** and **K'** to new states with wave-vectors $\mathbf{K}+\mathbf{k}$ and $\mathbf{K}-\mathbf{k}$. The matrix element of the Coulomb interaction could be written as a sum of four contributions:

$$H_{SS'}^{S_f S_f'} = \langle S \mid S_f \rangle \left\langle S' \,\middle|\, S_f' \right\rangle H_{dir} + \left\langle S \,\middle|\, S_f' \right\rangle \langle S' \mid S_f \rangle H_{exch}^{X} + S_{exch}^{e} H_{exch}^{e} + S_{exch}^{h} H_{exch}^{h}, \tag{4.12}$$

where the first term describes the direct Coulomb interaction, second term describes the exchange of the exciton as a whole, and the two last terms describe the electron and hole exchange. The authors have shown that $H_{dir} = 0$ when the $m_e = m_h$ or when $k = 0$. In other words, the direct scattering is inefficient in the case of excitons with small wave-vectors. The matrix elements for the exciton exchange interaction could be written as:

$$H_{exch}^{X}(\Delta K, k, \theta) = -\frac{1}{A}\frac{e^2}{\varepsilon} a_{2D} \left(\frac{2}{\pi}\right)^2 I_{dir}\left[\sqrt{(\Delta K)^2 + k^2 - 2\Delta K k \cos(\theta)}\right], \tag{4.13}$$

where

$$I_{dir}(q) = \frac{4\pi^3}{q a_{2D}} \left\{ \left[4 + (\mu_e q a_{2D})^2\right]^{-3/2} - \left[4 + (\mu_h q a_{2D})^2\right]^{-3/2} \right\}^2. \tag{4.14}$$

$\Delta K = |K - K'|$, θ is the angle between $K - K'$ and k, a_{2D} is the Bohr radius of the exciton and A is the normalization coefficient.

$I_{dir}(q)$ is zero for $q = 0$ and reaches its maximum value which is of order of 1 at very high q

The matrix element for electron and hole exchange process would take this form:

$$H_{exch}^{e,h}(\Delta K, k, \theta) = -\frac{1}{A}\frac{e^2}{\varepsilon} a_{2D} \left(\frac{2}{\pi}\right)^2 I_{exch}(\Delta K, k, \theta, \mu_{e,h}). \tag{4.15}$$

The value of I_{exch} could be found numerically and for the zero k it has the value -15 when the maximum value of $I_{dir}(q)$ is of the order of 1. It means that for small k the main mechanism of exciton-exciton interaction is coming from the electron-electron or the hole-hole exchange.

The light interacts with bright excitons and could form two polariton states: $|\pm 1>$, and thus there could be two different situations of polariton-polariton interaction - when polaritons are co- or cross-polarized. In the first case the final state of the exchange interaction is the same as the initial one, so electron or hole exchange

interaction increases the energy of polaritons proportionally to the overlapping of the wave-functions of their carriers, and the energy shift of the polaritons U_{ex}^{d} reads:

$$U_{ex}^{d} = \pi a_{2D} n X^2 \frac{e^2}{\varepsilon}, \tag{4.16}$$

where X is the Hopfield coefficient (excitonic fraction of the polariton) and n is the polariton density.

In the second case, when the polaritons are polarized oppositely, the exchange interaction turns them into dark states. As opposed to quantum well excitons, for which the dark states are close in energy to the bright states, in the strongly coupled system of cavity polaritons there is a significant energy gap between them Δ_{bd}, therefore, the exchange interaction between the two cross-polarized polaritons is relatively week.

Moreover, to consider the energy shift of two cross-polarized polaritons, we should consider the interactions conserving their states. This could be achieved by the consideration of the second-order processes involving the intermediate states such as the quantum confined state which causes the Van-der-Waals interaction[28], the dark states[29, 30] and the biexciton states[31].

The shift of the energy of particles obtained due to the second order scattering process involving the energy levels split by the value Δ reads [32]:

$$\Delta_0 = \frac{\Delta}{2}\left(\sqrt{1 - \frac{4M^2}{\Delta^2}} - 1\right), \tag{4.17}$$

where M is the matrix element of the scattering. So for the three mentioned above processes (Van-der-Waals interaction, scattering via dark and biexciton states) one could write three energy shift terms (U_{VdW}, U_{ex}^{i} and U_{be} respectively):

$$U_{VdW} = \frac{\Delta_{eo}}{2}\left(\sqrt{1 - \frac{\left(e^2 L_z n X^2\right)^2}{\varepsilon^2 \Delta_{eo}^2}} - 1\right), \tag{4.18}$$

$$U_{ex}^{i} = \frac{\Delta_{bd}}{2}\left(\sqrt{1 - \frac{\left(\pi e^2 a_{2D} n X^2\right)^2}{\varepsilon^2 \Delta_{bd}^2}} - 1\right), \tag{4.19}$$

$$U_{be} \approx \frac{\Delta_{be}}{2}\left(\sqrt{1 - \frac{\left((1-X^2)(X\hbar\Omega_R \pi a_{2D}^2 n\right)^2}{\Delta_{be}^2}} - 1\right). \tag{4.20}$$

Here, L_z is the quantum well size, Ω_R is the Rabi frequency and Δ_{eo}, Δ_{bd} and Δ_{be} are the sizes of the energy gaps between initial and virtual states.

The Van-der-Waals interaction affects both co- and cross-polarized polaritons, when the interaction via the dark and biexciton states shifts the energy only of cross-polarized polaritons. As they come from the scattering processes of the second order, all these interactions are attractive and cause the redshift of interacting

particles. The polariton-polariton interactions could be embedded in the spinor Gross-Pitaevskii equations to the interaction terms $\alpha_{1,2}$ this way:

$$\begin{aligned} \alpha_1 n &= U_{VdW} + U^d_{ex}, \\ \alpha_2 n &= U_{VdW} + U^i_{ex} + U_{be}. \end{aligned} \tag{4.21}$$

From the above discussion, it follows that the co-polarized polaritons show repulsive interactions, while cross-polarized polaritons attract each other, and usually $|\alpha_2| \ll |\alpha_1|$. The theory of polariton-polariton scattering was confirmed by numerous experimental works like [32, 33]. The spin anisotropy of polariton-polariton interaction led to the prediction and observation of a wide variety of remarkable phenomena, such as the inversion of the linear polarization during polariton-polariton scattering processes [33], the spin-Meissner effect [34], the stability of half-topological defects [35], and the polariton multistability [25, 26],

4.2.4 Multistability

The spin-anisotropy of the polariton-polariton interaction obviously should affect the polariton bistability effect whose properties should depend strongly on the polarization of the external pumping. The first prediction and theoretical description of the polariton multistability effect were made by N. A. Gippius et al. in [25]. The authors have considered a continuous wave quasi-resonant optical pumping of the polariton ground state. Coherent polariton state consists of two coupled components (ψ_+ and ψ_-) which energy shifts depends on their population as:

$$\Delta \mathrm{E}^{\pm} = \alpha_1 |\psi_{\pm}|^2 + \alpha_2 |\psi_{\mp}|^2. \tag{4.22}$$

The authors have started with simple spinor Gross-Pitaevskii equations from which they derive the relation between the pump properties (polarization ρ_p and intensity I) and the number of polaritons $N = |\psi_+|^2 + |\psi_-|^2$ and their polarization degree $\rho_c = (|\psi_+|^2 - |\psi_-|^2)/N$:

$$\begin{aligned} I/4\tau &= [\Omega^2 + \tau^{-2} + (\alpha_1 - \alpha_2)(1 - \rho_c^2)]\Omega N, \\ \rho_p I/4\tau &= [\Omega^2 + \tau^{-2} - (1/4)(\alpha_1 - \alpha_2)^2(1 - \rho_c^2)N^2]\rho_c N, \end{aligned} \tag{4.23}$$

where $\Omega = \omega_0 + \omega + \alpha_1 N$, ω is the frequency of the laser and ω_0 is the frequency of the polariton ground state, τ is the polariton lifetime.

Equations show that only when the external pumping is purely circularly polarized, the polarization degree of the transmitted beam coincides with it. In other cases ρ_c differs from the ρ_p and, moreover, the polaritons could be almost circularly polarized in the case of linearly polarized pumping. Also, if one considers the dependence of the polariton quantity or of the polariton polarization degree on the intensity of the excitation, which could be changed adiabatically, one could obtain the hysteresis-like curves (fig. 4.6).

Physically, the process could be described as follows. Linearly polarized excitation creates almost equal number of σ^+- and σ^--polarized polaritons, and the

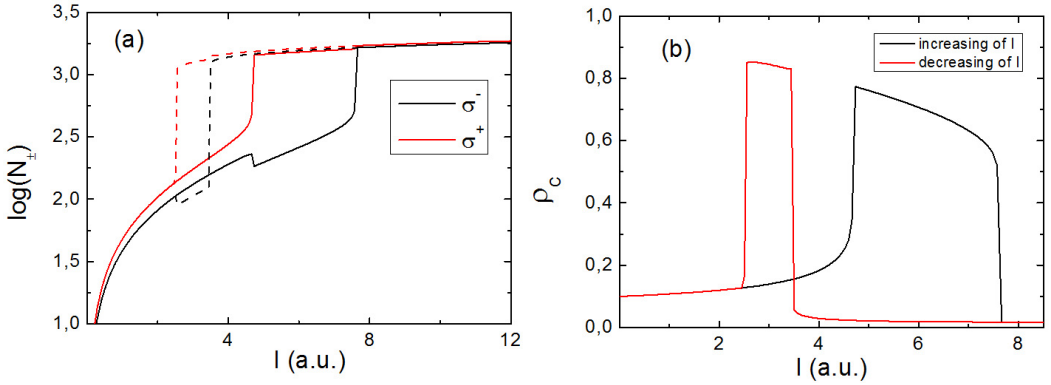

Figure 4.6: (a) Dependences of the polariton populations for σ^+- (red curve) and σ^-- (black curve) polarized components on the intensity of excitation. Solid (dashed) lines show the case when I was adiabatically increased (decreased). (b) Degree of polaritonic circular polarization for increasing (black curve) and decreasing (red curve) of the pump intensity. Calculations were performed for almost linearly polarized excitation and for the case of $\alpha_2 = -0.1\alpha_1$.

blueshift of their energy is proportional to their quantity. Above some intensity of the excitation, one of the components passes its threshold, and its population increases abruptly. Because of the negative sign of α_2, this decreases the energy of the second component and moves it far from the frequency of the excitation laser. This is why, the threshold intensity for the second component is quite larger than for the first. When the excitation intensity is between these two thresholds, the polarization of the transmitted beam is almost circular. The same situation occurs on the way back, when the intesity of excitation is decreased. When one component sharply goes down, other component remains highly populated, and moreover, it moves upwards from the excitation level, which slightly reduces its population.

The multistability effect was studied in different experiments done with continuous wave [6, 36] and pulsed [37, 38] pumping schemes. Indeed, the multistability of polariton population was observed, however, the effects differed from what was expected. For example, let us consider the work done by Paraiso et al. [6]. The authors studied the GaAs/AlAs quantum well embedded in the optical microcavity. However, on top of the cavity spacer, the $6nm$ height and $3\mu m$ diameter mesas were patterned, providing the effective potential well for polaritons. Thus the ground polariton state corresponds to totally confined 0D-polaritons and it is split in the energy from the 2D exciton level by the value of $\delta' = 1.5meV$.

The dependencies of the transmitted power and of the polarization degree of transmitted light on the pump power and on the polarization degree of excitation were measured for different cases. Fig. 4.7 shows the hysteresis-like curves for the quantity of polaritons vs the excitation power for different polarizations of excitations. On contrary to what was predicted theoretically, even at slightly elliptical excitation, the population of two components jumps up simultaneously (Fig. 4.7

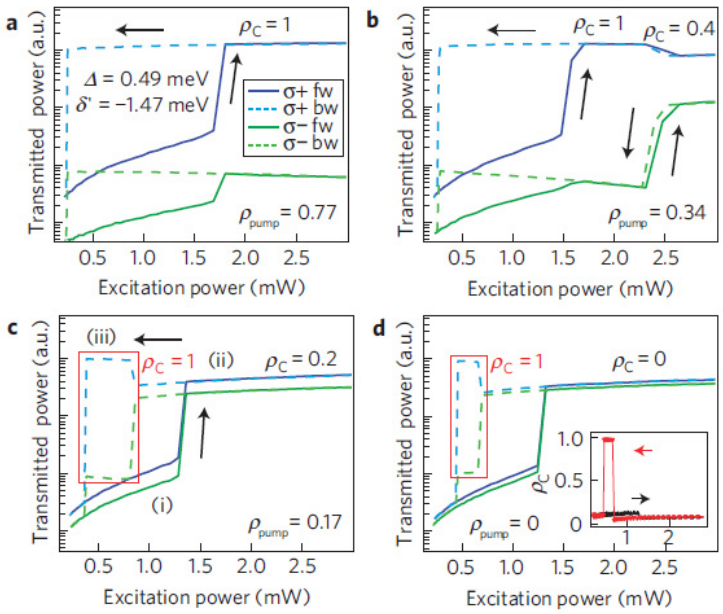

Figure 4.7: Transmitted power vs power of excitation for different values of the pumping degree of circular polarization: (a)$\rho_p = 1$, (b)$\rho_p = 0.4$, (c)$\rho_p = 0.2$, (d)$\rho_p = 0$. Blue (green) lines are for σ^+- (σ^--) polarized light. Inset on (d) shows the degree of polarization of the transmitted light. Image was taken from [6].

(c), (d)). This effect could be obtained if one will put positive α_2 what contradicts to the theory of polariton-polariton interaction.

Another strange effect occurs on the "way back", when the excitation intensity was adiabatically decreased in the case of almost linearly polarized excitation, namely, when the σ^- component jumps down, the σ^+ suddenly jumps up. Indeed it could not be explained just by the positive α_2 since in this case the lower threshold should be also the same for both components.

Thus, this experiment has revealed that the theoretical conception of polariton-polariton interaction was not complete.

4.3 Exciton reservoir

4.3.1 Idea of the reservoir

A set of experiments done on polariton multistability under pulsed excitation should be also noted [37, 38]. In these works, the cavity containing 6 quantum wells was excited by nanosecond pulses and the dynamics of the transmission intensity and polarization was studied. The intensity of the transmitted signal followed very well the intensity of the input signal and its polarization showed remarkable behavior, namely, when the cavity was excited by linearly polarized light, if the excitation intensity was strong enough, the transmitted light becomes elliptically polarized for

some time. The degree of circular polarization of the transmitted light has reached the values of 0.5. However, one more remarkable effect was observed - despite the fact, that intensity of the transmitted light decreased very fast, with the decreasing of the excitation intensity, the energy of emission showed a different behavior. It grew at the beginning of the pulse, what is natural, because the energy of polariton-polariton interaction grew with the polariton density. However, when the intensity of light diminished, and thus the number of polaritons strongly decreased, the energy of the emission remained shifted (fig. 4.8).

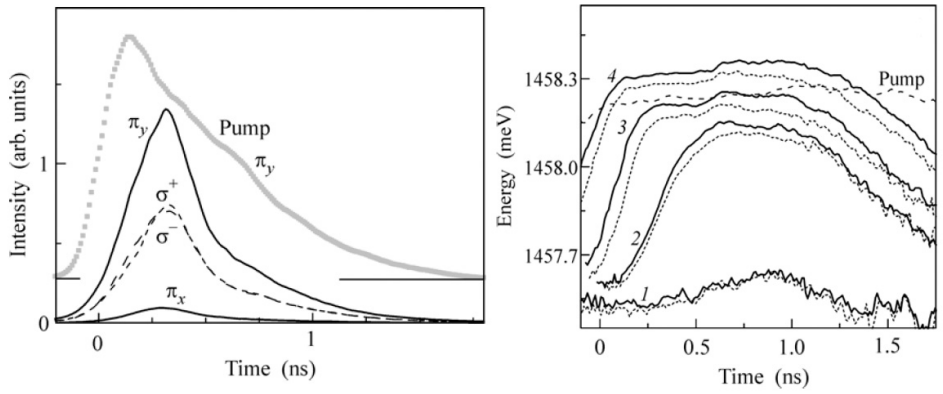

Figure 4.8: Left panel: the time profile of the intensity of the excitation (grey squares) and of the emission (black lines) for different components. Right panel: the energy of the transmitted light measured for different excitation powers. Image was taken from [37].

These measurements have shown, that a long-living component appears in the system under strong excitation, whose characteristic lifetime is of the order of nanoseconds. The authors have developed a phenomenological model that couples the system of polaritons with a noncoherent exciton reservoir system. Then, the following five equations were written:

$$\begin{aligned} i\dot{E}_\pm &= (\omega_c - i\gamma_c)E_\pm + \alpha F_\pm + \beta P_\pm, \\ i\dot{P}_\pm &= \left[\omega_x + V_1|P_\pm|^2 + V_2|P_\mp|^2 + V_1' N/2 - i(\gamma_x + \gamma_{xr} + V_r|P_\mp|^2)\right] P_\pm + AE_\pm, \\ \dot{N} &= -\gamma_r N + 2\gamma_{xr}\left(|P_+|^2 + |P_-|^2\right) + 4V_r|P_+|^2|P_-|^2. \end{aligned} \tag{4.24}$$

Here $F_\pm$, $E_\pm$, $P_\pm$, N describe respectively the external excitation, cavity electromagnetic field, polarization wave and the density of the exciton reservoir, $\gamma_{c,x,r}$ are the broadening of the cavity, exciton and reservoir lines, $\omega_{c,x}$ are the eigenfrequencies of the cavity photon and exciton, α, β, A are the coupling polariton constants. $V_{1,2}$ states the exciton-exciton interaction constants, γ_{xr} states the scattering of the excitons to the reservoir linear by the exciton density, when V_r is the ratio of the scattering process in which two oppositely polarized excitons are involved.

The reservoir is considered to be unpolarized and it shifts the energies of the

σ^+ and the σ^- components equally. The constant $V_1^{'}$ is responsible for this. From the equations 4.24, the authors have successfully described the measured behavior of the system. Also, the exciton reservoir renormalizes effectively the constants of polariton-polariton interaction what could lead to the effective repulsion between cross-polarized components. Indeed, if the density of the reservoir is linear by the density of the ground state $N = \theta(|P_+|^2 + |P_-|^2)$ then one could express the shift of the energy of the ground state as:

$$U_\pm = V_1|P_\pm|^2 + V_2|P_\mp|^2 + V_1^{'}\theta(|P_+|^2 + |P_-|^2) = (V_1 + V_1^{'}\theta)|P_\pm|^2 + (V_2 + V_1^{'}\theta)|P_\mp|^2. \tag{4.25}$$

As one can see, in the cases, when $(V_2 + V_1^{'}\theta) > 0$ the effective interactions between cross-polarized component of the polariton field mediated by the reservoir are repulsive. By this one could describe the problem of the upper threshold in the multistability experiment (that is, the one corresponding to increasing pumping power), discussed in the previous section. The effective repulsive interaction between cross-polarized components will lead to the simultaneous increasing of their populations. However, with the linear dependence of the reservoir density on the polariton density its impossible to describe the problem of the lower threshold.

In order to describe the polariton-polariton interaction more completely, one should consider the mechanism of the reservoir formation in details. One could distinguish three possible types of the reservoir: the reservoirs of biexcitons and of dark excitons formed by the scattering processes between two cross-polarized polaritons. The rates of these processes should be proportional to the product $|P_+|^2|P_-|^2$. The third type of the reservoir consists of simple excitons and it could be formed by the thermal heating of the polariton system. This process should be linear by the density of the ground state and thus it should be dominant in the case of the low densities. In our work [7] we consider the formation of such reservoir.

In this work, we describe theoretically the thermal generation of an excitonic reservoir from a resonantly pumped low energy polariton state. There is a wide literature which has been devoted to the opposite process, namely when an excitonic reservoir is generated from a non-resonant pump. In such a case, particles are injected in long living states (reservoir state) and then dissipate their energy in order to reach short living states, possessing a large photonic fraction. Here, we consider the case when a short living state is populated by a *cw* laser, which generates a distribution function characterized by $T = 0$. The interaction with the lattice phonons warms up the exciton-polariton gas. To our knowledge, this effect has never been studied, being always considered as negligible. As we are going to show below, this is essentially incorrect in structures showing a small Rabi splitting at zero or positive detunings, namely in the widely-studied GaAs-based cavities containing a single QW. In such a case, excitonic states can be populated by a single scattering event on an acoustic phonon. Because of the long life time of these states, excitons can accumulate in the system forming a thermal distribution. The idea of the process is schematically illustrated on fig. 4.9.

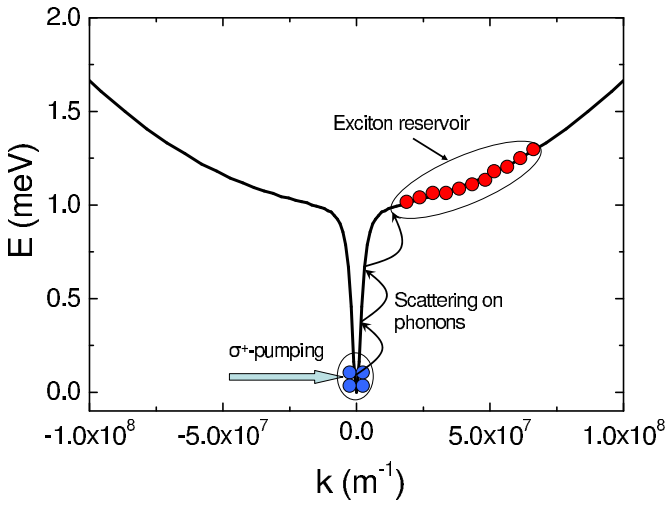

Figure 4.9: The scheme of the process we considered. The circularly polarized pumping is in the ground state. The interaction with phonons provides an exchange of polaritons between the condensate and the reservoir.

The structure we consider is exactly the type of structure which has been used so far in multistability experiments [36, 6]. In the beginning we will solve the semi-classical Boltzmann equations with the ground state being continuously pumped by a resonant, circularly polarized (σ^+) laser as sketched on the figure 4.9. This way of using Boltzmann equations is extremely unusual for the field of exciton-polaritons, since such equations are typically used in order to describe the non-resonant pumping case and the *relaxation* of reservoir excitons toward the lower energy states [39]. We show that in the above-mentioned type of structures, the resonant pumping results in the formation of a thermal exciton reservoir of a moderate density, which we assume to be unpolarized whatever the polarization of the pumping laser. This assumption might not be fully correct, since the interactions with the strongly polarized pumped state should split the circularly polarized reservoir state, which might slow down the standard exciton spin relaxation mechanisms [40]. In the absence of any data allowing to verify the presence of such effect, we assumed in our paper that the exciton spin relaxation time is much shorter than the reservoir exciton lifetime, leading to an unpolarised reservoir.

This reservoir can provoke a blue shift of both polariton spin components by a fraction of meV, comparable with the energy shifts induced by the resonantly pumped state occupation. This can result in an apparent positive α_2, induced by the reservoir. In the second part of the work we solve self-consistently the coupled spinor Gross-Pitaevskii–Boltzmann equations, using the proper attractive α_2 constant for polariton-polariton interaction. We show that the correct accounting for the reservoir generation by acoustic phonons is sufficient to describe the most important features of the experiment of Ref.[6].

4.3.2 Analytical approximation

We begin with a simple analytical model allowing to estimate the importance of the effect we would like to discuss, that is, the population of an exciton reservoir by scattering with phonons up from the coherently pumped condensate. The spatially homogeneous condensate and the reservoir are described by the occupation numbers. In what follows we will use lowercase letters to describe the surface densities (e.g. the condensate density $n_0 = N_0/S$) and uppercase ones for the occupancy of the states.

In the most general case the semi-classical Boltzmann equation for the occupation number of the state with wave-vector $\vec{k}$ reads [41]:

$$\frac{dN_{\vec{k}}}{dt} = P_{\vec{k}} - \Gamma_{\vec{k}} N_{\vec{k}} - N_{\vec{k}} \sum_{\vec{k}'} W_{\vec{k}\to\vec{k}'}(1 + N_{\vec{k}'}) + (1 + N_{\vec{k}}) \sum_{\vec{k}'} W_{\vec{k}'\to\vec{k}} N_{\vec{k}'}. \qquad (4.26)$$

Here the terms with W are the scattering rates between different states, P is the pumping and Γ are the decay rates of the corresponding states. The terms $(1 + N_{\vec{k}})$ account for the bosonic nature of the particles involved, allowing to describe bosonic stimulation towards strongly populated states.

This system of equations will be solved as a whole below, but first we will discuss an approximated solution allowing analytical treatment. Indeed, if one assumes the conditions when single-phonon assisted scattering is stronger than multi-scattering channels, the reservoir states become only coupled with the ground state, and not between each other. In QW-based structures, the exciton-phonon coupling arises between 2D excitons and 3D phonons. The wave vector in the plane is therefore conserved, which is not the case for the wave vector of phonons in the z direction (q_z). This specificity allows to organize energy-conserving scattering processes even in the very sharp polariton dispersion. This process is however limited by a wave vector cutoff provided by $q_{z,max} \sim 1/L$, L being the well width. In practice this cutoff limits the energy exchanged during a polariton-acoustic phonon scattering event to $2 - 3meV$. So qualitatively, one expects single-scattering processes to be dominant if the energy difference between polariton ground state and the excitonic reservoir is smaller than $3meV$, and multi-scattering processes if this energy difference is larger than $3meV$.

In the framework of the above-mentioned assumptions, the equation of motion for the reservoir state $\vec{k}$ writes:

$$\frac{dN_{\vec{k}}}{dt} = -\Gamma_{\vec{k}} N_{\vec{k}} - N_{\vec{k}} W_{\vec{k}\to 0}(1 + N_0) + (1 + N_{\vec{k}}) W_{0\to\vec{k}} N_0. \qquad (4.27)$$

Using the Fermi golden rule and assuming Lorentzian broadening of polariton lines, one can calculate the scattering rate for polariton-acoustic phonon interaction:

$$W^{phon}_{\vec{k}\to\vec{k}'} = \frac{2\pi}{\hbar}\sum_{\vec{q}_z}|M(\vec{q})|^2(0,1+N^{\vec{q}=\vec{k}-\vec{k}'+\vec{q}_z}_{ph})\times\frac{\hbar\gamma_{\vec{k}'}/\pi}{(E(k')-E(k)\pm\hbar\omega_{\vec{q}})^2+(\hbar\gamma_{k'})^2}. \tag{4.28}$$

Here γ_k is the broadening of the polariton line corresponding to the decay rate $\Gamma_{\vec{k}}$ in the Boltzmann equations, ω_q - the phonon frequency, $N^{\vec{q}=\vec{k}-\vec{k}'+\vec{q}_z}_{ph}$ - number of phonons, $M(q)$ - the matrix element of polariton-phonon interaction, taking into account the excitonic fraction of each of the states involved. This exact formulation will be used when a full numerical solution of the Boltzmann equations is obtained. However, it is instructive to further simplify the problem in order to be able to find an analytical solution. To do so, we simplify the above-mentioned scattering rates by assuming that the only dependence of $W^{phon}_{\vec{k}\to\vec{k}'}$ between the ground state and the reservoir state is via the number of phonons $N^{\vec{k}}_{ph}$: $W_{0\to\vec{k}} = WN^{\vec{k}}_{ph}$ and $W_{\vec{k}\to 0} = W(N^{\vec{k}}_{ph}+1)$ where $N^{\vec{k}}_{ph} = 1/(\exp(-\Delta E_k/k_BT)-1)$. We take the value of W as an adjustable parameter, which is determined by comparison between the analytical formula we will derive below and the result of the full numerical simulation. It will be shown in section IV to possess a value of order $10^7 s^{-1}$ using an exciton decay rate $\Gamma_k \approx \hbar/400$ ps. The main approximation performed in the analytical approach is to neglect the above-mentioned wavevector cutoff together with the wavevector dependence of the interaction with acoustic phonons, and the only dependence that is kept is the exponential decrease of phonon occupation numbers for large energies exchanged.

For this system of equations, one can analytically obtain the stationary values of the occupation numbers:

$$N_{\vec{k}} = \frac{N^{\vec{k}}_{ph}}{N_0+N^c_0}N_0. \tag{4.29}$$

from which the total reservoir density can be straightforwardly obtained. Here $N^c_0 = N^{\vec{k}}_{ph}+1+\Gamma_{\vec{k}}/W$ - critical value for N_0, discussed below.

From the previous equation, one can see the existence of two distinct regimes. If N_0 is smaller than N^c_0, the reservoir density increases linearly with N_0. It then saturates when $N_0 \gg N^c_0$. In the latter regime, the reservoir density does not depend on pumping anymore and is proportional to the phonon distribution function. In this regime, the reservoir distribution function is therefore exactly Bose distribution function with chemical potential equal to the energy difference between the the bottom of the bare excitonic branch (the zero energy) and the pumped polariton state [42]. It is anyway always very well approximated by a Boltzmann distribution function, which is fully confirmed by the numerical simulations, whatever the conditions.

The value N^c_0 in fact depends on the wave-vector of the final state and is slightly different for different states, however for the scattering process from the ground

polariton state to the exciton branch, its variation with $\vec{k}$ is not significant. Nevertheless, this variation will be accounted further.

The results of the calculations are presented on the figure 4.10. The dashed lines show the reservoir density n_r calculated with the procedure described above in the saturated regime versus the exciton-photon detuning for 3 different temperatures. The Rabi splitting of the structure is $4meV$, which corresponds to the case of a GaAs cavity containing a single QW [36, 6]. Going towards positive detuning reduces the energy splitting between the ground state and the reservoir, which increases the number of phonons. One can also increase the number of phonons directly, by simply increasing the temperature. In both cases, the reservoir density increases. One should note that with the Rabi splitting of $4meV$ and a positive detuning of $3meV$ the polariton dispersion remains substantially different from the bare exciton dispersion. The photonic fraction is about 0.2 and the energy difference between the polariton and bare exciton energy at $k = 0$ is $1meV$.

Next, in order to check the validity range of our analytical approximation, we have solved numerically the whole system of semi-classical Boltzmann equations where all possible scattering paths are taken into account Eq.4.26. The pumping term is different from zero only for ground state $P_0 \neq 0$. The simulation is carried out until the system reaches a steady-state distribution $N_{\vec{k}}$, that takes about $2ns$. An essential aspect to get a reliable result, is to consider the proper reciprocal space area for the pumped state which is given by $4\pi^2/S$ where S is the system surface. We will take $S = (3\mu\text{m})^2$, in order to be in agreement with the experimental conditions of [6].

The results of the numerical simulations are presented on the figure 4.10 with solid curves. As expected, the analytical approach shows a good accuracy in the positive detuning range when the energy difference between the polariton ground state and the excitonic reservoir is small. In that range, and at $20K$, the densities found are likely to destroy the strong coupling regime, and anyway to provoke strong blue shift due to exciton-exciton interactions. By going to negative detuning, the generated reservoir density drops very rapidly, becoming completely negligible. This drop is explained by the fast decay of the direct scattering processes and the inefficiency of the multiple scattering channels. One should also note that the accounting for polariton-polariton scattering mechanisms brings no change to the present picture as soon as only the polariton ground state is pumped.

The simulations using the complete system of Boltzmann equations have also been performed for a GaAs microcavity showing a significantly larger Rabi splitting of $12meV$. The results are presented on the Fig. 4.11. In that case, the reservoir density generated by the resonant pumping is completely negligible, keeping below to 10^8 cm^{-2} for the values of detuning considered, and the analytical approximation of single-phonon scattering is not applicable.

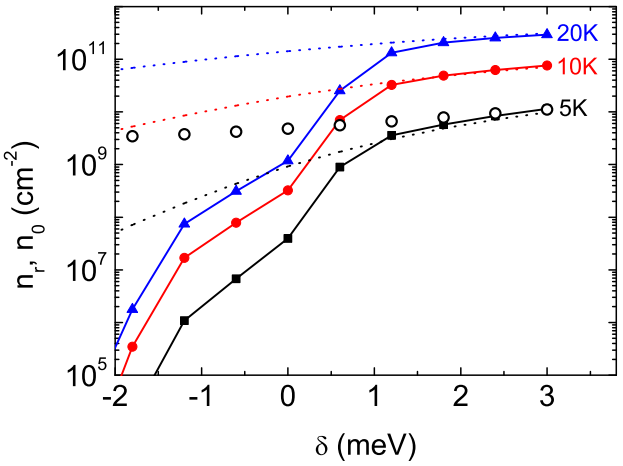

Figure 4.10: Densities of excitons versus detuning for different values of temperature, solid lines - numerically calculated, dashed lines - analytical approximation. Open circles - density of condensate n_0. Rabi splitting $4meV$.

4.3.3 Influence of the reservoir on energy shifting

Our next step is now to consider the impact of the excitonic reservoir, generated under quasi-resonant pumping, on the energy of the two spin components of the condensate. The interaction between excitons has been previously studied theoretically and experimentally, both in the scalar[27] and spinor cases[33, 32], taking the account the fact that the excitons are composite bosons [30]. We assume that this interaction is the same, whether the excitons concerned are both in the condensate, or one of them is in the reservoir.

In the triplet configuration the 2D interaction constant comes mostly from the exchange Coulomb interaction. It can be calculated in the Born approximation yielding the approximate formula $\alpha_1 = 3E_b a_B^2$. In the singlet configuration, the exciton-exciton interaction is a second-order process passing either through the dark exciton states possessing spin ± 2 or trough bi-exciton states. These latter states are usually several meV above the polariton states, which has two consequences: the matrix element of interaction becomes reduced and obtains a negative sign, as any second-order correction for the ground state. We should note, however, that it is possible to have the biexciton state close to the polariton ground state, if the Rabi splitting is small and the detuning is strongly positive[32]. In what follows, we assume that the singlet interaction constant is $\alpha_2 = -0.1\alpha_1$.

The corrections of the energies of the two polarization components of the condensate take into account both interaction constants:

$$\Delta E^+ = \alpha_1 n_+ + \alpha_2 n_-, \tag{4.30}$$

$$\Delta E^- = \alpha_1 n_+ - \alpha_2 n_+, \tag{4.31}$$

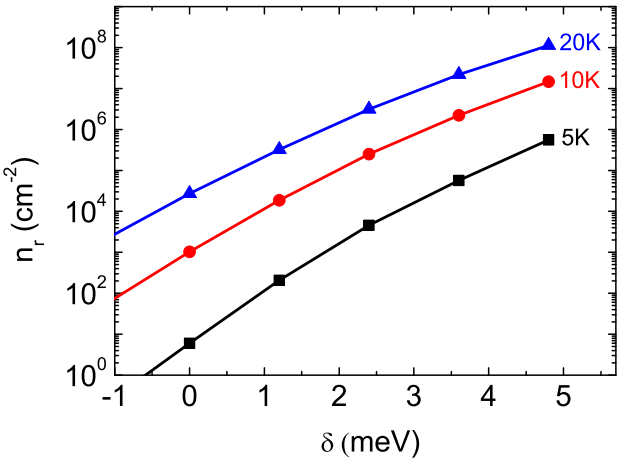

Figure 4.11: Densities of excitons versus detuning for different values of temperature. Rabi splitting $12meV$

where $E^{+,-}$ are the energy shifts of the σ^+ and σ^- polarized component, $n_{+,-}$ are the exciton densities (including both the condensate and the reservoir) and $\alpha_{1,2}$, the interaction constants. If we decompose the total exciton density into reservoir density n_r (the reservoir is not polarized) and condensate density n_0 (the condensate is polarized σ^+, as the pump), we can write the energy shifts as follows:

$$\Delta E^+ = \alpha_2 \frac{n_r}{2} + \alpha_1 \left(\frac{n_r}{2} + n_0 \right), \tag{4.32}$$

$$\Delta E^- = \alpha_2 \left(\frac{n_r}{2} + n_0 \right) + \alpha_1 \frac{n_r}{2}. \tag{4.33}$$

Using this formula, we plot on the figure 4.12 the energy shifts of the two components of the condensate as a function of the detuning, using the values of the reservoir density obtained by solving the full Boltzmann equations. The results presented on the figure correspond to a Rabi splitting of $4meV$ and a temperature $5K$.

We see that in the conditions of this simulation, namely, at relatively small Rabi splittings and quasi-resonant *cw* pumping (as opposed to pulsed excitation), the contribution of the reservoir can totally modify the observed energy shifts. Indeed, at negative detuning the reservoir is not strongly populated, and a redshift of the σ^- component is observed, as one would naturally expect from the negative sign of the α_2 constant. However, at positive detuning the reservoir starts to play a role. Since the reservoir is depolarized, it contains a large number of σ^- excitons which induce a blue shift for the σ^- component of the condensate via the stronger repulsive interactions, which dominate the weak redshift induced by the σ^+ excitons.

Therefore, a measurement of the energy shift of the σ^- component at positive detunings, without including the filling of long-lived reservoir states, can lead to

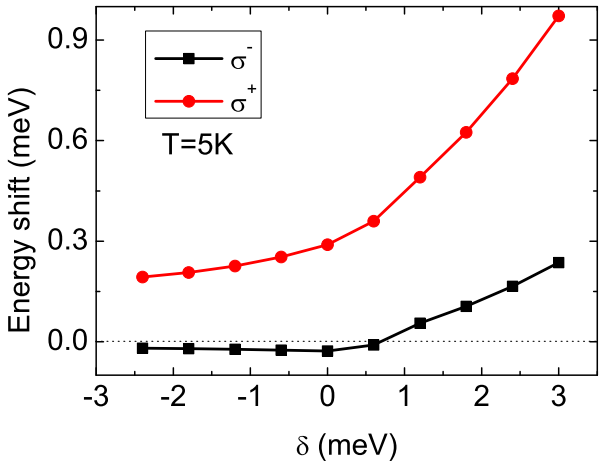

Figure 4.12: Energy shift of σ^+ (red circles) and σ^- (black squares) components of condensate . Rabi splitting $4meV$, temperature $5K$.

inexact conclusions concerning the wrong sign and the magnitude of the polariton-polariton interaction constants.

4.3.4 Application of the model

One of the important effects based on the energy shifts of the polariton mode is the bistability (or multistability in the spinor case) of the polariton mode under quasi-resonant pumping. Indeed, if the system is pumped with a *cw* laser whose frequency is above that of a bare polariton mode, blue shift of the macrooccupied mode will bring it closer to the laser, increasing the efficiency of the pumping. Therefore, at some pumping intensity the mode becomes unstable and the population jumps up abruptly. This effect has been predicted to occur also in the spinor case[25], but if one takes into account the negative sign of α_2, it is logical to expect that the jump of one polarization component under elliptical pumping will prevent the jump of the other component by moving it off-resonance.

In the first experimental work on polariton multistability[6], the authors have, in particular, observed an abrupt simultaneous increase of the amplitudes of both components, when the polarization of the excitation light is almost linear, but slightly elliptic (Fig 1(d,e) in Ref.[6]). This contradicts the expected behavior mentioned above, and was explained by the authors by introducing a positive sign of α_2, that is, repulsive interactions for excitons with opposite spins.

In this section we show how the formation of an excitonic reservoir in this particular type of experiment influences the observed behavior of the polariton modes in the multistable regime. In order to describe correctly the behavior of the macrooccupied modes under quasi-resonant pumping, we write the coupled Gross-Pitaevskii equations with pumping and decay for both polarization components $\Psi_\pm$, taking

into account the interactions with the reservoir.

$$i\hbar\frac{d\Psi_\pm}{dt} = \left[-i\frac{\gamma}{2} + \frac{\alpha_1}{S}|\Psi_\pm|^2 + \frac{\alpha_2}{S}|\Psi_\mp|^2 + \frac{(\alpha_1+\alpha_2)}{2}n_r\right]\Psi_\pm + P_\pm e^{i\Delta/\hbar t}. \quad (4.34)$$

Here, γ defines the broadening of the polariton line, S the surface area of the polariton spot, $P_\pm$, the excitation density and n_r, the density of excitons in the reservoir. The detuning between the laser and the pumped polariton state $\Delta = 0.5meV$, as in the experiment. We do not account the spatial distribution of the $\Psi_\pm$ as far as we want to consider quasi homogeneous (0D) case. The density of the reservoir can be obtained analytically, following the approach introduced in the beginning:

$$n_r = \frac{1}{2\pi}\int_0^\infty \frac{N_{ph}^k\left(|\Psi_+|^2 + |\Psi_-|^2\right)}{N_{ph}^k + 1 + |\Psi_+|^2 + |\Psi_-|^2 + \Gamma_k/W_k} kdk. \quad (4.35)$$

Taking an average value for $\frac{\Gamma_k}{W_k}$ and considering parabolic exciton dispersion, we can evaluate this integral analytically and obtain the solution for n_r as a function of $\left(|\Psi_+|^2 + |\Psi_-|^2\right)$:

$$\begin{aligned} n_r &= \frac{1}{4\pi}\left(|\Psi_+|^2 + |\Psi_-|^2\right)\frac{B}{C}\ln\left|1+\frac{C}{A}\right|, \quad (4.36)\\ A &= \left[|\Psi_+|^2 + |\Psi_-|^2 + 1 + \frac{\Gamma}{W}\right]e^{\frac{\delta'}{k_BT}},\\ B &= \frac{2m_X k_B T}{\hbar^2},\\ C &= -\left[|\Psi_+|^2 + |\Psi_-|^2 + \frac{\Gamma}{W}\right]. \end{aligned}$$

By introducing the above expression in the eq. 4.34, we get a closed equation for the amplitude of the pumped polariton mode. An essential parameter of the model is the ratio $\frac{\Gamma}{W}$ (which has to be assumed constant in order to obtain analytical results). It can be estimated by calculating with the full system of semi-classical Boltzmann equations the value of the reservoir density n_r as a function of the condensate density $n_0 = \frac{|\Psi_+|^2+|\Psi_-|^2}{S}$. We have then fitted the results obtained numerically by the analytical formula 4.36. The results of this fitting are presented on fig. 4.13. The value obtained for the fitting parameter $\frac{\Gamma}{W}$ was around 300.

By changing the pump density slowly in time from 0 to some value and back again we can obtain the evolution of the populations of both circularly polarized polariton components and of the excitonic reservoir. The results are presented on the fig. 4.14. Indeed, a simultaneous jump of both circular components, and of the reservoir is visible when increasing the pumping power. The strong rise of the σ^+ polariton density associated with the passage of the bistable threshold leads to a strong rise of the population of the unpolarized excitonic reservoir which provokes

a blue shift of the polariton energy of the σ^- component. This blue shift overcomes by far the red shift induced by the attractive interaction between the opposite spin components of the condensate. It leads to the passage of the bistable threshold for the σ^- component as well.

Another experimental effect is well reproduced when the system is on the upper stability branch and the pumping power is decreased. The σ^--component has a smaller population and therefore jumps down first. At the same time, the population of the other component σ^+ strongly increases. This effect is easy to understand as well. When σ^- jumps down, the energy of σ^+ is still higher that the laser frequency. The jump of σ^- leads to a reduction of the total reservoir density n_r, bringing the frequency of the σ^+ component *closer* to the laser frequency. This makes the pumping more efficient and increases the σ^+ population. When this amplitude in its turn abruptly decreases, the reservoir density jumps down once more, and this causes a second jump down of the σ^--component. So, while the pumping power is decreased, the amplitude of σ^--component undergoes two steps, as it was observed in experiment.

4.3.5 Conclusion

In this chapter we have discussed the numerous non-linear optical effects in different systems. After the description of the general historical background, I have paid attention to the NLO effects observed in optical microcavities and, particularly, to the effects of multistabilities. It was shown, that recent experiments revealed the problems in the understanding of polariton-polariton interactions. Finally, I have presented our work, in which we proposed the mechanism of the exciton reservoir formation.

In this work we present the microscopic mechanism for the build up of the excitonic reservoir and predict strong dependence of the reservoir density on the detuning and the temperature. We have studied the generation of an excitonic reservoir in the case of quasi-resonant pumping of a polariton mode. Exciton-polaritons from the condensate are scattered up with phonons. It was shown that in structures with small Rabi splitting and positive exciton-photon detuning, this process provides a strongly populated reservoir which influences the behavior of the resonantly pumped polariton modes. Because of the reservoir, it is possible to observe a blueshift of the polariton condensate component polarized opposite to excitation, while the exciton-exciton interaction constant for opposite spins remains negative (attractive interaction). An analytical model allowed us to describe the multistable behavior of the polariton system recently evidenced experimentally [36, 6].

The present calculations support the phenomenological theory [37, 38] for the case of small detuning between the polaritons and the excitons. The successful description of experimental data for both time-resolved and *cw* resonant pumping shows the important role of the "reservoir" in these experiments. This concept also allows to resolve several contradictions in the interpretation of data obtained in *cw* and ps-range pulsed excitation experiments (see also detailed discussion in

Ref.[38]). A coupling with the reservoir also had to be introduced to describe OPO polarization dynamics in earlier experiments [43]

However, in the framework of this model, we have not yet been able to fully describe the experimental behavior reported in [6] for large circular polarization degree of the pump. We believe that the hypothesis of the fully unpolarized excitonic reservoir might be no more valid in the case of quasi-circular pumping. Indeed, the jump up of one circular component only induces an energy splitting between σ^- and σ^+ excitons in the reservoir, which may substantially slow down the spin relaxation. Thus, the reservoir may become spin polarized which would strongly affect the behavior of the pumped modes. The proper analysis of these phenomena requires a more complete description of the dynamics of the coupled condensate-reservoir system and will be addressed in future works.

Also, the consideration of the homogeneous states is the approximation of our model. Finite size of the pumping spot should result in the initial distribution of polaritons over all states. Also, the propagation of polaritons should lead to the effective decreasing of their life-time inside the spot. On the other side, reservoir excitons are very slow comparing to the near ground state polaritons and anyway could be considered as static objects.

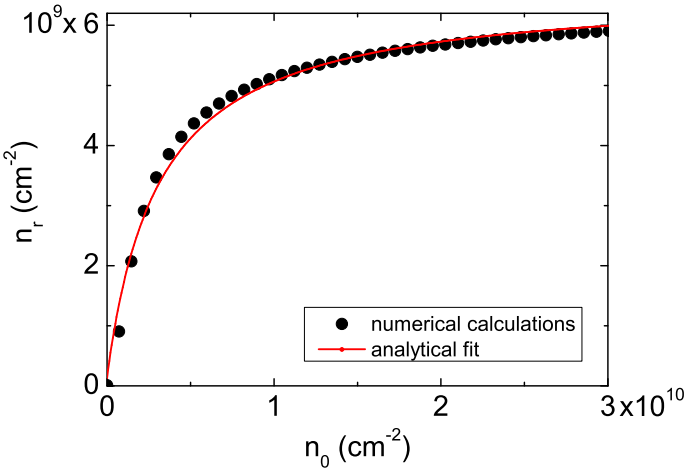

Figure 4.13: Black circles - dependence of n_r on n_0 calculated numerically. Red curve - fit of this data by the eqs. 4.36. Fitting gives $\frac{\Gamma}{W} = 274$. This value corresponds to $n_0^c = \frac{N_0^c}{S} = 3 \cdot 10^9 cm^{-2}$

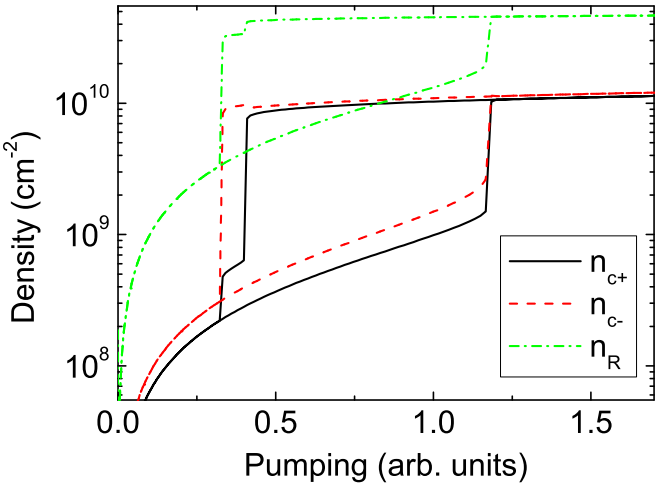

Figure 4.14: Dependence of the amplitudes of σ^+ (red dashed line) and σ^- (black solid line) components on pump power, when it increases and decreases. Polarization of pumping $\rho_{pump} = 0.1$

Bibliography

[1] P. A. Franken, A. E. Hill, C. W. Peters, and G. Weinreich, Generation of Optical Harmonics, *Phys. Rev. Lett.* **7**, 118 (1961). (Cited on pages 79 and 81.)

[2] P. G. Savvidis, J. J. Baumberg, R. M. Stevenson, M. S. Skolnick, D. M. Whittaker, and J. S. Roberts, Angle-Resonant Stimulated Polariton Amplifier, *Phys. Rev. Lett.* **84**, 1547 (2000). (Cited on pages 80, 84 and 85.)

[3] R. M. Stevenson, V. N. Astratov, M. S. Skolnick, D. M. Whittaker, M. Emam-Ismail, A. I. Tartakovskii, P. G. Savvidis, J. J. Baumberg, and J. S. Roberts, Continuous Wave Observation of Massive Polariton Redistribution by Stimulated Scattering in Semiconductor Microcavities, *Phys. Rev. Lett.* **85**, 3680 (2000). (Cited on pages 80, 84 and 86.)

[4] Cristiano Ciuti, Paolo Schwendimann, and Antonio Quattropani, Parametric luminescence of microcavity polaritons, *Phys. Rev. B* **63**, 041303(R) (2001). (Cited on pages 80 and 85.)

[5] A. Baas, J.-Ph. Karr, M. Romanelli, A. Bramati, and E. Giacobino, Optical bistability in semiconductor microcavities in the nondegenerate parametric oscillation regime: Analogy with the optical parametric oscillator, *Phys. Rev. B* **70**, 161307 (2004). (Cited on pages 80, 86 and 87.)

[6] T. K. Paraiso, M. Wouters, Y. Leger, F. Morier-Genoud and B. Deveaud-Pledran, Multistability of a coherent spin ensemble in a semiconductor microcavity, *Nature Materials* **9**, 655 (2010). (Cited on pages 80, 87, 91, 92, 95, 98, 101, 103 and 104.)

[7] D. V. Vishnevsky, D. D. Solnyshkov, N. A. Gippius, and G. Malpuech, Multistability of cavity exciton polaritons affected by the thermally generated exciton reservoir, *Phys. Rev. B* **85**, 155328 (2012). (Cited on pages 80 and 94.)

[8] Serge Haroche, Essay: Fifty Years of Atomic, Molecular and Optical Physics in Physical Review Letters, *Phys. Rev. Lett.* **101**, 160001 (2008). (Cited on page 81.)

[9] J. Wildenauer, Generation of the ninth, eleventh, and fifteenth harmonics of iodine laser radiation, *Journal of Applied Physics* **62**, 41 (1987). (Cited on page 81.)

[10] G. H. C. New and J. F. Ward, Optical Third-Harmonic Generation in Gases, *Phys. Rev. Lett.* **19**, 556 (1967). (Cited on page 81.)

[11] N. H. Burnett, H. A. Baldis, M. C. Richardson, and G. D. Enright, Harmonic generation in CO_2 laser target interaction, *Appl. Phys. Lett.* **31**, 172 (1977) (Cited on page 81.)

[12] A. McPherson, G. Gibson, H. Jara, U. Johann, T. S. Luk, I. A. McIntyre, K. Boyer, and C. K. Rhodes, Studies of multiphoton production of vacuum-ultraviolet radiation in the rare gases, *JOSA B* **4**, 595 (1987) (Cited on page 81.)

[13] M Ferray, A L'Huillier, X F Li, L A Lompre, G Mainfray and C Manus, Multiple-harmonic conversion of 1064 nm radiation in rare gases, *J. Phys. B: At. Mol. Opt. Phys.* **21**, L31 (1988) (Cited on page 81.)

[14] W. H. Louisell, A. Yariv and A. E. Siegman, Quantum Fluctuations and Noise in Parametric Processes. I., *Phys. Rev.* **124**, 1646 (1961). (Cited on page 82.)

[15] J. P. Gordon, W. H. Louisell and L. R. Walker, Quantum Fluctuations and Noise in Parametric Processes. II., *Phys. Rev.* **129**, 481 (1963). (Cited on page 82.)

[16] W. G. Wagner and R. W. Hellwarth, Quantum Noise in a Parametric Amplifier with Lossy Modes, *Phys. Rev.* **133**, A915 (1964). (Cited on page 82.)

[17] B. E. Harris, M. K. Oshman, and B. L. Byer, Observation of tunable optical parametric fluorescence, *Phys. Rev. Lett.* **18**, 733 (1967). (Cited on page 82.)

[18] D. Magde and H. Mahr, Study in ammonium dihydrogen phosphate of spontaneous parametric interaction tunable from 4000 to 16000 A, *Phys. Rev. Lett.* **18**, 906 (1967). (Cited on page 82.)

[19] Chiao R Y, Townes C H and Stoicheff B P, Stimulated Brillouin Scattering and Coherent Generation of Intense Hypersonic Waves, *Phys. Rev. Lett.* **12**, 592 (1964). (Cited on page 83.)

[20] B.Ya. Zel'dovich, V.I.Popovichev, V.V.Ragulskii and F.S.Faisullov,Connection between the wavefronts of the reflected and exciting light in stimulated Mandelshtam Brillouin scattering, *Sov. Phys. JETP* **15**, 109 (1972). (Cited on page 83.)

[21] R. L. Carman, R. Y. Chiao and P. L. Kelley, Observation of Degenerate Stimulated Four-Photon Interaction and Four-Wave Parametric Amplification, *Phys. Rev. Lett.* **17**, 1281 (1966). (Cited on page 83.)

[22] Govind P. Agrawal, Four-wave mixing and phase conjugation in semiconductor laser media, *Optics Letters* **12**, 4 (1987). (Cited on page 83.)

[23] Makoto Kuwata-Gonokami, Shin Inouye, Hidekatsu Suzuura, Masayuki Shirane, Ryo Shimanoy, Takao Someya and Hiroyuki Sakaki, Parametric Scattering of Cavity Polaritons, *Phys. Rev. Lett.* **79**, 7 (1997). (Cited on page 86.)

[24] Masayuki Shirane, C. Ramkumar, Yu. P. Svirko, Takatsu-ku, Hidekatsu Suzuura, Shin Inouye, Ryo Shimano, Takao Someya, Hiroyuki Sakaki, Makoto

Kuwata-Gonokami, Degenerate four-wave mixing measurements on an exciton-photon coupled system in a semiconductor microcavity, *Phys. Rev. B* **58**, 12 (1998). (Cited on page 86.)

[25] N. A. Gippius, I. A. Shelykh, D. D. Solnyshkov, S. S. Gavrilov, Yuri G. Rubo, A. V. Kavokin, S. G. Tikhodeev, and G. Malpuech, Polarization Multistability of Cavity Polaritons, *Phys. Rev. Lett.* **98**, 236401 (2007). (Cited on pages 87, 90 and 101.)

[26] S.S. Gavrilov, N.A. Gippius, S.G. Tikhodeev, and V.D. Kulakovskii, *Journal of Experimental and Theoretical Physics*, **110**, 825 (2010). (Cited on pages 87 and 90.)

[27] C. Ciuti, V. Savona, C. Piermarocchi, A. Quattropani and P. Schwendimann, Role of the exchange of carriers in elastic exciton-exciton scattering in quantum wells, *Phys. Rev. B* **58**, 7926 (1998). (Cited on pages 88 and 99.)

[28] C. Schindler and R. Zimmermann, Analysis of the exciton-exciton interaction in semiconductor quantum wells, *Phys. Rev. B* **78**, 045313 (2009). (Cited on page 89.)

[29] L. Klopotowski, M. D. Martin, A. Amo, L. Vina, I. A. Shelykh, M. M. Glazov, G. Malpuech, A. V. Kavokin, and R. Andre, Optical anisotropy and pinning of the linear polarization of light in semiconductor microcavities, *Solid State Commun.* **139**, 511 (2006). (Cited on page 89.)

[30] M. M. Glazov, H. Ouerdane, L. Pilozzi, G. Malpuech, A. V. Kavokin, and A. D'Andrea, Polariton-polariton scattering in microcavities: A microscopic theory, *Phys. Rev. B* **80**, 155306 (2009). (Cited on pages 89 and 99.)

[31] M. Wouters, Resonant polariton-polariton scattering in semiconductor microcavities, *Phys. Rev. B* **76**, 0453196 (2007). (Cited on page 89.)

[32] M. Vladimirova, S. Cronenberger, D. Scalbert, K. V. Kavokin, A. Miard, A. Lemaitre, J. Bloch, D. Solnyshkov, G. Malpuech, A. V. Kavokin, Polariton-polariton interaction constants in microcavities, *Phys. Rev. B* **82**, 075301 (2010). (Cited on pages 89, 90 and 99.)

[33] Renucci P., Amand T., Marie X., Senellart P., Bloch J., Sermage B., Kavokin K. V., Microcavity polariton spin quantum beats without a magnetic field: A manifestation of Coulomb exchange in dense and polarized polariton systems, *Phys. Rev. B* **72**, 075317 (2005). (Cited on pages 90 and 99.)

[34] Yu. G. Rubo, A.V. Kavokin, and I.A. Shelykh, Suppression of superfluidity of exciton-polaritons by magnetic field, *Phys. Lett. A* **358**, 227 (2006). (Cited on page 90.)

[35] D.D. Solnyshkov, H. Flayac, G. Malpuech, Stable magnetic monopoles in spinor polariton condensates, Phys. Rev. B 85, 073105 (2012). (Cited on page 90.)

[36] D. Sarkar, S. S. Gavrilov, M. Sich, J. H. Quilter, R. A. Bradley, N. A. Gippius, K. Guda, V. D. Kulakovskii, M. S. Skolnick, and D. N. Krizhanovskii, Polarization Bistability and Resultant Spin Rings in Semiconductor Microcavities, *Phys. Rev. Lett.* **105**, 216402 (2010). (Cited on pages 91, 95, 98 and 103.)

[37] S.S. Gavrilov, A.S. Brichkin, A.A. Dorodnyi, S.G. Tikhodeev, N.A. Gippius, V.D. Kulakovskii, Polarization Instability in a Polariton System in Semiconductor Microcavities, *JETP Letters* **92**, 171 (2010). (Cited on pages 91, 92, 93 and 103.)

[38] S. S. Gavrilov, A. S. Brichkin, A. A. Demenev, A. A. Dorodnyy, S. I. Novikov, V. D. Kulakovskii, S. G. Tikhodeev, and N. A. Gippius, Bistability and nonequilibrium transitions in the system of cavity polaritons under nanosecond-long resonant excitation, *Phys.Rev.B* **85**, 075319 (2012) (Cited on pages 91, 92, 103 and 104.)

[39] A. V. Kavokin, J. J. Baumberg, G. Malpuech, F. P. Laussy, *Microcavities* (Oxford University Press, 2007). (Cited on page 95.)

[40] M.Z. Maialle, E.A. De Andrada Silva, L.J. Sham, Exciton spin dynamics in quantum wells, *Phys. Rev. B*, **47**, 15776, (1993). (Cited on page 95.)

[41] A. Kavokin and G. Malpuech, Cavity Polaritons (Elsevier, 2003). (Cited on page 96.)

[42] Of course bare excitons with very small wave vectors do not exist because of their coupling with photons. This is however neglected in the analytical discussion, regarding the fact that the corresponding region of reciprocal space is completely negligible on the excitonic scale. (Cited on page 97.)

[43] D.D. Solnyshkov et al, Semiconductors 41, 1080 (2007). (Cited on page 104.)

Chapter 5

Indirect excitons

Contents

As it was mentioned in the first chapter, bosonic particles could form at low temperatures the new state of matter - Bose-Einstein condensates. However, real bosons, like atoms, are very massive, so the temperature of the transition is extremely low. Because quasi-particles in semiconductors are often much lighter than atoms, they are considered as good candidates to obtain the BEC at reasonable temperatures [1, 2]. On the other hand their finite and often small lifetime complicates the process of thermalization. Thus polaritons or excitons usually recombine emitting light before they interact enough with phonons. The total density of particle usually is also low due to the short lifetime, what demands extremely small critical temperatures for the condensation.

There are several ways to increase the lifetime of the quasi-particles. For example in the case of polaritons, very high-quality cavities were constructed. In order to increase the lifetime of excitons and to observe their condensation, the separation of carriers was proposed either in reciprocal [3, 4, 5] or in the real space [6, 7, 8]. The proposition has initiated the intensive investigation of such so-called *indirect excitons*, and very recently the typical properties of condensates (such as spontaneous coherence) were observed [9].

On the other hand, bosonic condensates show the quantum fluid properties, and numerous stable topological defects could be observed, like quantized vortices [10], solitons [11], skyrmions [12] etc.

In this chapter I will discuss the condensation of the indirect excitons and the polarization of their photoluminescence. First I will describe in more details the idea of the indirect excitons condensation. Then I will show several works, reporting the condensate properties in the system of indirect excitons. And then I will discuss the polarization dynamics of indirect excitons and their spin patterns.

5.1 Condensation of the indirect excitons

5.1.1 The idea of the indirect excitons

First attempts to overcome the negative effects coming from the fast exciton recombination where done in the semiconductors with indirect bandgaps, like Cu_2O [3, 4, 5]. Separation of carriers in the reciprocal space indeed made the electron-hole pairs live longer than it was necessary for the thermalization. However, excitons in such systems would rather form the electron-hole plasma droplets than go to the condensed state.

In 1975, Y. E. Lozovik and V. I. Yudson considered the possibility of superfluidity of coupled electrons and holes [6]. In order to overcome the effects of the interband transitions, which prevent the superfluidity in the excitonic liquid [13], the authors have proposed to separate the carriers spatially. They proposed to consider two mutually parallel conducting plates, separated by a dielectric. In such structure, the carriers of different types would be localized in different plates. However, the interaction between them would be strong enough to couple them into pairs. Also, the authors have derived that such 2D indirect excitons would interact with each other repulsively, according to the interacting potential:

$$V(r) = \frac{2e^2}{\varepsilon}\left(\frac{1}{r} - \frac{1}{\sqrt{r^2 + D^2}}\right), \tag{5.1}$$

where D is the width of the dielectric layer.

It was an important result, since such repulsive interaction prevents the formation of biexcitons, exciton droplets, etc. and ensures the stability of the exciton gas.

The idea was developed in 1990 by Fukuzawa et al. who proposed to use a double quantum well with applied voltage in order to obtain the condensation of indirect excitons [8]. The matrix element of the electron-hole interaction is proportional to the overlapping of their wave-functions which is small in such systems, which results in the long radiative life-time of excitons. The scheme of the DQW as well as the carrier wavefunctions are illustrated at fig. 5.1.

As long as the spatially separated electron-hole pairs (SEHP) were considered first with respect to their superfluid properties, the theory of their condensation was developed in the superfluidity formalism (BCS theory). Thus, the crucial parameter in the system is the gap in the spectrum of the elementary excitations, which for the SEHP could be expressed as:

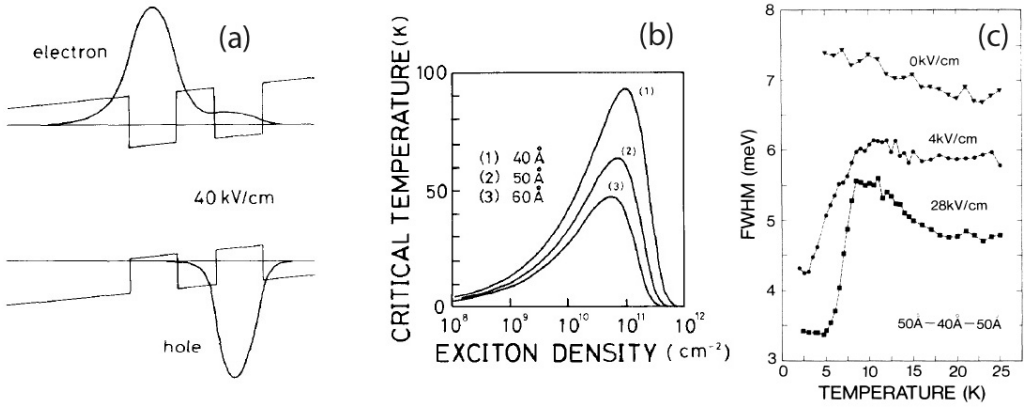

Figure 5.1: (a) The schematic representation of the double quantum well and the electron and hole wave-functions. (b) Critical temperature of the condensation as a function of the exciton density. (c) FWHM of the PL spectra from double quantum well with different voltage applied as a function of the temperature. (a),(b) were taken from [8], (c) was taken from [14]

$$\begin{aligned} \Delta_0 &= v p_\alpha \exp\left[-1/\zeta\right], \\ \zeta &= 8\alpha \left(\frac{p_\alpha}{p_0}\right)^2 \frac{e^2 m}{p_0^2 a_0}. \end{aligned} \tag{5.2}$$

Here $\alpha \sim 1$ is a numerical factor, p_0 is the Fermi momentum and a_0 is the mean distance between particles. p_0 and a_0 are defined by the exciton density n in the following way: $p_0 = \hbar k = \hbar\sqrt{2\pi n}$, $a_0 = 2\pi/k$. m is the exciton reduced mass and $p_\alpha = \hbar d$, d is the spatial separation between the quantum wells and v is the sum of electron hole velocities at the Fermi surface.

From this equation, one can find that the critical temperature of the Bose condensation is $T_c = 2\Delta_0/3.5k_B$. T_c calculated for different values of the carrier density and the spatial separation is plotted on fig. 5.1 (b).

The same year the same group has performed an experiment on the system of double quantum wells, measuring the spectral width of the photoluminescence. Authors observed that when the temperature of the sample has passed some critical value T_c, the width of the PL peak has decreased abruptly almost twice 5.1 (c). The authors have attributed this narrowing to a phase transition of the exciton system into an ordered state. However, the conditions were unlikely for the BEC formation and the results were not enough to say for sure about the origin of such phase transition.

Since then, a large number of works were done on the investigation of the exciton condensation in the system of coupled quantum wells [15, 16, 17]. The changes of numerous properties of excitons were reported, like changes of PL spectra, large increase of the exciton diffusivity and of radiative decay rate as well as stimulated scattering to the low-energy states.

5.1.2 Macroscopically ordered state in an exciton system

In 2002, the group of L. Butov studied the photoluminescence from the double quantum well, whose spatial profile at low excitation densities just followed the laser excitation [18]. However, at large pumping intensities two concentric rings in the PL around the pumping spot were observed. First ring (inner ring) had a small diameter comparable to the size of the excitation spot, while the diameter of the second (outer) ring has been increasing dramatically with the excitation density (fig. 5.2). Also the external ring was fragmented into spots that formed a periodic array over macroscopic lengths, up to around $1mm$.

Moreover, between the inner and the outer ring, a lot of bright spots were observed. Their position was fixed, so they were called localized bright spots (LBS).

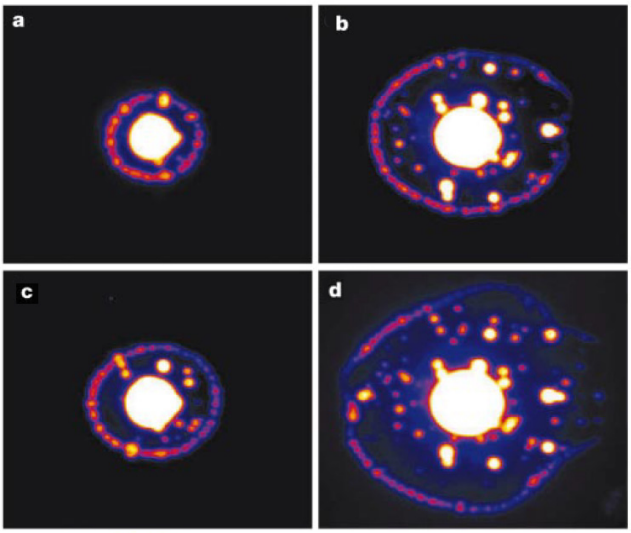

Figure 5.2: Spatial structure of the photoluminescence measured at different values of the excitation density. Image was taken from [18]

The observation of such composite structure has put a lot of questions about its origin and many of them have not been solved at the time of writing of this thesis. The formation of the inner ring was described in the original paper as a photoluminescence from the photoexcited excitons which propagated a bit in space during their lifetime pushed by the exciton-exciton repulsive forces. Also, the authors proposed a description of the outer ring formation. According to their version, the excitons, which have not decayed in first few moments after their creation, could obtain the kinetic energy large enough to get out from the light cone and the decoupling between light and excitons could occur. After that, they propagate for significant distances and relax in energy to the states inside the light cone. After that they recombine emitting light and this forms the outer ring.

However, such scheme had to be reviewed in the works [19, 20]. Different additional measurements have shown the inconsistence of the previous theory. Thus, for example, in the case of two pumping spots, situated not far from each other, the two

outer rings did not cross each other as it should be expected but merged together, forming one halo around both pumping spots [19]. Also, the formation of the outer rings was observed only when the excitation energy was above the AlGaAs barrier band gap energy [20].

These observations led to the formation of the new theory of the outer ring developed independently by two groups. Photoexcited carriers have two options - either to drift towards the electrodes, or to be captured by the quantum wells. It was assumed, that holes have larger probability to be captured than the electrons, which creates a hole-rich region close to the pumping spot. However, far from the spot, there is an electron-rich region, because of the modulation doping of the sample. Outer ring appears at the interface between the two regions, where electrons from outer region and holes from inner region couple to the excitons. This scheme could be phenomenologically described by four kinetic equations for the populations of the hot n, p_{hot} and cold n, p_{cold} carriers:

$$\begin{aligned}
\frac{\partial n_{hot}}{\partial t} &= D^e_{hot}\nabla^2 n_{hot} - \frac{n_{hot}}{\tau^e_{cool}} - \frac{n_{hot}}{\tau^e_{drift}} + Af(r),\\
\frac{\partial p_{hot}}{\partial t} &= D^h_{hot}\nabla^2 p_{hot} - \frac{p_{hot}}{\tau^h_{cool}} - \frac{p_{hot}}{\tau^h_{drift}} + Af(r),\\
\frac{\partial n_{cold}}{\partial t} &= D^e_{cold}\nabla^2 n_{cold} + \frac{n_{hot}}{\tau^e_{cool}} - \frac{n_{cold}-n_{eq}}{\tau^e_{leak}} - \xi n_{cold}p_{cold},\\
\frac{\partial p_{cold}}{\partial t} &= D^h_{cold}\nabla^2 p_{cold} + \frac{p_{hot}}{\tau^h_{cool}} - \frac{p_{cold}}{\tau^e_{leak}} - \xi n_{cold}p_{cold}.
\end{aligned} \tag{5.3}$$

Here $\tau^{e,h}_{cool}, \tau^{e,h}_{drift}, \tau^{e,h}_{leak}$ describe the rates of the cooling, drifting of hot carriers and leakage to or from the contacts of cold carriers, $D^{e,h}_{hot,cold}$ are the diffusion coeffecients, $Af(r)$ states the pumping and ξ is the electron-hole recombination rate. n_eq is the electron equilibrium density in the absence of the external pumping.

Numerous models were proposed in order to describe the fragmentation of the outer ring into the bright spots [21, 22, 23, 24]. Among the assumptions of the driving mechanism were such as the stimulated scattering of excitons [21], the formation of the BEC [22], the exciton-electron-hole Coulomb interaction [24], etc. However, still none of the proposed models gives the exhaustive answer on the nature of the ordered array formation and it still remains an open question.

The origin of the LBS, so far as their position is constant, is usually referred to the defects of the structure which locally increase the electron density. Thus, LBS could be considered as point sources of the hot excitons.

5.2 BEC as a quantum fluid

Condensates, whose motion is well described by Gross-Pitaevskii equations, exhibit the properties of quantum fluids, like, for example, superfluidity. The stable topological defects, like vortices, therefore are of a great interest in such systems. The spinor degree of freedom leads to the possibility of the formation of new objects: half-vortices and skyrmions. This section will be devoted to the discussion of the topological defects in the Bose-Einstein condensates.

5.2.1 Topological defects

Let us consider a simple 1D Gross-Pitaevskii equation:

$$i\frac{\partial}{\partial t}\psi(x,t) = -\frac{\hbar^2}{2m}\frac{\partial^2}{\partial^2 x}\psi(x,t) + \alpha|\psi(x,t)|^2\psi(x,t), \tag{5.4}$$

where we can write a wave-function of the condensate as $\psi(x,t) = \sqrt{n(x,t)}\exp\left[i\theta(x,t)\right]$, $n(x,t)$ is the local density of condensate and $\theta(x,t)$ is its phase.

Let us now consider the repulsive interaction $\alpha > 0$. Then, apart from the trivial homogeneous solution and its weak excitations (bogolons), considered in the first chapter, there is a stable solution of the Gross-Pitaevskii equation which is called the soliton solution:

$$\psi_S(x,t) = \sqrt{n_\infty}\left[\sqrt{1-\frac{v_s^2}{c^2}}\tanh\left(\frac{x-v_s t}{\xi\sqrt{2}}\sqrt{1-\frac{v_s^2}{c^2}}\right) + i\frac{v_s}{c}\right]. \tag{5.5}$$

This solution describes a dip in the density of the condensate, propagating with velocity $v_s = c\sqrt{n(0)/n_\infty}$, where $n(0)$ and n_∞ are the values of the condensate density in the center of soliton and far away from it (fig. 5.3 (a)). Also, the width of the dip is given by the so-called healing length $\xi = \hbar/\sqrt{2m\mu}$, modulated by a Lorentz prefactor $\sqrt{1-v_s^2/c^2}$, where μ is a chemical potential of the condensate and c is the speed of sound.

If the density in the soliton center is zero, then its velocity also turns to zero and the soliton is not propagating. The equation 5.5 turns to just a $\tanh(x/\sqrt{2}\xi)$ function. Such soliton is called a dark soliton. Its phase has a discontinuity in the center, representing the Heaviside function (fig. 5.3 (b)).

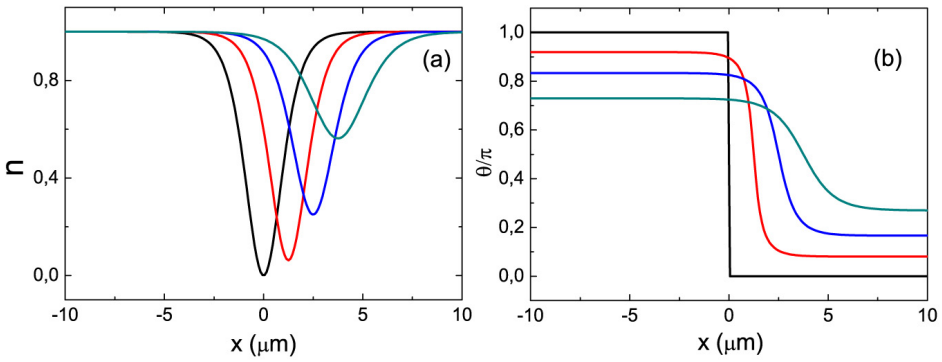

Figure 5.3: The soliton solution for different values of v_s showing (a) the density of the condensate and (b) its phase θ.

In 2D systems, the analogue of the solitons are the quantized vortices, which were first predicted by Lars Onsager in 1947 in connection with superfluid helium[25], but were considered even earlier in the seminal paper of Dirac in 1931 [26]. The idea is

that any spatial variation of the condensate's phase θ around a closed path should be proportional to 2π:

$$\oint \nabla\theta(r,t) = 2l\pi, \tag{5.6}$$

where l is an integer. The cases when $l \neq 0$ requires the phase to have a singularity inside the closed path, what leads to a quantized topological defect - quantized vortex.

The wavefunction describing the condensate would be in this case the product of the radial function $f_l(r)$ and the phase prefactor $\exp[il\varphi]$:

$$\psi_v(r,\varphi) = f_l(r)e^{il\varphi}. \tag{5.7}$$

The radial function $f_l(r)$ has to be evaluated variationally. For the case of $l = 1$ it reads:

$$f_1(r) = \sqrt{n_\infty}\frac{r/\xi}{\sqrt{(r/\xi)^2 + 2}}. \tag{5.8}$$

In the center of the vortex, where is located the phase singularity, the density of the condensate turns to zero as in the center of the dark soliton.

Vortices were observed both in atomic [10, 27] and polaritonic BECs [28].

For multicomponent condensates, like the spinor BECs, the situation gets a bit more complicated. Depending on the strength and on the type of interaction between two components, different type of topological defects could occur. In linearly polarized condensates, in the case of spin-anisotropic interactions (which is the case of polaritons and excitons) the perturbation in one component could occur while the other remains almost undisturbed. In such cases the half-integer topological defects [29] like half-solitons [30] or half-vortices [31] are provided.

In 1962 Tony Skyrme considered the possibility of the construction of a theory of self-interacting meson fields, which will admit states that have the phenomenological properties of fermion particles [32]. He considered an extended nonlinear sigma model and he found the family of classic stationary solutions to the equation of motion derived from the Lagrangian, which could be written in a form:

$$U_S = \exp\{i\tau\mathbf{r}F(r)\}, \tag{5.9}$$

where the phase factor $F(r)$ should satisfy the boundary conditions:

$$F(r \to \infty) = 0, \qquad F(r \to 0) = N\pi, \tag{5.10}$$

where N is the winding number.

This particle, corresponding to the solution was called *skyrmion* particle. So far skyrmions are particles produced by meson fields, showing the barion properties.

It was shown that in the circularly polarized Bose-Einstein condensates in the case of the spin-isotropic interactions the coreless vortex [12, 34] could be observed.

The solution which leads to such vortex is the same as for skyrmion particles, so the vortices are also called skyrmions. Such defects are presented by a dip in the density of the main component and the peak in the density of the other, so the total density of condensate remains constant. In general skyrmions in condensate could be considered as the projection of the Poincare sphere on a plane.

5.2.2 Optical Spin-Hall effect

In 1971, Dyakonov and Perel' have predicted the effect of the spin accumulation on the lateral surfaces of a sample under applied electric current [35] in absence of an external magnetic field. Under the forces of spin-orbit interaction, the scattering of the flowing carriers becomes spin-dependent and an effective spin current appears in the system. The effect was reconsidered by Hirsch in 1999 [36], who named it the Spin-Hall effect (SHE) by the analogy with the Hall effect, where charge separation under external magnetic field occurs. Experimentally, the SHE was observed in semiconductors in 2004 [37, 38].

The idea was extended to the case of photonic-like particles, namely polaritons, by A. Kavokin et al. who proposed so-called Optical Spin-Hall effect (OSHE) [39]. Cavity polaritons, propagating radially from the point of the source, feel the effective in-plane magnetic field provided by the TE-TM splitting, whose direction depends on the direction of polariton propagation and the polariton Hamiltonian could be written as:

$$\hat{H} = \frac{\hbar^2 k^2}{2m^*} + (\sigma \mathbf{\Omega_k}), \tag{5.11}$$

where σ is the pseudospin Pauli matrix and $\mathbf{\Omega_k}$ is the in-plane vector describing the effective magnetic field and its components depend on the wave-vector components $k_{x,y}$ as:

$$\Omega_x = \frac{\Omega}{k^2}\left(k_x^2 - k_y^2\right), \ , \qquad \Omega_x = 2\frac{\Omega}{k^2}\left(k_x k_y\right). \tag{5.12}$$

By this, a polarized polariton would feel the effective in-plane magnetic field, and its pseudospin $\mathbf{s}$ would precess according to the formula:

$$\frac{\partial \mathbf{s}}{\partial t} = \mathbf{s} \times \mathbf{\Omega_k} + \mathbf{f}(t) - \frac{\mathbf{s}}{\tau}. \tag{5.13}$$

Here, the first part describes the Larmor precession of the pseudospin, the second part corresponds to the source of polarized polaritons and the final term takes into account the polariton spin relaxation.

The OSHE was observed in 2007 by C. Leyder et al. in [40]. The authors injected polaritons resonantly with a well-defined wave vector and then considered the Rayleigh scattering of polaritons on the elastic ring. They observed the separation of the polariton polarizations both in real and reciprocal space.

Later the works were done with the consideration of the normal non-resonant excitation of the polariton system [41, 42, 43] in both linear and non-linear cases. In

such schemes, the polaritons are initially settled on the elastic ring in the reciprocal space with some polarization defined by the external excitation (fig. 5.4 (a),(b)). The works have shown the spatial oscillations of the degree of the potoluminescence polarization coming from the cavity , followed by the spatial domains of different polarizations (as in fig. 5.4 (c)).

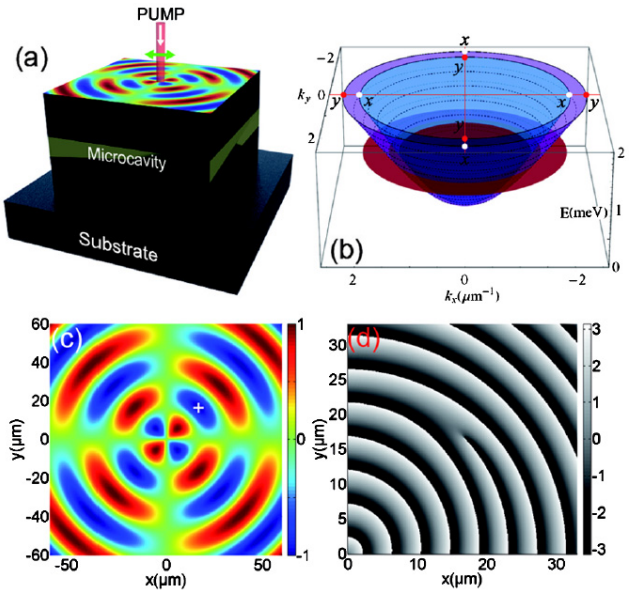

Figure 5.4: (a) Scheme of a typical experiment. (b) 2D dispersions of TE (purple or outer surface) and TM (blue or inner surface) polarized polaritons. The red disk is the Fourier image of the pump laser (x polarized). (c) Degree of circular polarization of photoluminescence (d) The phase of σ^+ component within one polarization domain. Image was taken from [43]

Also it was mentioned in [43] that the polarization structure observed in OSHE resembles the structure of skyrmions despite the fact that that OSHE could be observed in the linear regime. Indeed, within one polarization domain the density of one component goes to zero when the density of the other rises up. At the same time, the total polariton density remains constant. The phase singularity of the first component is presented by a fork-like dislocation in a phase (see fig. 5.4 (d)). Thus, in spite of the spin anisotropy of polariton-polariton interaction, the skyrmions could be obtained in polariton condensates under the forces of TE-TM splitting. Moreover, these topological defects could be obtained in the linear regime.

5.3 Polarization patterns of the exciton condensates

5.3.1 Spontaneous coherence in a cold exciton gas

In the recent paper of High et al., the spontaneous coherence in the indirect exciton condensate was observed [9]. The authors considered the coherence of the light

emitted by the exciton system and studied it by the shift interferometry. The light was divided on two parts, each of them passed through one of two arms of a Mach-Zehnder interferometer. The images were shifted with respect to each other by a value δx to measure the coherence between spatially separated excitons. Authors observed the extended spontaneous coherence in the vicinity of the bright spots - both LBS and bright spots of outer ring (fig. 5.5). However, the interference structure was blurred directly in the center of spots.

The authors have claimed that the spots are the sources of the cold excitons, which propagate radially from each spot and cool down to the lattice temperature forming a condensed state. As the state formed is coherent, this coherency is exhibited in the emitted light.

The polarization of the light emitted from the bright spots is of a particular interest (fig. 5.5 (d),(e),(i),(j)). It shows a well-defined structure and both its linear and circular polarization degrees depend on the direction of exciton propagation. It is a direct evidence that the exciton pseudospin behavior is wave-vector dependent.

The studies of the phase of the emitted light in the region of LBS have revealed two phase singularities presented by forks in the interference pattern and located symmetrically with respect to the center of the spot. The distance between them was independent to the changing of the parameter δx, which means that the singularities were not provided by a single quantized vortex in the center of the LBS.

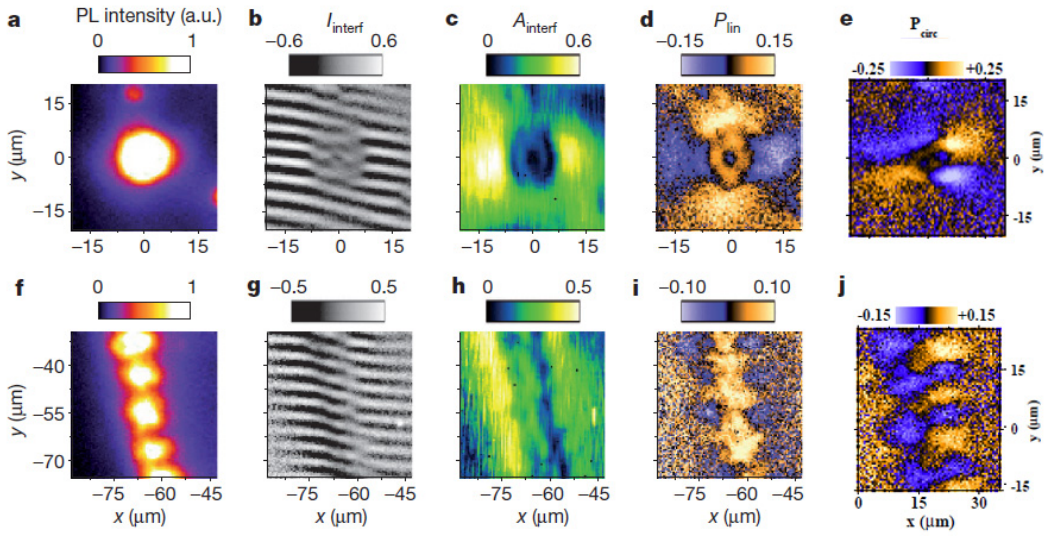

Figure 5.5: Coherence of indirect excitons in the vicinity of LBS ((a)-(e)) and spots on outer ring ((f)-(j)). (a),(f) PL intensity, (b),(g) The interference pattern, (c),(h) The amplitude of the interference, (d),(i) Linear polarization degree, (e),(j) Circular polarization degree. Image was taken from [9].

In our work [44] we discuss the spin dynamics of the propagating indirect excitons. We develop the theory of the indirect exciton spin-orbit interaction discussed

in [45, 46], which allows us to qualitatively reproduce the experimental features. First, we take into account the internal structure of excitons and shows how the relative motion of electron and hole affects the SOI. Especially, the hole SOI is found to become comparable to that of the electron. Second, we assume that a bright indirect exciton condensate with a well defined spin state is locally formed at the center of the LBS, as assumed in Ref.[9]. Then, unlike the approach of Ref.[9], we consider the coherent expansion of the resonantly created exciton cloud by direct numerical solution of the spinor Schroedinger equation, in the presence of the Dresselhaus SOI. The renormalization of the dispersion induces a radial flow of excitons outwards from the pump spot. The repulsive exciton-exciton interactions can also contribute to this effect, but we neglect them in the present work. Since the typical time scale of the scattering of indirect excitons on phonons is of about a few ns, the ballistic propagation length is expected to be of the order of $10 - 20$ microns. Within this length scale, we reproduce both the polarization pattern, and the presence of phase singularities of the wave function components, which are associated with the formation of Skyrmions. These topological defects appear thanks to the interplay between the radial flow and the SOI, as recently shown theoretically [43] for cavity polaritons flowing in a TE-TM effective magnetic field. Inspired by the experimental results, we propose a configuration leading to the onset of circular polarization domains, fully equivalent to the one observed in the optical spin-Hall effect[39]. This happens despite the fact that the wavevector dependence of the effective magnetic field of the Dresselhaus SOI is completely different from the one given by the TE-TM splitting in the microcavities.

5.3.2 The model

.

Indirect excitons are composite bosons formed from electrons and heavy holes separated in space. The projection of the electron's spin (angular momentum of heavy hole) on the growth axis can take two values $\pm 1/2$ ($\pm 3/2$) respectively, so the total angular momentum of exciton can take four values ± 2 and ± 1. The bright $|\pm 1\rangle$ states are coupled with $\sigma^{\pm}$-polarized light, while the states $|\pm 2\rangle$ are dark. Their radiative recombination is forbidden by selection rules.

In planar structures, these four states can be coupled via the inter-exciton interactions, the application of an external magnetic field, or by spin-orbit interactions of carriers originating from the violation of the inversion symmetry. The interactions of the first type are density-dependent. There are two kinds of spin-orbit coupling for carriers: Dresselhaus and Rashba SOIs. Both interactions act as effective in-plane k-dependent magnetic fields coupling different carrier spin states. However, in the sample used in the experiments of reference [9, 46], the Dresselhaus SOI has been found to be much larger than the Rashba SOI, and thus the latter shall be neglected in the following.

For a gas of free 2D electrons, Dresselhaus SOI is linear versus the electron wavevector and the corresponding term of the Hamiltonian in the basis $(+1/2, -1/2)^T$

takes the form:

$$H_e^D = \tilde{\beta}_e(\sigma_+ k_-^e + \sigma_- k_+^e), \tag{5.14}$$

where $\tilde{\beta}_e$ is a Dresselhaus interaction constant. Here and after we use the following notations: $k_\pm^\gamma = k_x^\gamma \pm i k_y^\gamma$, $k_{x,y}^\gamma$ are x- and y-components of wave-vector k^γ, and γ =e, h or X for electrons, holes or excitons respectively. $\sigma_\pm = \sigma_x \pm i\sigma_y$ when $\sigma_{x,y}$ are Pauli matrices.

As it was discussed in the Chapter 1, the SOI for the 2D free heavy-holes is linear by the wave vector [47]. Usually the linear term is considered as dominant and higher order terms are neglected. However, in our work we show, that the terms with cubic dependence could be reduced to the linear by the averaging of the hole motion inside the exciton. We start with the following cubic by k term in the Hamiltonian for the free heavy-hole for Dresselhaus and Rashba type interactions [48]:

$$H_h^{\mathrm{R}} = i\tilde{\alpha}_h(\sigma_+ k_-^3 - \sigma_- k_+^3), \tag{5.15a}$$

$$H_h^{\mathrm{D}} = -\tilde{\beta}_h(\sigma_+ k_- k_+ k_- + \sigma_- k_+ k_- k_+). \tag{5.15b}$$

Here $\tilde{\alpha}_h$ and $\tilde{\beta}_h$ are interaction constants. To do the averaging, we decouple the relative motion of electron and holes from the motion of the excitonic center of mass:

$$\Psi(k^X, q) = \Psi_{\mathrm{c.m.}}(k^X)\Psi_{\mathrm{rel}}(q). \tag{5.16}$$

Here $q = k^e - k^h$ is relative wavevector of electron and hole in the exciton, that is of the order of inverse exciton Bohr radius ($1/a_B$), and k^X is excitonic center of mass wavevector that is much smaller for the cold excitons. Electron and hole wave-vectors are expressed in these values as $k^e = \nu_e k^X + q/2$ and $k^h = \nu_h k^X - q/2$, where $\nu_{e,h} = m_{e,h}/(m_e + m_h)$ is the ratio of the electron (hole) mass to the exciton mass. The averaging of the Hamiltonian (5.15) over the internal exciton e-h-motion in ground state gives rise to an additional term for holes which has the Dresselhauss geometry and is linear in k^X:

$$H_h^D = \int |\Psi_{\mathrm{rel}}(q)|^2 H_h^D d^2q = \beta_h \nu_h(\sigma_+ k_-^X + \sigma_- k_+^X), \tag{5.17}$$

while the Rashba term under similar averaging remains cubic in k^X and can be anyway safely neglected. Here $\beta_h = -\tilde{\beta}_h/2\langle q^2\rangle$ is the effective Dresselhaus constant for holes. Note that $\langle q^2\rangle \sim a_{\mathrm{B}}^{-2} \gg (k^X)^2$, where a_{B} is the excitonic Bohr radius. An analogous procedure for electrons does not change the form of (5.14) but renormalizes electron interaction constants. Finally, one may write a SOI term for both electron and hole bound into exciton as:

$$H_{e,h}^D = \beta_{e,h}\nu_{e,h}(\sigma_+ k_-^X + \sigma_- k_+^X). \tag{5.18}$$

Here $\beta_{e,h}$ are the effective Dresselhaus interaction constants of electrons and holes.

In addition to the SOIs, k-independent energy splitting between linearly polarized states, e.g. parallel and perpendicular to crystallographic axis can occur, and

can be described as k-independent constant effective magnetic fields. Finally, we can write the Hamiltonian for indirect excitons on the basis of the four spin states $\begin{pmatrix} +2 & +1 & -1 & -2 \end{pmatrix}^T$ as follows:

$$H = \begin{pmatrix} E_{+2}\left(k^X\right) & \nu_e\beta_e k_+^X & \nu_h\beta_h k_-^X & -\delta_d \\ \nu_e\beta_e k_-^X & E_{+1}\left(k^X\right) & -\delta_b & \nu_h\beta_h k_-^X \\ \nu_h\beta_h k_+^X & -\delta_b & E_{-1}\left(k^X\right) & \nu_e\beta_e k_+^X \\ -\delta_d & \nu_h\beta_h k_+^X & \nu_e\beta_e k_-^X & E_{-2}\left(k^X\right) \end{pmatrix}. \tag{5.19}$$

Here $E_{\pm1,\pm2}(k) = E_0(k) = \hbar^2(k^X)^2/2m_X$ are the parabolic dispersions of the bare indirect exciton states, $\delta_{b,d}$ give the energy splittings between linearly polarized bright (dark) states. We take the exciton energy at $k^X = 0$ as the zero point. Putting $\delta_b = \delta_d = 0$, the Hamiltonian diagonalization is straightforward and yields the following set of isotropic eigenmodes:

$$\begin{pmatrix} E_I\left(k^X\right) \\ E_{II}\left(k^X\right) \\ E_{III}\left(k^X\right) \\ E_{IV}\left(k^X\right) \end{pmatrix} = \begin{pmatrix} E_0\left(k^X\right) + \left(\nu_h\beta_h + \nu_e\beta_e\right)k^X \\ E_0\left(k^X\right) + \left(\nu_h\beta_h - \nu_e\beta_e\right)k^X \\ E_0\left(k^X\right) - \left(\nu_h\beta_h - \nu_e\beta_e\right)k^X \\ E_0\left(k^X\right) - \left(\nu_h\beta_h + \nu_e\beta_e\right)k^X \end{pmatrix}, \tag{5.20}$$

and the corresponding eigenstates:

$$\begin{aligned} \psi_I &= \begin{pmatrix} 1 \\ +e^{-i\phi} \\ +e^{+i\phi} \\ 1 \end{pmatrix}, \psi_{II} = \begin{pmatrix} -1 \\ +e^{-i\phi} \\ -e^{+i\phi} \\ 1 \end{pmatrix} \\ \psi_{III} &= \begin{pmatrix} -1 \\ -e^{-i\phi} \\ +e^{+i\phi} \\ 1 \end{pmatrix}, \psi_{IV} = \begin{pmatrix} 1 \\ -e^{-i\phi} \\ -e^{+i\phi} \\ 1 \end{pmatrix}. \end{aligned} \tag{5.21}$$

Here ϕ is the polar angle in reciprocal space. The combinations of Eqs.5.21 correspond to linear polarizations of the bright (rows 2 and 3) part given the usual identities $\psi_\pm = \psi_X \pm i\psi_Y$. While dark components are isotropic, the bright components have a linear polarization that is ϕ-dependent and the polarization changes from X to Y when ϕ is changed by $\pi/2$. In other words, the bright spin component exhibits a 2ϕ relative phase. This peculiarity is analogue to the exciton-polariton case in the presence of the so-called TE-TM splitting that gives birth to the optical spin-Hall effect (OSHE). One of the main differences between the two systems is that the TE-TM splitting acts mostly on the photonic part of the exciton polaritons while here, the effective magnetic field involving both the electron and hole spin, is more complex from the point of view of the global system. We will demonstrate below, that the OSHE polarization texture can be reproduced for the indirect exciton under proper excitation of the bright states.

The isotropic dispersion branches given by the Eq.(5.20) are plotted on the Fig.5.6 in the case $\delta_b = \delta_d = 0$. One can clearly see the energy splittings between

the branches coming from the Dresselhaus SOI contribution. Experimentally, one can detect only the emission coming from bright excitons with small wave-vectors inside the light cone ($2.6 \times 10^7 \mathrm{m}^{-1}$). In this region the dispersion branches are linear. Interestingly, the calculated ground state of excitons has a significant wave vector completely out of the light cone. Thus a condensate in the ground state, even possessing some "bright" exciton component, is expected to be completely dark. It is moreover degenerate, and may demonstrate rich phenomenology of topological defects. The Liouville equation allows us to derive the reciprocal space dynamics of

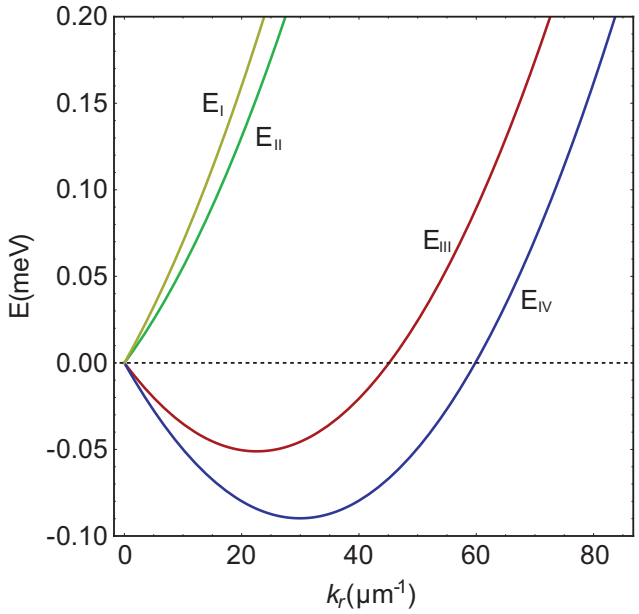

Figure 5.6: Isotropic dispersion branches of the indirect exciton eigen modes [see Eqs.(5.20)].

the spinor field $\mathbf{\Psi} = (\psi_{+2}, \psi_{+1}, \psi_{-1}, \psi_{-2})^T$ with Eq.(5.19) yielding:

$$i\hbar \frac{\partial \mathbf{\Psi}}{\partial t} = H\mathbf{\Psi} - \frac{i\hbar}{2\tau}\mathbf{\Psi} + \mathbf{P}, \tag{5.22}$$

where we have phenomenologically introduced the exciton decay with a lifetime τ and a local source $\mathbf{P}(\mathbf{k}^X) = \mathbf{A}_P\left(\mathbf{k}^X\right)\delta\left(\omega - \omega_P\right)$ with frequency ω_P (in our calculations we took $\hbar\omega_P = 2\mu eV$) acting on each component, where $\mathbf{A}_P(\mathbf{k}^{\mathbf{X}})$ are 2D Gaussians. The formation of the condensate of indirect excitons coming from a hot reservoir and the process of their relaxation towards ground state are complex and need further investigations. Within this simplified model we consider a narrow pump spot (broad in reciprocal space) exciting laterally the dispersion branches and assume a ballistic propagation of the exciton. As said above, the ballistic propagation time is of order of a few ns, during which the evolution of the created cloud is expected to be coherent.

In the idealized case of a Dirac delta source in real space, the excitation of

an eigenstate can be found analytically. For example, the dynamical equation for $\psi_I(k^X)$ reads:

$$i\hbar\frac{\partial\psi_I\left(\mathbf{k}^{\mathbf{X}},t\right)}{\partial t}=\frac{\hbar^2}{2m}(k^X)^2\psi_I\left(\mathbf{k}^{\mathbf{X}},t\right)+i\Delta\beta k^X\psi_I\left(\mathbf{k}^{\mathbf{X}},t\right)+A_P e^{i\omega_P t}, \tag{5.23}$$

and the stationary radial solutions are found writing $\psi_I(k_r^X,t) = \psi_I(k_r^X)\exp(i\omega_P t)$ which yields:

$$\hbar\omega_P\psi_I\left(k_r^X\right)=\left(\frac{\hbar^2}{2m}(k_r^X)^2+i\Delta\beta k^X\right)\psi_I\left(k_r^X\right)+A_P, \tag{5.24}$$

the Green's function of the problem reads

$$G_I\left(k^X\right)=-\frac{A_P}{\frac{\hbar^2}{2m}(k_r^X)^2+i\Delta\beta k_r^X-\hbar\omega_P}, \tag{5.25}$$

whose Fourier transform gives

$$G_I\left(r\right)=\frac{A_P\kappa_1}{\kappa_2-\kappa_1}\left[\begin{array}{l}\log\left(\frac{2}{\kappa_1}\right)\frac{J_0(\kappa_1 r)}{2}-\frac{\pi}{2}\mathbf{H}_0\left(\kappa_1 r\right)\\ +{}_0F_1\left(1,-\frac{\kappa_1^2r^2}{4}\right)\end{array}\right], \tag{5.26}$$

$$-\frac{A_P\kappa_2}{\kappa_2-\kappa_1}\left[\begin{array}{l}\log\left(\frac{2}{\kappa_2}\right)\frac{J_0(\kappa_2 r)}{2}-\frac{\pi}{2}\mathbf{H}_0\left(\kappa_2 r\right)\\ +{}_0F_1\left(1,-\frac{\kappa_2^2r^2}{4}\right)\end{array}\right], \tag{5.27}$$

which is nothing but $\psi_I(r)$ for the delta source. $\kappa_{1,2}$ are the poles of Eq.(5.25) and Eqs.(5.26,5.27) require that $\kappa_1 > 0$ and $\kappa_2 < 0$ which means that $\hbar\omega_P > 0$. The solutions for the other eigenstates are found with a similar procedure and one can therefore construct any combination using the eigenstates (5.21).

For a numerical simulation, we first consider a linearly polarised ($P_{\pm2} = 0$, $P_{\pm1} \neq 0$) bright exciton state as initial condition. The exact values of the Dresselhaus constants are not known, so we took them to be comparable to what was observed in recent experiment [9] (several μeV). Taking different but of the same order constants for electrons and holes would not change qualitatively the final pictures, so for simplicity we took them to be equal: $\beta_{e,h} = 6\mu eV\cdot\mu m$. The masses are $m_e = 0.07m_0$, $m_h = 0.5m_0$, where m_0 is the free electron mass.The figure 5.7(a,b,c) shows the stationary real space images of a linear, circular polarization degree and phase of bright states. One can observe the formation of a Skyrmion lattice associated with the formation of the spin domains. The situation is analogous with the polaritonic optical spin Hall effect. This similarity is expectable, since the effective field acting on the bright states is exactly equivalent to the case of exciton polaritons in the presence of the so-called TE-TM splitting. Fig.5.7 (c) shows the density profile of bright states along the diagonal line [white dashed line on Fig.5.7(b)]. Densities of σ^+ and σ^- states are oscillating while the total density decays in space with r. Phase structure of σ^+-polarized bright state is plotted on Fig.5.7(d). However, the linear

polarization pattern that we observe in this particular simulation (8 polarization domains), differs from the one measured in [9] (4 domains).

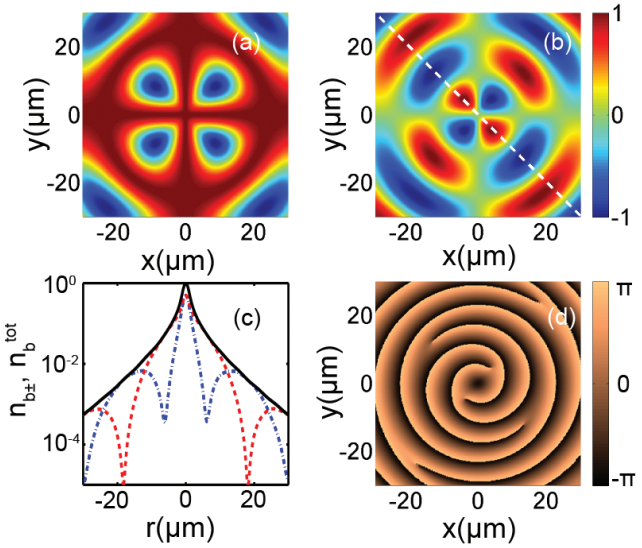

Figure 5.7: Excitonic optical spin-Hall effect. (a) Degree of linear polarization of bright states. (b) Degree of circular polarization of bright states. (c) Density profile for σ^+- (n_{b+}, red dashed line),σ^-- (n_{b-}, blue dashed line) polarized bright states and total density (n_b^{tot}, black solid line) of bright states along the diagonal line $y = -x$ (white dashed line in (b)). (d) Phase of σ^+-polarized bright component.

In order to reproduce the experiment, we therefore consider a different initial spin state for the condensate (Fig. 3). We consider first a condensate of dark states with a slight asymmetry between the dark components ($P_{-2}/P_{+2} = 0.9$, $P_{+1} = P_{-1} = 0$). Then, in order to mix the circularly polarized bright states, we introduce an additional constant splitting between the linearly polarized bright states along and perpendicular to the main crystallographic axis of the sample $\delta_b = 1\mu eV$.

Fig. 5.8 (a,b) shows the spatial distribution of linear and circular polarization degree, while Fig.5.8(d) shows the phase of the X-component. Both circular and linear polarization structures present 4 domains and are stretched along the x axis (because of δ_b) as it was observed in experiment[9]. Interestingly, we also observe pairs of phase singularities (red crosses), situated symmetrically with respect to the exciton source. This phase singularity is accompanied by a density dip only in the Y component. This topological defect is therefore similar to a Skyrmion, but in the linear polarization basis. Our approach shows that the appearance of phase singularities is a general feature of radial flows of particles in the presence of coupling between the spin and motional degree of freedom.

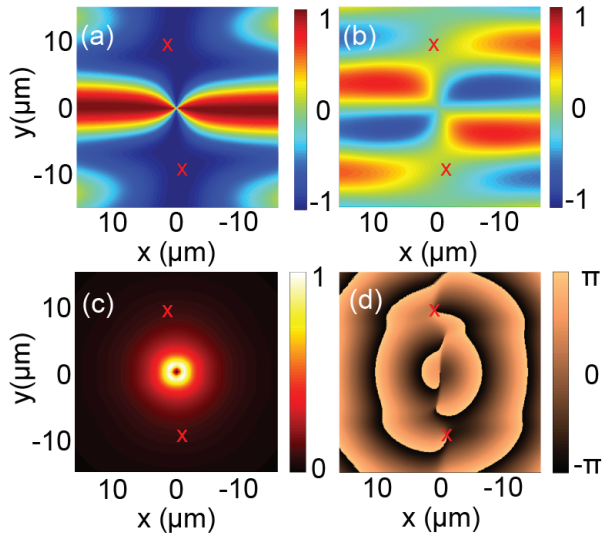

Figure 5.8: (a) Degree of linear polarization of bright states. (b)Degree of circular polarization of bright states. (c) Total density of bright states. (d) Phase of x-component of bright states. Red crosses mark the phase singularities in x-component

5.3.3 Conclusion

Thus we have shown that an expanding cloud of indirect excitons can form polarization textures and phase singularities thanks to the interplay between the flow and spin-orbit interactions. Their structure strongly depends on the polarization of initial state, so changing the excitation conditions one can strongly modify the number of polarization domains and qualitatively reproduce experimental data. Additionally, we were able to mimic the optical spin-Hall effect for bright excitons.

Bibliography

[1] I.M. Blatt. K.W. Boer and W. Brandt, Bose-Einstein Condensation of Excitons, *Phys. Rev.* **126**, 1691 (1962) (Cited on page 111.)

[2] L.V. Keldysh and A. N. Kozlov, Collective Properties of Excitons in Semiconductors, *Sov. Phys. JETP* **27**, 521 (1968) (Cited on page 111.)

[3] A. Mysyrowicz, Exciton as a new quantum system, *J. Phys. (Paris)* **41**, 7, 281 (1980) (Cited on pages 111 and 112.)

[4] D. Hulin, A. Mysyrowicz, and C. Benoit a la Guillaume, Evidence for Bose-Einstein Statistics in an Exciton Gas, *Phys. Rev. Lett.* **45**, 1970 (1980) (Cited on pages 111 and 112.)

[5] D. Snoke, J. P. Wolfe and A. Mysyrowicz , Quantum saturation of a Bose gas: Excitons in Cu_2O, *Phys. Rev. Lett.* **59**, 827 (1987) (Cited on pages 111 and 112.)

[6] Y. E. Lozovik and V. I. Yudson, Feasibility of superfluidity of paired spatially separated electrons and holes; a new superconductivity mechanism, *JETP Lett.* **22**, 274 (1975) (Cited on pages 111 and 112.)

[7] S. l. Shevchenko, , *Sov. J. Low Temp. Phys.* **2**, 505 (1976) (Cited on page 111.)

[8] T. Fukuzawa, S. S. Kano, T. K. Gustafson, and T. Ogawa, Possibility of coherent light emission from Bose condensed states of SEHPs, *Surf. Sci.* **228**, 482 (1990) (Cited on pages 111, 112 and 113.)

[9] A. High, J. R. Leonard, A. T. Hammack, M. M. Fogler, L. V. Butov, A. V. Kavokin, K. L. Campman, and A. C. Gossard, Spontaneous coherence in a cold exciton gas, *Nature* **483**, 584588 (2012) (Cited on pages 111, 119, 120, 121, 125 and 126.)

[10] M. R. Matthews, B. P. Anderson, P. C. Haljan, D. S. Hall, C. E. Wieman, and E. A. Cornell, Vortices in a Bose-Einstein Condensate, *Phys. Rev. Lett.* **83**, 2498 (1999) (Cited on pages 111 and 117.)

[11] O. A. Egorov, D. V. Skryabin, A. V. Yulin, and F. Lederer, Bright Cavity Polariton Solitons, *Phys. Rev. Lett.* **102**, 153904 (2009) (Cited on page 111.)

[12] Usama Al Khawaja and Henk Stoof, Skyrmions in a ferromagnetic Bose-Einstein condensate, *Nature* **411**, 6840 (2001) (Cited on pages 111 and 117.)

[13] R.R. Guseinov, L.V. Keldysh, Nature of the Phase Transition under the Conditions of an "Excitonic" Instability in the Electronic Spectrum of a Crystal, *JETP* **36**, 1193 (1972) (Cited on page 112.)

[14] T. Fukuzawa, E. E. Mendez and J. M. Hong, Phase Transition of an Exciton System in GaAs Coupled Quantum Wells, *Phys. Rev. Lett.* **64**, 25 (1990) (Cited on page 113.)

[15] L. V. Butov, A. Zrenner, G. Abstreiter, G. Bohm, and G. Weimann, Condensation of Indirect Excitons in Coupled AlAs/GaAs Quantum Wells, *Phys. Rev. Lett.* **73**, 304 (1994) (Cited on page 113.)

[16] L. V. Butov and A. I. Filin, Anomalous transport and luminescence of indirect excitons in AlAs/GaAs coupled quantum wells as evidence for exciton condensation, *Phys. Rev. B* **58**, 1980 (1998) (Cited on page 113.)

[17] L.V. Butov, A. L. Ivanov, A. Imamoglu, P. B. Littlewood, A. A. Shashkin, V. T. Dolgopolov, K. L. Campman, and A. C. Gossard, Stimulated Scattering of Indirect Excitons in Coupled Quantum Wells: Signature of a Degenerate Bose-Gas of Excitons, *Phys. Rev. Lett.* **86**, 24 (2001) (Cited on page 113.)

[18] L. V. Butov, A. C. Gossard and D. S. Chemla, Macroscopically ordered state in an exciton system, *Nature* **418**, 751 (2002) (Cited on page 114.)

[19] L. V. Butov, L. S. Levitov, A. V. Mintsev, B. D. Simons, A. C. Gossard, and D. S. Chemla, Formation Mechanism and Low-Temperature Instability of Exciton Rings, *Phys. Rev. Lett.* **92**, 117404 (2004) (Cited on pages 114 and 115.)

[20] R. Rapaport, Gang Chen, D. Snoke, Steven H. Simon, Loren Pfeiffer, Ken West, Y. Liu, and S. Denev, Charge Separation of Dense Two-Dimensional Electron-Hole Gases: Mechanism for Exciton Ring Pattern Formation, *Phys. Rev. Lett.* **92**, 117405 (2004) (Cited on pages 114 and 115.)

[21] L. S. Levitov, B.D. Simons, and L.V. Butov, Pattern Formation as a Signature of Quantum Degeneracy in a Cold Exciton System, *Phys. Rev. Lett.* **94**, 176404 (2005) (Cited on page 115.)

[22] A.V. Paraskevov and T.V. Khabarova, On the microscopic theory of the exciton ring fragmentation, *Phys. Lett. A* **368**, 151 (2007) (Cited on page 115.)

[23] V. I. Sugakov, Islands of exciton condensed phases in a two-dimensional system, the distribution of their sizes and coherence in position, *Solid State Commun.* **134**, 63 (2005) (Cited on page 115.)

[24] J. Wilkes, E. A. Muljarov, and A. L. Ivanov, Drift-Diffusion Model of the Fragmentation of the External Ring Structure in the Photoluminescence Pattern Emitted by Indirect Excitons in Coupled Quantum Wells, *Phys. Rev. Lett.* **109**, 187402 (2012) (Cited on page 115.)

[25] L. Onsager, Statistical hydrodynamics, *Nuovo Cimento* **6**, 249 (1949). (Cited on page 116.)

[26] P. A. M. Dirac, Quantized Singularities in Electromagnetic Field, *P. R. Soc. A* **133**, 60 (1931). (Cited on page 116.)

[27] K. W. Madison, F. Chevy, W. Wohlleben, and J. Dalibard, Vortex Formation in a Stirred Bose-Einstein Condensate, *Phys. Rev. Lett.* **84**, 806 (2000). (Cited on page 117.)

[28] K. G. Lagoudakis, M. Wouters, M. Richard, A. Baas, I. Carusotto, R. André, Le Si Dang, and B. Deveaud-Plédran, Quantized vortices in an exciton-polariton condensate, *Nature Physic*, **4**, 706 (2008). (Cited on page 117.)

[29] G. E. Volovik, V. P. Mineev, Line and point singularities in superfluid ^{3}He, *JETP Lett.* **24**, 561 (1976). (Cited on page 117.)

[30] M. M. Salomaa and G. E. Volovik, Half-solitons in superfluid ^{3}He-A: Novel *pi*/2-quanta of phase slippage, *J. Low Temp. Phys.* **74**, 3-4 (1989). (Cited on page 117.)

[31] J. R. Kirtley, C. C. Tsuei, Martin Rupp, J. Z. Sun, Lock See Yu-Jahnes, A. Gupta, M. B. Ketchen, K. A. Moler, and M. Bhushan, Direct Imaging of Integer and Half-Integer Josephson Vortices in High- T_c Grain Boundaries, *Phys. Rev. Lett.* **76**, 1336 (1996). (Cited on page 117.)

[32] T.H.R. Skyrme, A unified field theory of mesons and baryons, *Nucl. Phys.* **31**, 556 (1962). (Cited on page 117.)

[33] U. A. Khawaja and H. Stoof, Skyrmions in a ferromagnetic Bose-Einstein condensate, *Nature* **411**, 918 (2001). (Not cited.)

[34] K. Kasamatsu, M. Tsubota, and M. Ueda, Spin textures in rotating two-component Bose-Einstein condensates, *Phys. Rev. A* **71**, 043611 (2005). (Cited on page 117.)

[35] M. I. Dyakonov and V. I. Perel', Possibility of orientating electron spins with current, *Sov. Phys. JETP Lett.* **13**, 467 (1971). (Cited on page 118.)

[36] J. E. Hirsch, Spin Hall Effect, *Phys. Rev. Lett.* **83**, 1834 (1999). (Cited on page 118.)

[37] Y. K. Kato, R. C. Myers, A. C. Gossard and D. D. Awschalom, Observation of the Spin Hall Effect in Semiconductors, *Science* **306**, 1910 (2004). (Cited on page 118.)

[38] J. Wunderlich, B. Kaestner, J. Sinova and T. Jungwirth, Experimental Observation of the Spin-Hall Effect in a Two-Dimensional Spin-Orbit Coupled Semiconductor System, *Phys. Rev. Lett.* **94**, 047204 (2005). (Cited on page 118.)

[39] A. Kavokin, G. Malpuech, and M. Glazov, Optical spin-Hall effect, *Phys. Rev. Lett.* **95**, 136601 (2005). (Cited on pages 118 and 121.)

[40] C. Leyder, M. Romanelli, J.-Ph. Karr, E. Giacobino, T. C. H. Liew, M. M. Glazov, A. V. Kavokin, G. Malpuech and A. Bramati, Observation of the optical spin-Hall effect, *Nature Phys.* **3**, 628 (2007). (Cited on page 118.)

[41] W. Langbein, I. A. Shelykh, D. D. Solnyshkov, G. Malpuech, Y. G. Rubo, and A. Kavokin, Polarization beats in ballistic propagation of exciton-polaritons in microcavities, *Phys. Rev. B* **75**, 075323 (2007). (Cited on page 118.)

[42] E. Kammann, T. C. H. Liew, H. Ohadi, P. Cilibrizzi, P. Tsotsis, Z. Hatzopoulos, P. G. Savvidis, A.V. Kavokin, and P. G. Lagoudakis, Nonlinear Optical Spin Hall Effect and Long-Range Spin Transport in Polariton Lasers, *Phys. Rev. Lett.* **109**, 036404 (2012). (Cited on page 118.)

[43] H. Flayac, D. D. Solnyshkov, I. A. Shelykh, and G. Malpuech, Transmutation of Skyrmions to Half-Solitons Driven by the Nonlinear Optical Spin Hall Effect, *Phys. Rev. Lett.* **110**, 016404 (2013). (Cited on pages 118, 119 and 121.)

[44] D. V. Vishnevsky, H. Flayac, A. V. Nalitov, D. D. Solnyshkov, N. A. Gippius, G. Malpuech, Skyrmion Formation and Optical Spin-Hall Effect in an Expanding Coherent Cloud of Indirect Excitons, *Phys. Rev. Lett.* **110**, 246404 (2013). (Cited on page 120.)

[45] O. Kyriienko, E. B. Magnusson, and I. A. Shelykh, Spin dynamics of cold exciton condensates, *Phys. Rev. B* **86**, 115324 (2012). (Cited on page 121.)

[46] M. Matuszewski, T. C. H. Liew, Y. G. Rubo, and A. V. Kavokin, Spin-orbit coupling and the topology of gases of spin-degenerate cold excitons in photoexcited GaAs-AlGaAs quantum wells, *Phys. Rev. B* **86**, 115321 (2012). (Cited on page 121.)

[47] E. I. Rashba and E. Ya. Sherman, Spin-Orbital Band Splitting in Symmetric Quantum Wells, *Phys. Lett. A* **129**, 35 (1988) (Cited on page 122.)

[48] Denis V. Bulaev and Daniel Loss, Spin Relaxation and Decoherence of Holes in Quantum Dots, *Phys. Rev. Lett.* **95**, 076805 (2005) (Cited on page 122.)

Appendix I. Numerical methods.

During my thesis I used to make a lot of numerical simulations, so it would be fare to discuss the methods and the features of my calculations. Almost all simulations were done in `MATLAB v7.11.0`. The exception was the calculations based on the full set of the semi-classical Boltzmann equations (Chapter 4) which were carried out using a code written in `C`.

In most of the situations, the problems were described by the ordinary differential equations in partial derivatives (Gross-Pitaevskii equations in Chapters 2, 4 and 5 and a set of Maxwell-Bloch equations in Chapter 3), which we were solving over time. In order to carry out the time integration of the equations I used the built-in `MATLAB` solver function `ode45()`, which is based on the explicit 4th order Runge-Kutta method. It is a one-step solver, what means that in order to obtain the value of the function on n-th step $\psi(t_n)$ only the value on the previous step $\psi(t_{n-1})$ is needed. The size of the time-step $\delta t = t_n - t_{n-1}$ is found automatically by the solver on each step and for most of problems it was of order of $10^{-16}s$.

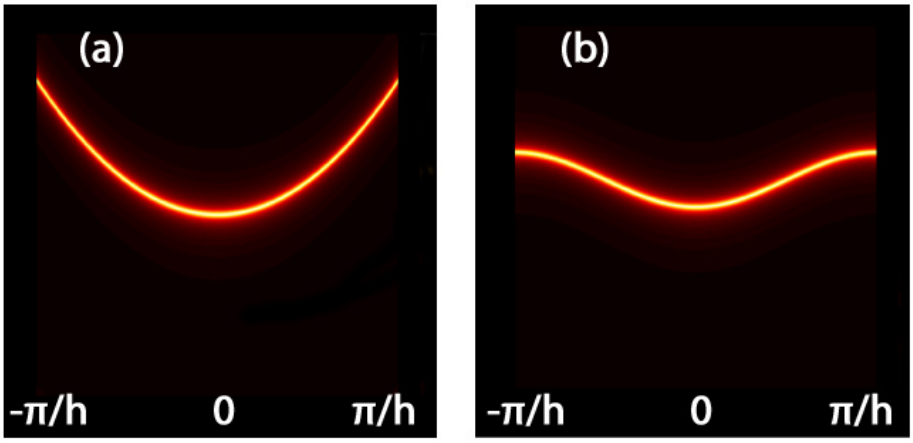

Figure A.1: The dispersion of free particle calculated by the (a) Fourier transform method and (b) method of finite differences. X,Y-axis corresponds to the wave-vector, energy.

The problems discussed in Chapters 2 and 5 required 1D or 2D GPE simulations and the spatial derivatives terms were included into ODE. Each spin component of the wave-function at each moment of time was described by a $n_x \times n_y$ matrix of double-precision complex numbers, where $n_{x,y}$ was the size of x, y vector. In the 1D case, $n_y = 1$. Discretization of the spatial vectors x, y imposes restrictions on possible the wave vectors of the wave-functions, whose value is limited by the spatial resolution:

$$-\frac{\pi}{h_{x,y}} < k_{x,y} < \frac{\pi}{h_{x,y}}, \tag{A.1}$$

where $h_{x,y}$ is the spatial step along x or y direction.

Solving the problem described in Chapter 2, in order to express the second order spatial derivative of the wave functions, I used the method of finite differences. Thus, the Laplacian of the function at the i-th position could be derived as:

$$\left(\frac{d^2\psi}{d(x,y)^2}\right)_i = \frac{\psi_{i+1} - 2\psi_i + \psi_{i-1}}{h_{x,y}^2}. \tag{A.2}$$

The boundary conditions were taken to be periodical, but one could also use other types of boundary conditions, such as infinitely high barriers or zero flux through the boundary. Unfortunately, this method of finite differences reproduces well the parabolic dispersion one expects from the Hamiltonian just in the vicinity of zero. Near the boundaries of the zone, the dispersion is bent showing the negative effective mass as it is shown on the figure A.1 (b). It means that the useful range of the wave-vectors is reduced by a factor of 3, requiring to decrease the spatial step.

In the later work, discussed in Chapter 5, I used another method. The spatial derivatives were described by a Fourier transform $F[]$ method (or rather its numerical implementation FFT), so the Laplacian could be written as:

$$\left(\frac{d^2\psi}{d(x,y)^2}\right) = F^{-1}\left[k_{x,y}^2 F\left[\psi\right]\right], \tag{A.3}$$

where $k_{x,y}$ are the x, y components of the wave-vector.

Such method gives a parabolic dispersion over the whole zone (fig. A.1 (a)). The difference between two methods becomes more important, when we consider a 2 component wave-function in the presence of spin-orbit interactions, which strongly renormalize the dispersion (figure A.2).

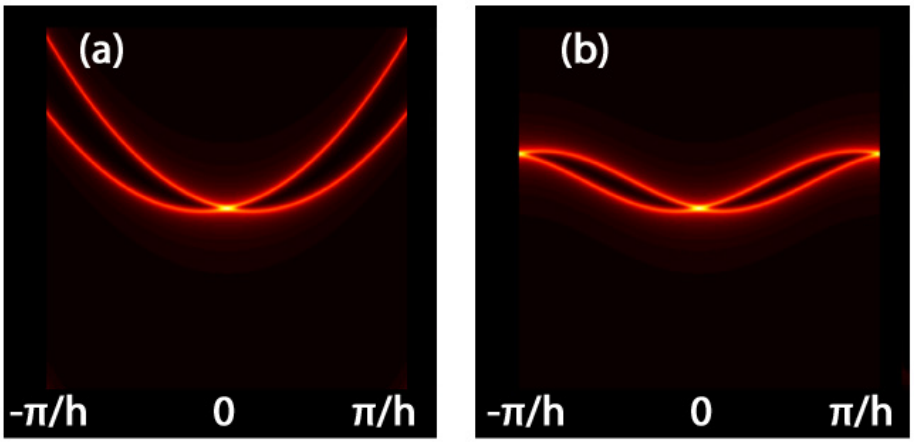

Figure A.2: The dispersion of free particle with spin in the presence of spin-orbit interactions, calculated by the (a) Fourier transform method and (b) method of finite differences. X,Y-axis corresponds to the wave-vector, energy.

The Fourier transform was realized by the `MATLAB` functions `fft(),fft2()` and

`ifft()` which implement the fast Fourier transform algorithm and the inverse transform. Most efficiently these algorithms work in cases, when the matrix dimensions n_x, n_y equal to the 2^m, where m is some integer. In my calculations I used $n_{x,y} = 256$ or 512. The fast Fourier transform implements periodical boundary conditions automatically. These functions are implemented in such way that they can be executed in parallel, if supported by the hardware. This is very useful when one deals with large matrices.

The semi-classical Boltzmann equations discussed in Chapter 4 were simulated by a program written in `C`. The algorithm was based on the 4th order Runge-Kutta method with a variable step.

Conclusions

In order to sum up all what was written in this manuscript, I can say that I tried to show the evolution of different subjects of semiconductor physics, like, Bose-Einstein condensation of quasi-particles, non-linear optics, lasing, etc. through the XX and the beginning of XXI century. I discussed the general specifics of the subjects and attempted to show what are the actual main problems and goals in these fields. I tried to show that recent technological progress gives a reach field of activity to work on, enabling to investigate the nanoworld more and more precisely and to create new impressive technologies. Also, I have presented the works, in which I took the participation, aimed at the solving of some of the problems of modern solid-state physics.

Publications

1. Roman V. Cherbunin, Sergey Yu. Verbin, Thomas Auer, Dmitri R. Yakovlev, Dirk Reuter, Andreas D. Wieck, Ilya Ya. Gerlovin, Ivan V. Ignatiev, Dmitry V. Vishnevsky, and Manfred Bayer, Dynamics of the nuclear spin polarization by optically oriented electrons in a (In,Ga)As/GaAs quantum dot ensemble, *Phys. Rev. B*, **80** 035326 (2009).

2. R. V. Cherbunin, S. Yu. Verbin, K. Flisinski, I. Ya. Gerlovin, I. V. Ignatiev, D. V. Vishnevsky, D. Reuter, A. D. Wieck, D. R. Yakovlev and M. Bayer, Time-resolved Hanle effect in (In,Ga)As/GaAs quantum dots, *J. Phys.: Conf. Ser.*, **245** 012055 (2010).

3. D. V. Vishnevsky, D. D. Solnyshkov, G. Malpuech, N. A. Gippius, and I. A. Shelykh, Coherent interactions between phonons and exciton or exciton-polariton condensates, *Phys. Rev. B*, **84** 035312 (2011).

4. D. V. Vishnevsky, D. D. Solnyshkov, N. A. Gippius, and G. Malpuech, Multistability of cavity exciton polaritons affected by the thermally generated exciton reservoir, *Phys. Rev. B.* **85**, 155328 (2012).

5. D. V. Vishnevsky, N. A. Gippius, Acoustic control of the lasing threshold in QDs ensemble coupled to an optical microcavity, *arXiv:1210.3199* (Submitted to Phys. Rev. B) (2012).

6. D. V. Vishnevsky, H. Flayac, A. V. Nalitov, D. D. Solnyshkov, N. A. Gippius, G. Malpuech, Skyrmion Formation and Optical Spin-Hall Effect in an Expanding Coherent Cloud of Indirect Excitons, *Phys. Rev. Lett.* **110**, 246404 (2013).

7. H. S. Nguyen, D. V. Vishnevsky, C. Sturm, D. Tanese, D. Solnyshkov, E. Gallopin, A. Lemaitre, I. Sagnes, A. Amo , G. Malpuech, and J. Bloch, Polariton nonlinear resonant tunneling diode, *Phys. Rev. Lett.* **110**, 236601 (2013).

Conferences

Oral Contributions

1. The 17^{th} Int. Symp. "Nanostructures: Physics and Technology", Minsk, Belarus, June 22-26, 2009.

2. Meeting of Spin-Optronics project, Madrid, Spain, June 28-29, 2011.

3. 13^{th} International Conference on Physics of Light-Matter Coupling in Nanostructure, Hangzhou, China, June 19-23, 2012.

4. International Conference on Spin-Optronics, Toulouse, France, June 10-14, 2013.

Poster Contributions

1. International School of Nanophotonics and Photovoltaics, Maratea, Italy, September 17-24, 2011.

2. International Polatom School, Toledo, Spain, May 21-23, 2012.

3. International Summer School of ITN "SPINOPTRONICS" (ISSO-2012), Saint-Petersburg, Russia, July 10-14, 2012.

Collective dynamics of excitons and exciton-polaritons in nanoscale heterostructures

Abstract: In my thesis I will discuss some aspects of collective dynamics of excitons and exciton-polaritons in nanoscale heterostructures. In the first Chapter I will make a brief introduction to the modern semiconductor physics and will describe the general elements and notions which will be used further. Other four chapters would be devoted to four works in which I participated, notably, in Chapter 2 I will speak about the coherent interactions between phonons and exciton or exciton-polariton condensates, in Chapter 3 I will discuss the quantum dots lasing and its amplification by an acoustic pulse. Chapter 4 and 5 will be devoted respectively to the polariton multistability and to the condensates of indirect excitons.

Keywords: Excitons, indirect excitons, exciton-polaritons, nanostructures, quantum wells, quantum dots, microcavities, acousto-optic interactions, lasers, nonlinear optics, Bose-Einstein condensation, spin dynamics, topological defects.